10/17 Hansen

DTIC FILE COPY 1

OSU

The Ohio State University

NEAR FIELD GAIN CORRECTION FOR STANDARD GAIN HORN ANTENNAS

H. H. Chung and R. C. Rudduck

The Ohio State University

ElectroScience Laboratory

Department of Electrical Engineering
Columbus, Ohio 43212

Technical Report 711587-1

March 1980

Contract N00014-76-A-0039-RZ01

2750th Air Base Wing/PMR
Specialized Procurement Branch
Building 1, Area C
Wright-Patterson Air Force Base, Ohio 45433

NOTICES

SECURITY CLASSIFICATION OF THIS PAGE (When Data Entered)

REPORT DOCUMENTATION PAGE		READ INSTRUCTIONS BEFORE COMPLETING FORM
1. REPORT NUMBER	2. GOVT ACCESSION NO.	3. RECIPIENT'S CATALOG NUMBER
4. TITLE (and Subtitle) NEAR FIELD GAIN CORRECTION FOR STANDARD GAIN HORN ANTENNAS		5. TYPE OF REPORT & PERIOD COVERED Technical Report
		6. PERFORMING ORG. REPORT NUMBER ESL 711587-1
7. AUTHOR(s) H. H. Chung and R. C. Rudduck		8. CONTRACT OR GRANT NUMBER(s) N00014-76-A-0039-RZ01
9. PERFORMING ORGANIZATION NAME AND ADDRESS The Ohio State University ElectroScience Laboratory, Department of Electrical Engineering, Columbus, Ohio 43212		10. PROGRAM ELEMENT, PROJECT, TASK AREA & WORK UNIT NUMBERS Project F692SB8187-0001 & 0002
11. CONTROLLING OFFICE NAME AND ADDRESS 2750th Air Base Wing/PMR, Specialized Procurement Branch, Building 1, Area C Wright-Patterson Air Force Base, Ohio 45433		12. REPORT DATE March 1980
		13. NUMBER OF PAGES 96
14. MONITORING AGENCY NAME & ADDRESS(if different from Controlling Office)		15. SECURITY CLASS. (of this report) Unclassified
		15a. DECLASSIFICATION DOWNGRADING SCHEDULE
16. DISTRIBUTION STATEMENT (of this Report)		
17. DISTRIBUTION STATEMENT (of the abstract entered in Block 20, if different from Report)		
18. SUPPLEMENTARY NOTES The material contained in this report is also used as a thesis presented to The Ohio State University as partial fulfillment for the degree Master of Science.		
19. KEY WORDS (Continue on reverse side if necessary and identify by block number) Standard gain antennas Horn antennas Antenna gain Geometrical Theory of Diffraction Corrugated horns		

20 ABSTRACT (Continue on reverse side if necessary and identify by block number)

Near field corrections are usually required when the far field gain is to be measured for horn antennas. In this research, the object was to investigate the use of the Geometrical Theory of Diffraction (GTD) for calculating near field corrections.

over

DD FORM 1 JAN 73 1473 EDITION OF 1 NOV 65 IS OBSOLETE

SECURITY CLASSIFICATION OF THIS PAGE (When Data Entered)

20.

Both the GTD method and the equivalent line source integration (LSI) method were used for the calculation of the on-axis near fields for non-corrugated pyramidal horns. For the corrugated horns, the aperture integration method (API) was used.

Keywords: Horn antennas; Gain (r—

ACKNOWLEDGMENT

The authors would like to express their sincere appreciation to Dr. W. D. Burnside for his suggestions and reading of the manuscript.

The efforts of the Measurement Standards and Microwave Laboratory at Newark Air Force Station in providing measured results on coupling data are greatly appreciated.

TABLE OF CONTENTS

CHAPTER I
INTRODUCTION

The customary method of measuring the gain of microwave antennas is by comparison with a standard gain pyramidal horn. The gain of the standard gain horn is determined either by calculation from the dimensions of the pyramidal horn or by measurements. If the far field gain is to be measured, near field corrections are frequently necessary for accurate gain measurements. In this research, the object was to investigate the use of the Geometrical Theory of Diffraction (GTD) for calculating near field corrections.

Both the GTD method and the equivalent line source integration (LSI) method were used for the calculation of the on-axis near fields for non-corrugated pyramidal horns. For small horn dimensions, the LSI method is recommended for somewhat better accuracy. For the corrugated horns, the aperture integration method (API) is used for better accuracy.

In most published research the range is defined as that between the two horn apertures. A more appropriate way to define the range is to use the distance between the amplitude centers of the two horns. The amplitude center of a horn is determined from its E- and H-plane phase centers. Because the range is defined as that between the amplitude centers, considerably less correction is required as compared to using the distance between the horn apertures.

The method for using the near field range correction to determine the far field gain from the measurements of coupling between two horns is discussed in Chapter VII. The measured coupling data used in this research are based on measurements taken at the Measurement Standards and Microwave Laboratory at Newark Air Force Station.

CHAPTER II
BASIC GTD THEORY

Wedge Diffraction

The basic GTD analysis for horn antennas [1-5] is the diffraction by a wedge as shown in Figure 1. There are three basic contributions to the field at the observation point, namely, the incident rays and reflected rays (called the geometric optics rays) and the diffracted rays as seen in the figure. Depending on the position of the observation point there may be no incident ray or no reflected ray as seen in Figure 2.

For an isotropic point source, the incident ray at the observation point (s,ϕ) is given by

$$E^i = \frac{e^{-jks_i}}{s_i} \tag{1}$$

where s_i is the distance between the source and observation points as shown in Figure 1b. The reflected ray at the observation point is given by

$$E^r = \pm \frac{e^{-jks_r}}{s_r} \tag{2}$$

where s_r is the distance between the image and observation points. The plus (+) sign is used for E-field polarization perpendicular to ray fixed plane of incidence and the minus (-) sign is used for parallel polarization. The diffracted fields at the observation point (s,ϕ) are given by [6]

$$E_{\parallel}^d = E_{\parallel}^i(Q_E) \cdot D_s(L,\phi,\phi_o,\beta_o,n)\ A(s)\ e^{jks} \tag{3}$$

$$E_{\perp}^d = E_{\perp}^i(Q_E) \cdot D_h(L,\phi,\phi_o,\beta_o,n)\ A(s)\ e^{-jks} \tag{4}$$

where $E_{\parallel}^i(Q_E)$ is the parallel component which parallel to ray fixed plane of incidence of the incident field at the diffraction point Q_E, $E_{\parallel}^d$ is the parallel component of the diffracted field at the

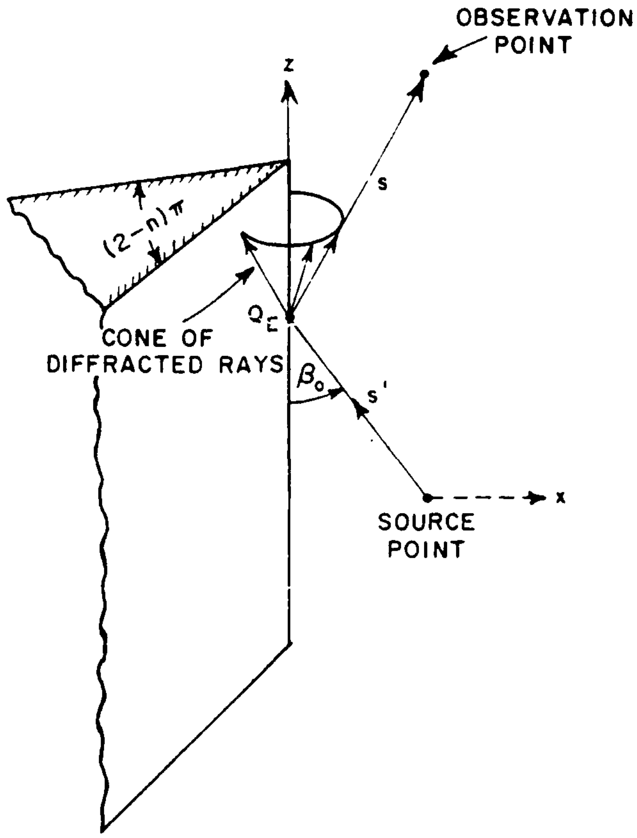

(a)

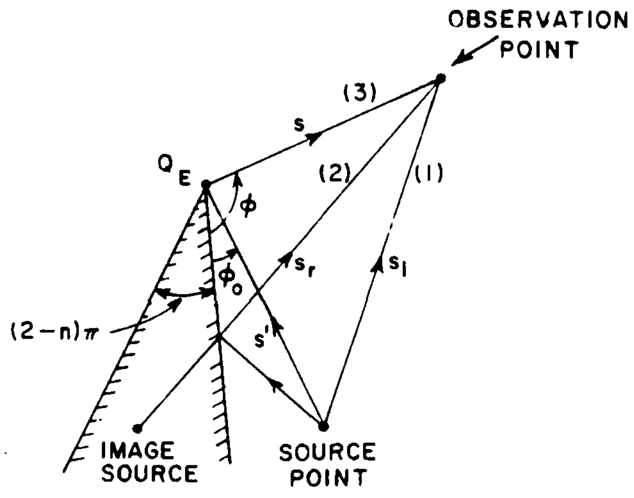

(b)

(1) Incident ray at the observation point.
(2) Reflected ray at the observation point.
(3) Diffracted ray at the observation point.

Figure 1. Geometry for three-dimensional wedge diffraction.

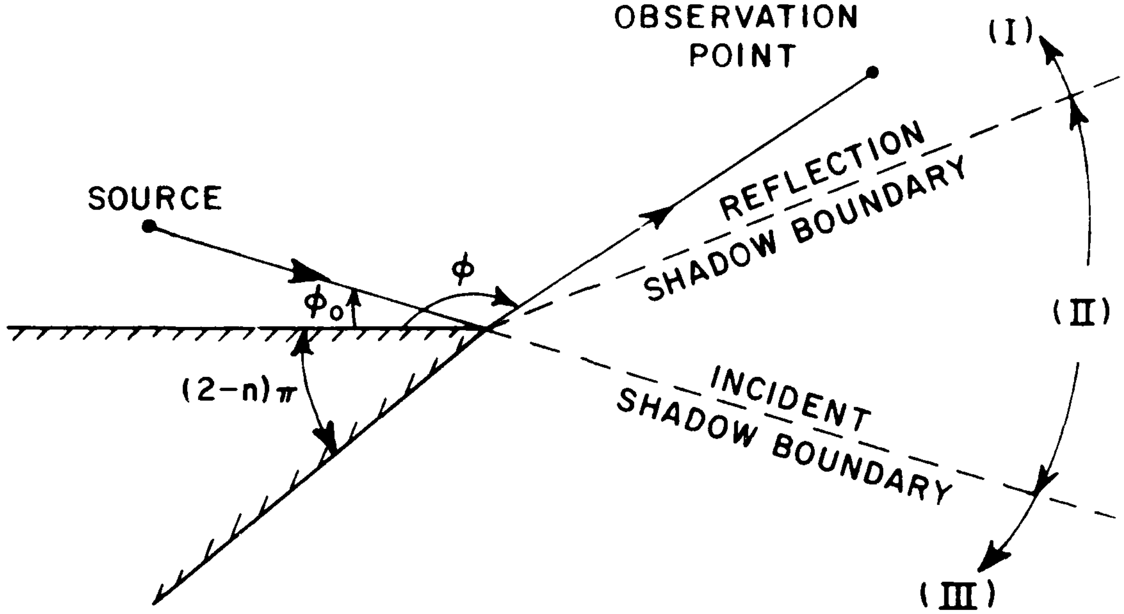

Figure 2. Boundary regions for the wedge problem.
Region I: Incident + reflected + diffracted diffracted rays.
Region II: No reflected ray.
Region III: No reflected and incident rays.

observation point, and $E^i_\perp(Q_E)$ and $E^d_\perp$ are the perpendicular components. For an isotropic point source located at (s',ϕ_0), the incident field at the diffraction point Q_E is given by

$$E^i(Q_E) = \frac{e^{-jks'}}{s'} \tag{5}$$

where s' is the distance between the source and diffraction points. The spreading factor, A(s), describes how the amplitude of the field varies along the diffracted ray,

$$A(s) = \sqrt{\frac{s'}{s(s'+s)}} \quad . \tag{6}$$

The diffraction coefficients, D_s and D_h, for each incident polarization are given by

$$D_{s,h}(L,\phi,\phi_0,\beta_0,n) = D_I(L,\phi-\phi_0,\beta_0,n) \mp D_I(L,\phi+\phi_0,\beta_0,n) \tag{7}$$

where the minus (-) sign applies for D_s and the plus (+) sign for D_h. The components of the diffraction coefficients are expressed in terms of

$$D_I(L,\psi,\beta_o,n) = \frac{e^{-j\frac{\pi}{4}}}{2n\sqrt{2\pi k}\sin\beta_o} \left[\cot\left(\frac{\pi+\psi}{2n}\right)F(kLa^+(\psi))\right.$$

$$\left. + \cot\left(\frac{\pi-\psi}{2n}\right)F(kLa^-(\psi))\right] \quad (8)$$

where β_o is the incident angle with respect to the edge. The wedge parameter n is given by

$$n = 2 - \frac{WA}{\pi} \quad (9)$$

where WA is the wedge angle in radians. The angle parameter is given by

$$\psi = \phi \pm \phi_o \quad (10)$$

and

$$a^{\pm}(\psi) = 2\cos^2\left(\frac{2n\pi N^{\pm} - \psi}{2}\right) \quad (11)$$

where $N^{\pm}$ are integers which most nearly satisfy the equations,

$$2\pi nN^+ - \psi = \pi \quad (12)$$

and

$$2\pi nN^- - \psi = -\pi \quad . \quad (13)$$

The transition function which is basically a Fresnel integral is given by

$$F(x) = 2j\sqrt{x}\, e^{jx} \int_{\sqrt{x}}^{\infty} e^{-j\tau^2}\, d\tau \quad . \quad (14)$$

For spherical wave incidence on a wedge with a flat surface, the distance parameter is given by

$$L = \frac{ss'}{s+s'} \sin^2\beta_o \quad . \quad (15)$$

The total field at the observation point is the sum of the incident, reflected, and diffracted fields as given by

$$E^t = E^i + E^r + E^d \quad . \tag{16}$$

For grazing incidence along the wedge surface (ϕ_0=0) the incident and reflected terms combine to give the total geometrical optics field effectively incident at the observation point. Thus,

$$E^{GO} = E^i + E^r = 2\,\frac{e^{-jks_i}}{s_i} \quad , \tag{17}$$

and the diffraction coefficient becomes

$$D_h = 2D_I\,(L,\phi,\beta_0,n) \quad . \tag{18}$$

It is usually more convenient to use a unit amplitude for the incident wave as given in Equation (1). Consequently, the geometrical optics field for grazing incidence is defined as

$$E^{GO} = \frac{e^{-jks_i}}{s_i} \quad , \tag{19}$$

and hence the diffracted field for grazing incidence is given by

$$E^d = E^i(Q_E)\; D_I(L,\phi,\beta_0,n)\; A(s)\; e^{-jks} \quad , \tag{20}$$

where

$$E^i(Q_E) = E^{GO}(Q_E) = \frac{e^{-jks'}}{s'} \quad . \tag{21}$$

Slope Diffraction

It is well known that the tangential component of the electric field vanishes on the surface of a perfectly conducting plane. Therefore, in the case of grazing incidence on a wedge, the parallel component of the incident field vanishes, and thus one needs to use slope diffraction in order to obtain the H-plane pattern. The slope diffracted fields are calculated in a way similar to ordinary edge diffraction except that the slope diffraction coefficients $\frac{\partial D_s}{\partial \phi_0}$ and $\frac{\partial D_h}{\partial \phi_0}$ and the slope of the incident field $\frac{\partial E^i}{\partial n}$ at the edge are used.

Slope diffraction can be derived from ordinary edge diffraction by considering a dipole source composed of two isotropic point sources as shown in Figure 3. The field of the dipole source is given by

$$E^{si} = I \frac{e^{-jks_+}}{s_+} - I \frac{e^{-jks_-}}{s_-} \tag{22}$$

where s_+ and s_- are the respective slant distances from each individual source. For small spacings $\ell << s_i$,

$$s_\pm = s_i \mp \frac{1}{2} \ell \sin\beta \sin\psi$$

where β is the angle measured from the z-axis as shown in Figure 3a, and ψ is measured from the xz plane as shown in Figure 3b. Thus, the source field can be expressed as

$$E^{si} = I \frac{e^{-jks_i}}{s_i} \left[e^{+j\frac{k\ell}{2}\sin\beta\sin\psi} - e^{-j\frac{k\ell}{2}\sin\beta\sin\psi} \right]$$

$$= 2\, j\, I \sin\left(\frac{k\ell}{2}\sin\beta\sin\psi\right) \frac{e^{-jks_i}}{s_i} \; . \tag{23}$$

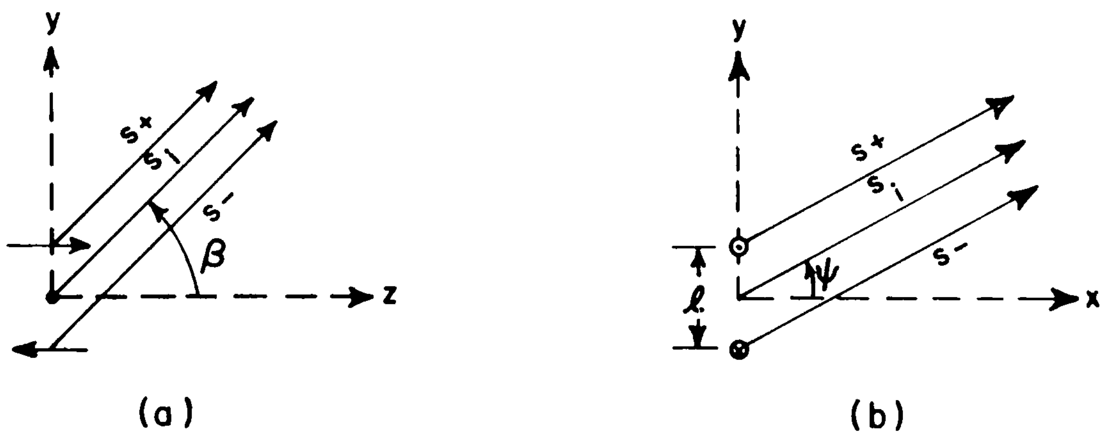

Figure 3. Dipole source for slope diffraction.

For a slope diffraction source $k\ell \to 0$, and thus

$$E^{si} = jkI\ell\sin\beta\sin\psi \frac{e^{-jks_i}}{s_i} \; . \tag{24}$$

The slope diffracted field can be derived by superposition of the diffracted fields from the individual sources as shown in Figure 4. Thus by using Equations (3) and (4)

$$E^{sd} = I \frac{e^{-jks'}}{s'} \left[D_{s,h}\left(\phi, \phi_0 + \frac{\Delta\phi_0}{2}\right) - D_{s,h}\left(\phi, \phi_0 - \frac{\Delta\phi_0}{2}\right) \right] A(s) e^{-jks} \tag{25}$$

where D_s is used for parallel polarization and D_h for perpendicular polarization. Since $\Delta\phi_0 \to 0$ for a dipole source, Equation (25) can be expressed as

$$E^{sd} = I \frac{e^{-jks'}}{s'} \frac{\partial D_{s,h}}{\partial \phi_0} \Delta\phi_0 \, A(s) \, e^{-jks} \quad . \tag{26}$$

Furthermore, the slope of the incident field at the diffraction point Q_E can be derived from Equation (24) as

$$\left.\frac{\partial E^{si}}{\partial \psi}\right|_{\pi} = - jkI\ell \sin\beta_0 \frac{e^{-jks'}}{s'} \tag{27}$$

where β_0 is the angle of the incident ray with respect to the edge. From Equation (27)

$$I \frac{e^{-jks'}}{s'} = \frac{-1}{jk\ell \sin\beta_0} \left.\frac{\partial E^{si}}{\partial \psi}\right|_{\pi} \tag{28}$$

and substituting into Equation (26) gives the slope diffracted field in terms of the slope of the incident field,

$$E^{sd} = - \frac{1}{jk\ell \sin\beta_0} \left.\frac{\partial E^{si}}{\partial \psi}\right|_{\pi} \frac{\partial D_{s,h}}{\partial \phi_0} \Delta\phi_0 \, A(s) \, e^{-jks} \quad . \tag{29}$$

From Figures 4a and b

$$\ell = \rho' \quad \Delta\phi_0 = s' \sin\beta_0 \, \Delta\phi_0 \tag{30}$$

and substituting into Equation (29) gives

$$E^{sd} = \frac{-1}{jks' \sin^2\beta_0} \left.\frac{\partial E^{si}}{\partial \psi}\right|_{\pi} \frac{\partial D_{s,h}}{\partial \phi_0} A(s) \, e^{-jks} \quad . \tag{31}$$

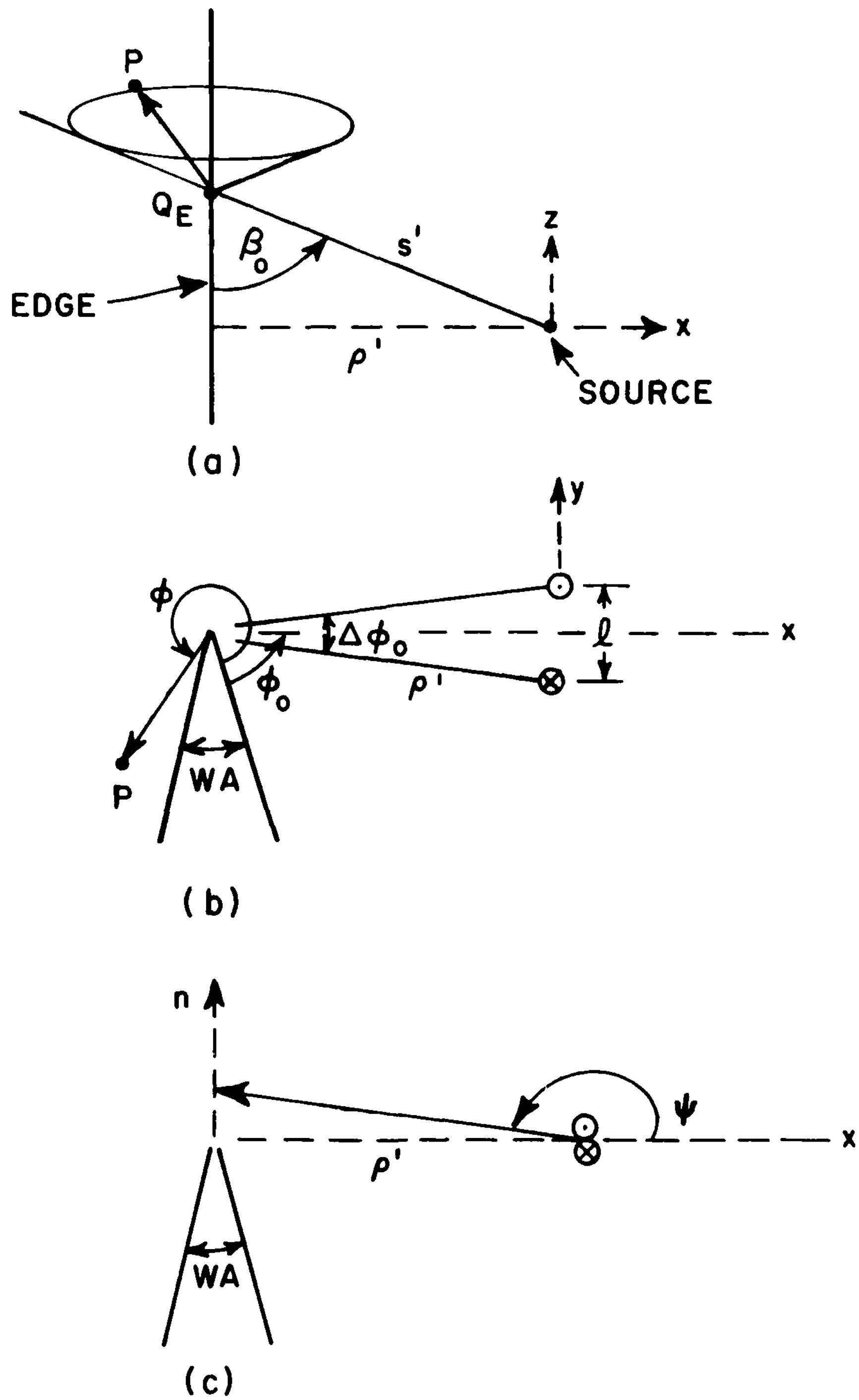

Figure 4. Slope diffraction for a wedge.

The slope of the incident field at the edge can be expressed in terms of the normal to the edge as shown in Figure 4c. Thus

$$\left.\frac{\partial E^{si}}{\partial \psi}\right|_{\pi} = -\rho' \frac{\partial E^{si}}{\partial n} = -s' \sin\beta_o \frac{\partial E^{si}}{\partial n} \, . \tag{32}$$

Thus the slope diffracted field can be expressed in terms of the normal derivative of the incident field at the diffraction point Q_E as

$$E^{sd} = \frac{1}{jk\sin\beta_o} \frac{\partial E^{si}}{\partial n} \frac{\partial D_{s,h}}{\partial \phi_o} A(s)\, e^{-jks} \tag{33}$$

For grazing incidence the parallel components of the incident and reflected waves combine to form the geometrical optics field as discussed before and, consequently,

$$E_{\shortparallel}^{sd} = \frac{1}{jk\sin\beta_o} \frac{\partial E^{si}}{\partial n} D_{PI}\,(L,\phi,\beta_o,n)\, A(s)\, e^{-jks} \tag{34}$$

where

$$D_{PI}(L,\phi,\beta_o,n) = \frac{D_I(L,\phi,\beta_o,n)}{\partial \phi_o} \tag{35}$$

Equation (34) applies for grazing incidence where D_{PI} is used in the same manner as D_I was used in Equation (20).

CHAPTER III
FAR-FIELD PATTERN ANALYSES

E-Plane Pattern

In the case of standard gain horn antennas, the feed waveguide dimension is small; therefore, the dominant propagating mode within the horn can be approximated as a spherical wave with a TE_{10} mode distribution,

$$E^{G.O.} = \frac{e^{-jkR_o}}{R_o} \cos \frac{\pi \tan\theta_H}{2\tan\theta_{oH}} \tag{36}$$

where R_o is the distance from the apex of horn to the observation point, θ_H is the angle measured from the H-plane, and θ_{oH} is the half-flare angle in the H-plane as shown in Figure 5. Here it is assumed that the source is located at the apex. From the TE_{10} mode distribution, one obtains a uniform amplitude distribution in the E-plane and a cosine amplitude distribution in the H-plane.

Our purpose for calculating the far field patterns is to find the phase center in each principal plane. Then the amplitude center for the on-axis radiated field can be determined from the phase center information as will be discussed later. The E-plane pattern can be approximated by superimposing the contributions from the geometrical optics field and the first order diffracted field from the two diffraction points Q_{E_1} and Q_{E_2} shown in Figures 5 and 6. The doubly diffracted field and higher-order fields are usually small for most horns and are often neglected. For a more detailed analysis in the E-plane pattern see Reference [3]. In the E-plane $\theta_H=0^0$, and thus the geometrical optics field is given by

$$E^{G.O.} = \frac{e^{-jkR_o}}{R_o} \ , \tag{37}$$

where R_o is the distance from the E-plane apex to the observation point. For far field distances,

$$R_o = R_{E1} + L_E \cos(\theta_{oE} - \theta) \ . \tag{38}$$

Since the source is located at the apex of the horn walls the E-plane diffracted fields are given by Equation (20) which applies for grazing incidence. Thus the diffracted field from the diffraction point Q_{E1} is given by

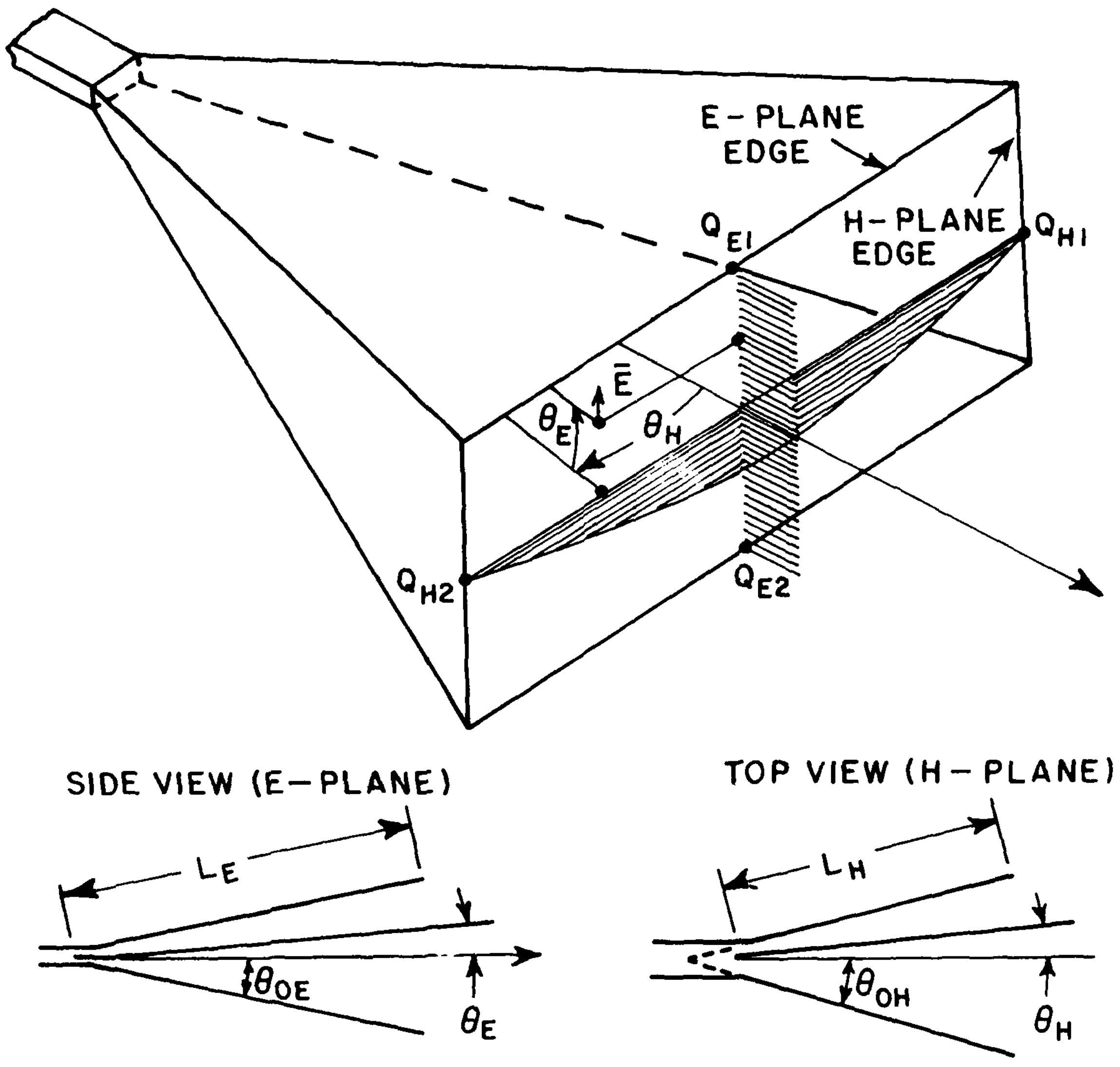

Figure 5. Horn geometry.

$$E_1^d = E^i(Q_{E1})\cdot D_I(L,\pi-\theta_{oE}+\theta,\beta_o,n)\cdot A(R_{E1})e^{-jkR_{E1}} \tag{39}$$

where

$$\beta_o = \frac{\pi}{2} \tag{40}$$

$$n = 2 \tag{41}$$

$$L = L_E \tag{42}$$

$$A(R_{E1}) = \sqrt{\frac{L_E}{R_{E1}(R_{E1}+L_E)}} \approx \sqrt{\frac{L_E}{R_{E1}}} \approx \frac{\sqrt{L_E}}{R_o} \quad \text{for } R_{E1} >> L_E \tag{43}$$

$$R_{E1} \approx R_o - L_E\cos(\theta_{oE}-\theta), \qquad \text{for } R_{E1}, R_o >> L_E \tag{44}$$

and

$$E^i(Q_{E1}) = \frac{e^{-jkL_E}}{L_E} \quad . \tag{45}$$

Thus the diffracted field from Q_{E1} can be expressed as

$$E_1^d = \frac{e^{-jkR_o}}{R_o} \cdot \frac{e^{-jkL_E}}{\sqrt{L_E}} \cdot D_I(L_E,\pi-\theta_{oE}+\theta,\frac{\pi}{2},2) \cdot e^{jkL_E\cos(\theta_{oE}-\theta)} \tag{46}$$

Similarly, the diffracted field from the diffraction point Q_{E2} is given by

$$E_2^d = \frac{e^{-jkR_o}}{R_o} \cdot \frac{e^{-jkL_E}}{\sqrt{L_E}} \cdot D_I(L_E,\pi-\theta_{oE}-\theta,\frac{\pi}{2},2) \cdot e^{jkL_E\cos(\theta_{oE}+\theta)} \tag{47}$$

For far field distances, the rays corresponding to the three terms, $E^{G.O.}$, E_1^d and E_2^d are almost parallel and thus the three field vectors can be summed as scalars. The total field in the E-plane pattern is given by

$$E^{TOT}(\theta) = E^{G.O.} + E_1^d + E_2^d \tag{48}$$

Also, these three terms have a common factor $\frac{e^{-jkR_o}}{R_o}$, which can be suppressed for the convenience of our E-plane pattern analysis.

Each term in Equation (48) contributes to the field only in certain regions as shown in Figure 7 because of shadowing by the horn walls. Each region and the terms used there are defined in Table 1.

Table 1

Boundary Regions for Geometrical Optics and diffracted fields

Region	θ_{min}	θ_{max}	Terms
I	$-\theta_o$	θ_o	$E^{G.O.} + E_1^d + E_2^d$
II	θ_o	$\frac{\pi}{2}$	$E_1^d + E_2^d$
III	$\frac{\pi}{2}$	$\pi - \theta_o$	E_1^d
IV	$\pi - \theta_o$	$-\pi + \theta_o$	$E_1^d + E_2^d$
V	$-\pi + \theta_o$	$-\frac{\pi}{2}$	E_2^d
VI	$-\frac{\pi}{2}$	$-\theta_o$	$E_1^d + E_2^d$

An example of an E-plane pattern is shown in Figure 8 for the Scientific-Atlanta (S/A) standard gain horn antenna (model number 12-8.2) for a frequency of 10 GHz. The flare angle of the S/A horn in the E-plane is 13^o and the aperture width is 14.4 cm or 4.8λ at 10 GHz.

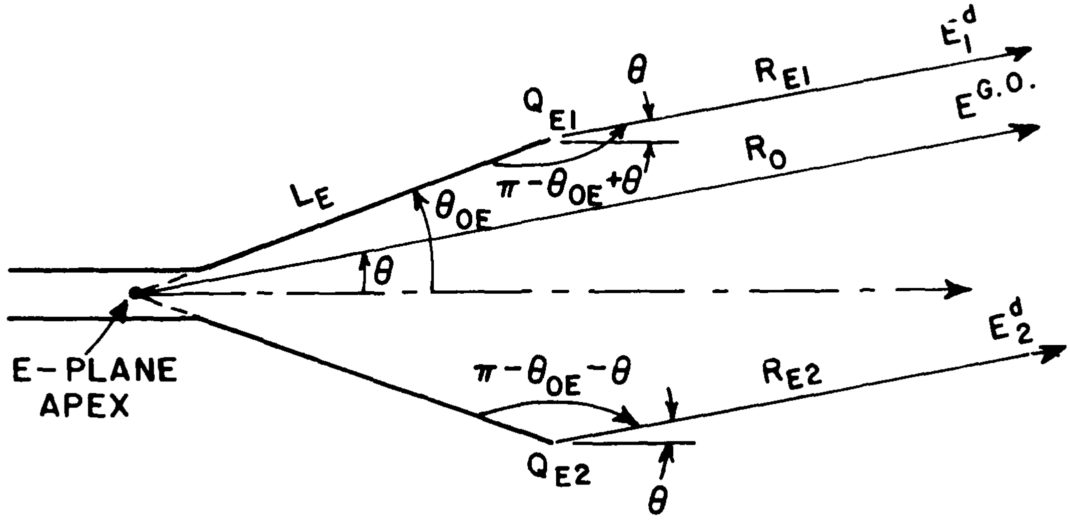

Figure 6. E-plane cross section of horn for far-field pattern analysis.

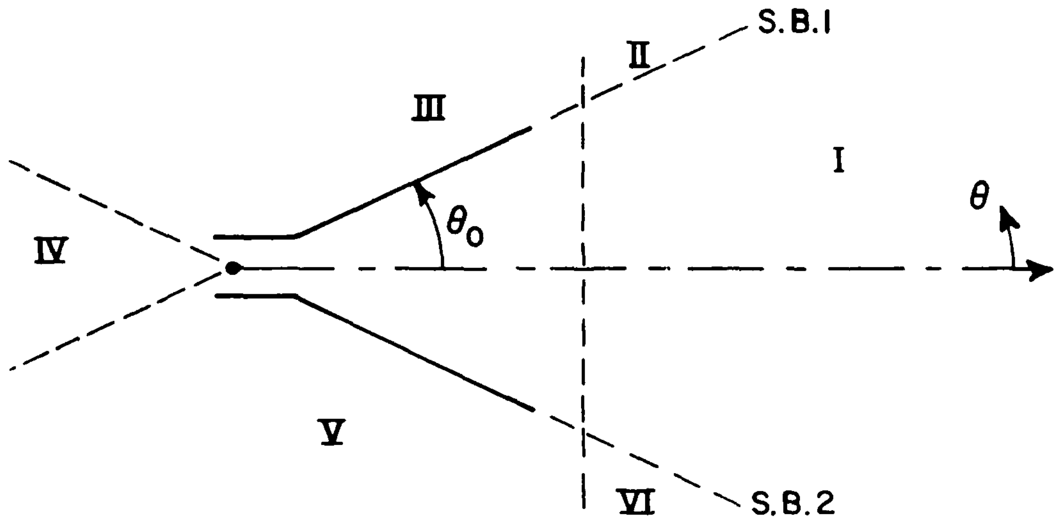

Figure 7. Boundary regions for geometric optics and diffracted fields.

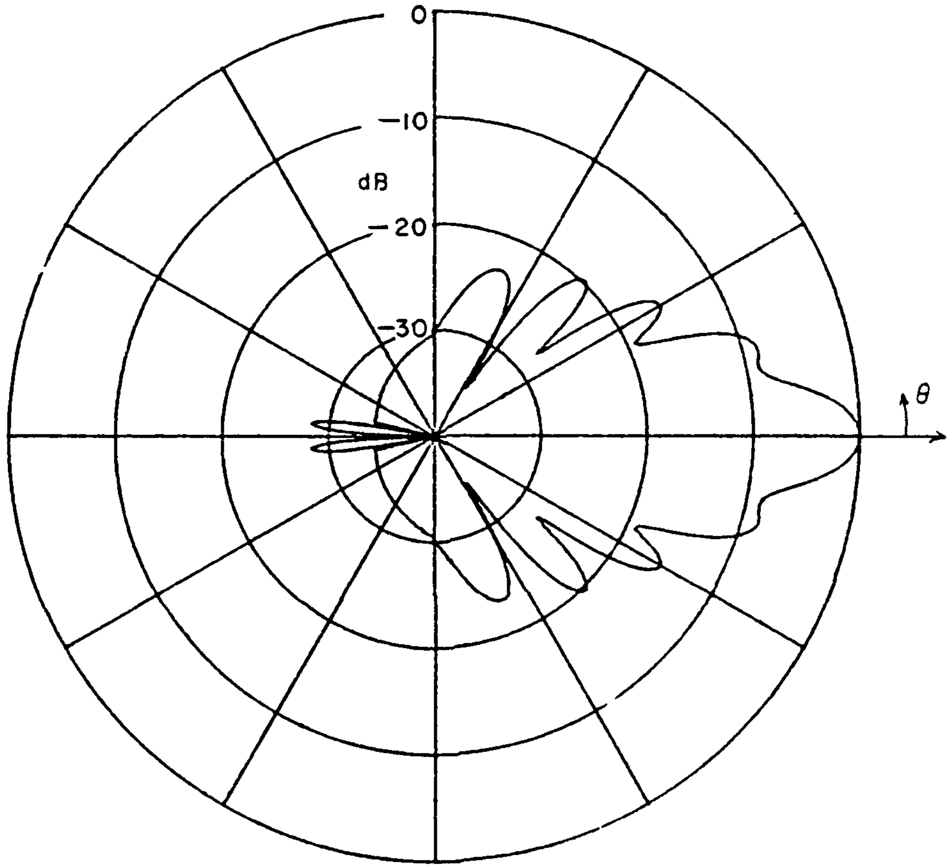

Figure 8. E-plane pattern for Scientific-Atlanta horn (model 12-8.2).

H-plane pattern

In Reference [4], GTD was used to calculate the H-plane pattern by representing the TE_{10} waveguide mode as a pair of plane waves. The analysis is tedious because there are multiple reflections between the horn walls. This makes it necessary to consider many reflections and diffractions in the process. The use of slope diffraction in conjunction with a simple source at the H-plane apex gives a much simpler model for the H-plane. Thus the slope diffraction concept [5] will be used here.

In the H-plane, for grazing incidence along the horn walls, the tangential component of the electric field vanishes on the surfaces and thus only slope diffraction is used to obtain the H-plane pattern. The H-plane pattern can be approximated by superimposing the contributions from the geometrical optics field and the slope diffracted fields from the two diffraction points Q_{H_1}, Q_{H_2} as shown in Figure 9. The contribution of the E-plane edge will not significantly affect the H-plane pattern shape but will slightly affect the computed front/back ratio. The contribution of doubly diffracted and higher order fields are usually small for most horns. Therefore, the contribution of the E-plane edge, doubly diffracted and higher order fields will not be included in our study.

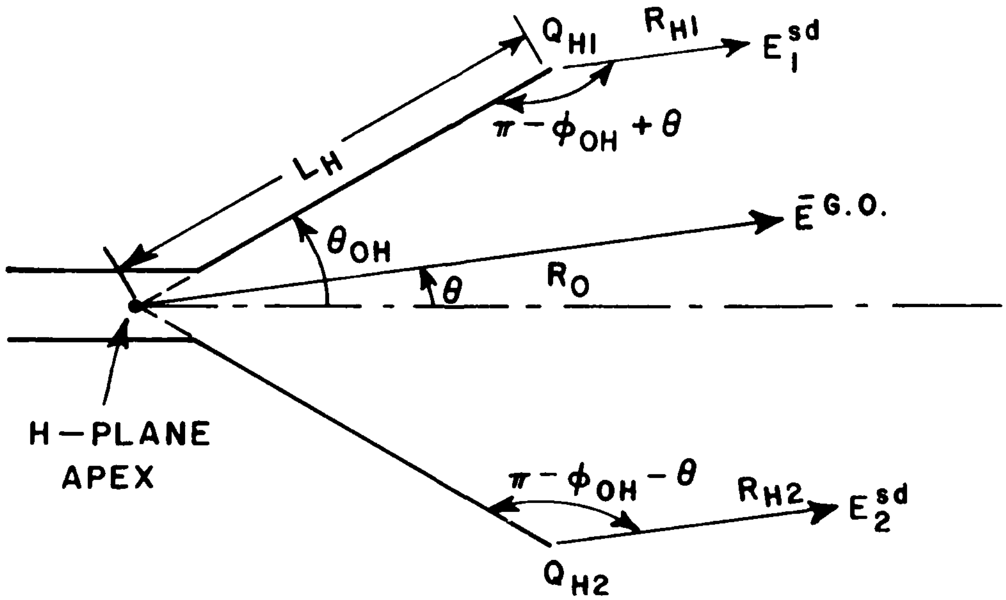

Figure 9. H-plane cross section of horn for far-field pattern analysis.

The phase reference is taken at the H-plane apex as shown in Figure 9. The geometrical optics field is approximated as

$$E^{G.O.} = \cos\left(\frac{\pi}{a} L_H \cos\theta_{oH} \tan\theta\right) \cdot \frac{e^{-jkR_o}}{R_o}$$

$$= \cos\left(\frac{\tan\theta}{2\tan\theta_{oH}}\right) \cdot \frac{e^{-jkR_o}}{R_o} \tag{49}$$

where $\quad a = 2L_H \sin\theta_{oH}$. (50)

For narrow flare angle ($\theta_{oH} < 20^o$) ,

$$E^{G.O.} \approx \cos\left(\frac{\pi\theta}{2\theta_{oH}}\right) \cdot \frac{e^{-jkR_o}}{R_o} . \tag{51}$$

Since the source is located at the apex, the H-plane diffracted fields are given by Equation (34) which applies for grazing incidence. The slope of the field incident on the diffraction points Q_{H1} and Q_{H2} is given by

$$\therefore \frac{\partial E^{si}}{\partial n} = \frac{1}{L_H} \cdot \frac{\partial E^i(Q_{H1,2})}{\partial \phi_o}$$

$$= -\frac{1}{L_H} \cdot \left.\frac{\partial E^i(Q_{H1,2})}{\partial \psi}\right|_{\psi=\pi}$$

$$= -\frac{1}{L_H} \cdot \left.\frac{\partial E^i(Q_{H1,2})}{\partial \theta}\right|_{\theta=\theta_{oH}}$$

$$= -\frac{e^{-jkL_H}}{L_H^2} \cdot \frac{\partial}{\partial\theta}\left(\cos\left(\frac{\tan\theta}{2\tan\theta_{oH}}\right)\right) \tag{52}$$

where the slope of the pattern is determined as

$$\frac{\partial}{\partial \alpha}\left(\cos\frac{\alpha\tan\alpha}{2\tan\alpha_{oH}}\right)\Bigg|_{\alpha=\alpha_{oH}} = -\frac{\pi}{\sin 2\alpha_{oH}} \tag{53}$$

Thus we get,

$$\frac{\partial E^{si}}{\partial n} = \frac{e^{-jkL_H}}{L_H^2}\ \frac{\pi}{\sin 2\alpha_{oH}} \tag{54}$$

$$A(s) = \sqrt{\frac{L_H}{R_{H1}(R_{H1}+L_H)}} \approx \frac{\sqrt{L_H}}{R_{H1}}, \quad \text{for } R_{H1} \gg L_H \tag{55}$$

$$\therefore E_1^{sd} = \frac{\pi}{jk\sin 2\alpha_{oH}} \cdot \frac{e^{-jkL_H}}{L_H^{3/2}} \cdot D_{PI}(L_H, \pi-\alpha_{oH}+\theta, \tfrac{\pi}{2}, 2) \cdot \frac{e^{-jkR_{H1}}}{R_{H1}} \tag{56}$$

Similarly,

$$E_2^{sd} = \frac{\pi}{jk\sin 2\alpha_{oH}} \cdot \frac{e^{-jkL_H}}{L_H^{3/2}} \cdot D_{PI}(L_H, \pi-\alpha_{oH}-\theta, \tfrac{\pi}{2}, 2)\ \frac{e^{-jkR_{H2}}}{R_{H2}} \tag{57}$$

For far field distances,

$$R_{H1} = R_0 - L_H\cos(\alpha_{oH} - \theta) \tag{58}$$

$$R_{H2} = R_0 - L_H\cos(\alpha_{oH} + \theta) \tag{59}$$

and for narrow flare angle ($\alpha_{oH} < 20^{o}$), the slope diffraction fields become

$$E_1^{sd} = \frac{\pi}{jk2\alpha_{oH}} \cdot \frac{e^{-jkL_H}}{L_H^{3/2}} \cdot D_{PI}(L_H, \pi-\alpha_{oH}+\theta, \tfrac{\pi}{2}, 2)\ \frac{e^{-jkR_0}}{R_0} \cdot e^{jkL_H\cos(\alpha_{oH}-\theta)} \tag{60}$$

$$E_2^{sd} = \frac{\pi}{jk2\theta_{oH}} \frac{e^{-jkL_H}}{L_H^{3/2}} D_{PI}\left(L_H, \pi-\theta_{oH}-\theta, \frac{\pi}{2}, 2\right) \frac{e^{-jkR_o}}{R_o} e^{jkL_H\cos(\theta_{oH}+\theta)} \tag{61}$$

The total field in the H-plane pattern is given by

$$E^{TOT}(\theta) = E^{G.O.} + E_1^{sd} + E_2^{sd} \tag{62}$$

The factor, $\frac{e^{-jkR_o}}{R_o}$, can be suppressed for the convenience of the H-plane pattern analysis.

The regions for the geometrical optics and the slope diffracted fields are the same as for the E-plane shown in Figure 7 and given in Table 1.

An example of an H-plane pattern is shown in Figure 10 for the S/A standard gain horn (model number 12-8.2) for a frequency of 10 GHz. The flare angle of the S/A horn in the H-plane is 16.5^o and the aperture width is 19.43 cm or 6.48λ at 10 GHz.

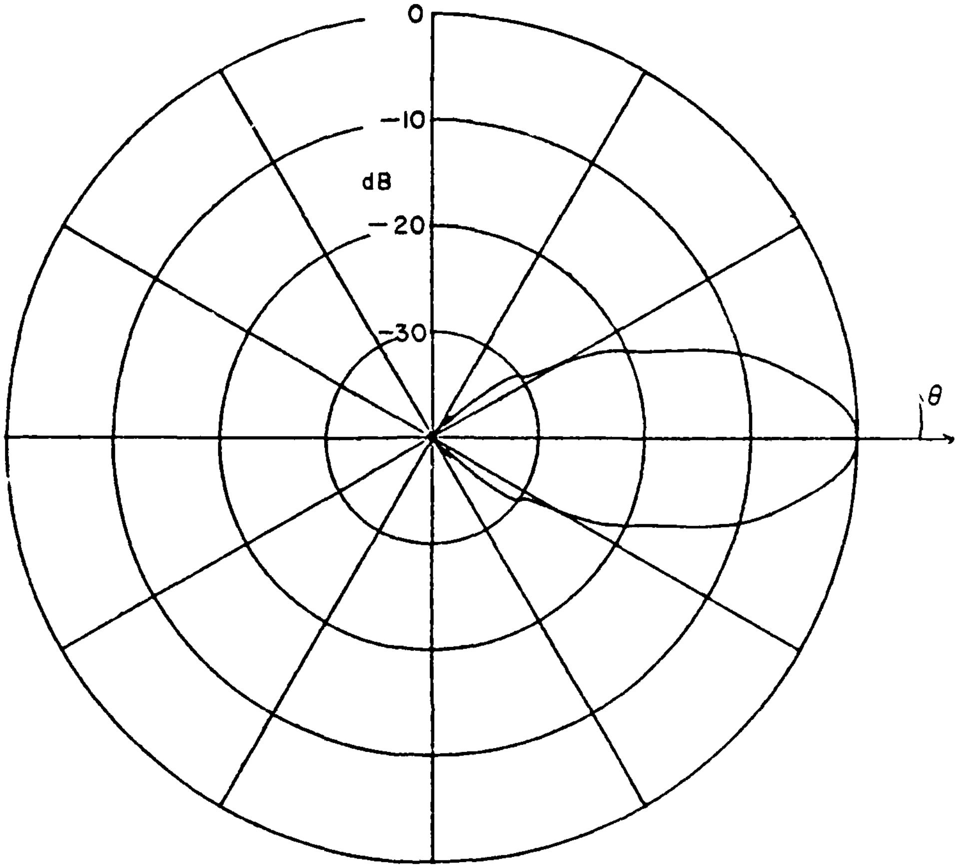

Figure 10. H-plane pattern for Scientific-Atlanta horn (model 12-8.2).

CHAPTER IV
ANALYSIS OF HORN'S ON-AXIS NEAR FIELD USING GTD

The GTD analysis of the on-axis near field radiated by a rectangular horn is similar to the far field pattern cases. As shown in Figure 11, the source is located at the apex, the total field at the observation point is the sum of incident and diffracted fields as given by

$$\overline{E}^{TOT} = \overline{E}^{G.O.} + \overline{E}_1^d + \overline{E}_2^d + \overline{E}_1^{sd} + \overline{E}_2^{sd} \tag{63}$$

where $\overline{E}^{G.O.}$, $\overline{E}_1^d$, $\overline{E}_2^d$, $\overline{E}_1^{sd}$ and $\overline{E}_2^{sd}$ are defined as before except that the distances, angle parameters, and spreading factors are modified for the near field case as will be defined later.

As shown in Figure 12, for the on-axis near field in the E-plane, the amplitudes of the two diffracted fields from Q_{E1} and Q_{E2} in the E-plane are equal because of symmetry in the ray geometry. Thus the diffracted fields are given by Equation (20), where

$$L = \frac{L_E R_{E1}}{L_E + R_{E1}} \tag{64}$$

$$S = R_{E1} = R_{E2} \tag{65}$$

$$\phi = \pi - \theta_{oE} - \theta' \tag{66}$$

$$\theta' = \tan^{-1} \frac{B}{2Z_A} \tag{67}$$

$$\therefore A(s) = \sqrt{\frac{L_E}{R_{E1}(R_{E1}+L_E)}} \tag{68}$$

$$\therefore E_1^d = E_2^d = \frac{e^{-jkL_E}}{\sqrt{L_E}} D_I \left(\frac{L_E R_{E1}}{L_E + R_{E1}}, \pi - \theta_{oE} - \theta', \frac{\pi}{2}, 2 \right) \cdot \frac{e^{-jkR_{E1}}}{\sqrt{R_{E1}(R_{E1}+L_E)}} \tag{69}$$

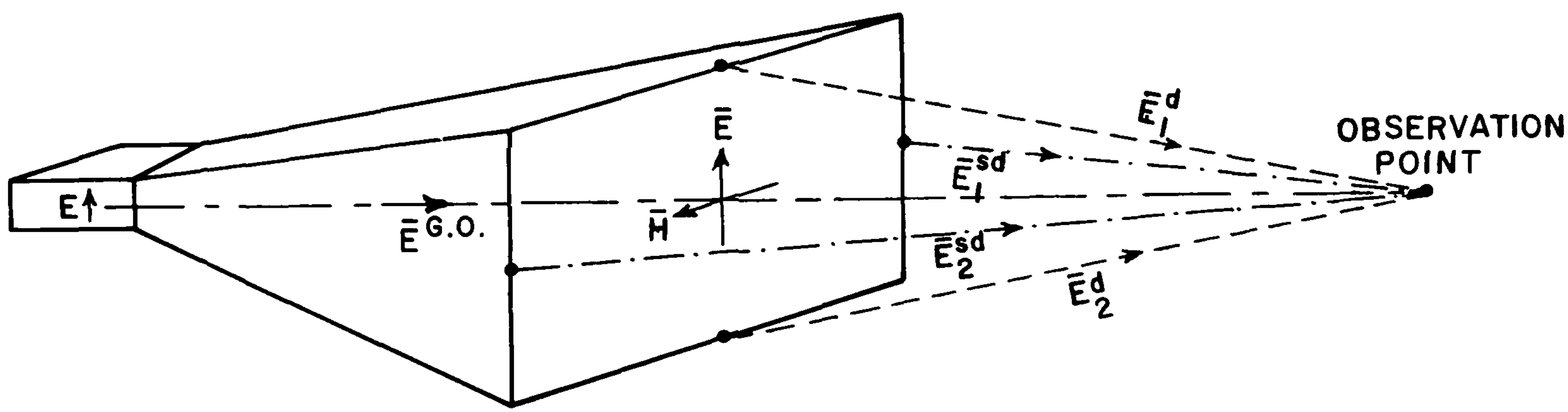

Figure 11. Basic field contributions for the pyramidal horn at the observation point.

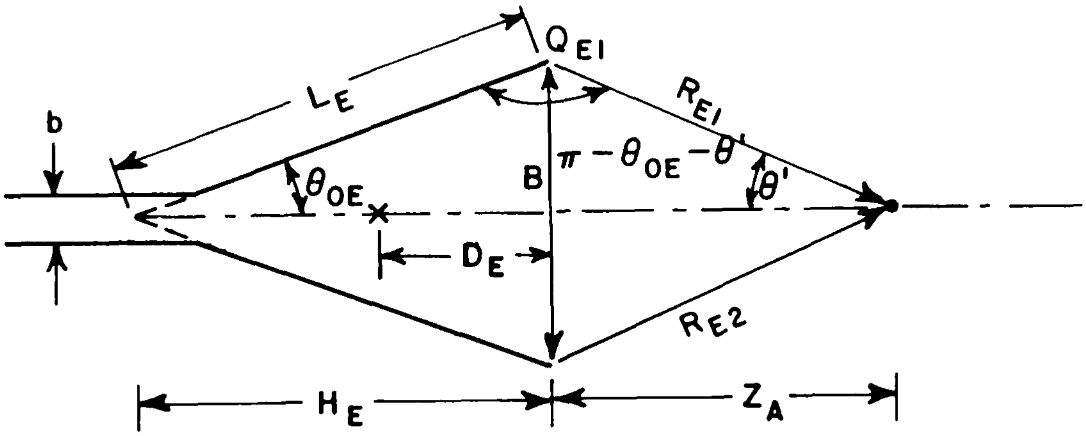

Figure 12. E-plane geometry.

However, the two diffracted electric field vectors are not in the same direction at the observation point as shown in Figure 13. The $\cos\theta'$ components are in the same direction and can be added together, but the sin components are in the opposite direction and cancel each other. Thus the sum of the diffracted fields from the diffraction points Q_{E1} and Q_{E2} in the E-plane is given by

$$E_{DIF} = (E_1^d + E_2^d)\cos\theta'$$

$$= 2 \cdot \frac{e^{-jkL_E}}{\sqrt{L_E}} \; D_I\left(\frac{L_E R_{E1}}{L_E+R_{E1}}, \pi-\theta_{oE}-\theta', \frac{\pi}{2}, 2\right) \frac{e^{-jkR_{E1}}}{\sqrt{R_{E1}(R_{E1}+L_E)}} \cos\theta' \tag{70}$$

Similarly, as shown in Figure 14, for the on-axis near field in the H-plane, the diffracted fields from points Q_{H1} and Q_{H2} are given by Equation (34), where

$$L = \frac{L_H R_{H1}}{L_H+R_{H1}} \tag{71}$$

$$S = R_{H1} = R_{H2} \tag{72}$$

$$\phi = \pi - \theta_{oH} - \theta'' \tag{73}$$

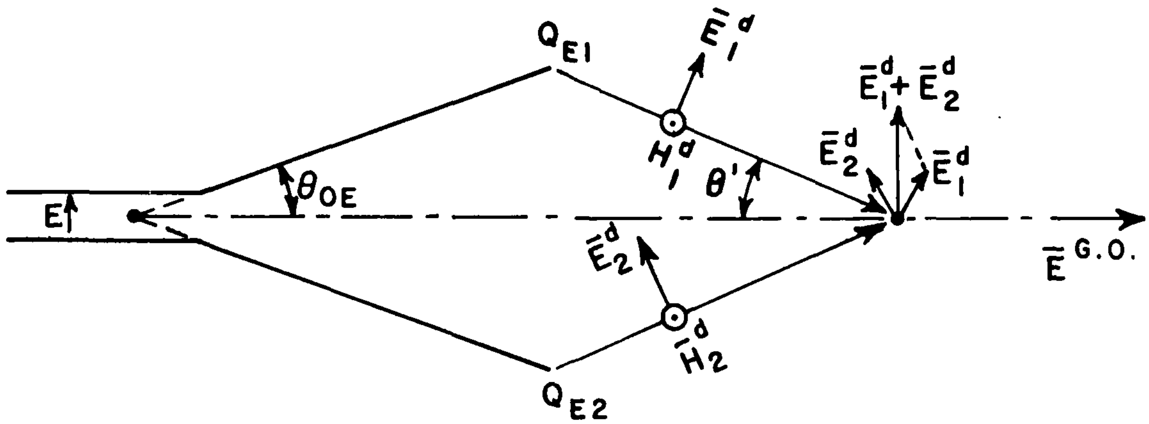

Figure 13. Analysis of the direction of EM field propagation in the E-plane.

$$\theta'' = \tan^{-1} \frac{A}{2Z_A} \tag{74}$$

$$A(s) = \sqrt{\frac{L_H}{R_{H1}(R_{H1}+L_H)}} \tag{75}$$

$$\therefore E_1^{sd} = E_2^{sd}$$

$$= \frac{\pi}{2\theta_{oH}} \cdot \frac{e^{-jkL_H}}{jkL_H^{3/2}} \cdot D_{PI}\left(\frac{L_H R_{H1}}{L_H+R_{H1}}, \pi-\theta_{oH}-\theta'', \frac{\pi}{2}, 2\right) \frac{e^{-jkR_{H1}}}{\sqrt{R_{H1}(R_{H1}+L_H)}} \tag{76}$$

Since the two diffracted E-fields are in the same direction at the observation point as shown in Figure 15, the sum of the diffracted fields from the diffraction points Q_{H1} and Q_{H2} is given b

$$H_{DIF} = E_1^{sd} + E_2^{sd}$$

$$= 2\left(\frac{\pi}{2\theta_{oH}}\right) \cdot \frac{e^{-jkL_H}}{jkL_H^{3/2}} \; D_{PI}\left(\frac{L_H R_{H1}}{L_H+R_{H1}}, \pi-\theta_{oH}-\theta'', \frac{\pi}{2}, 2\right) \cdot \frac{e^{-jkR_{H1}}}{\sqrt{R_{H1}(R_{H1}+L_H)}} \tag{77}$$

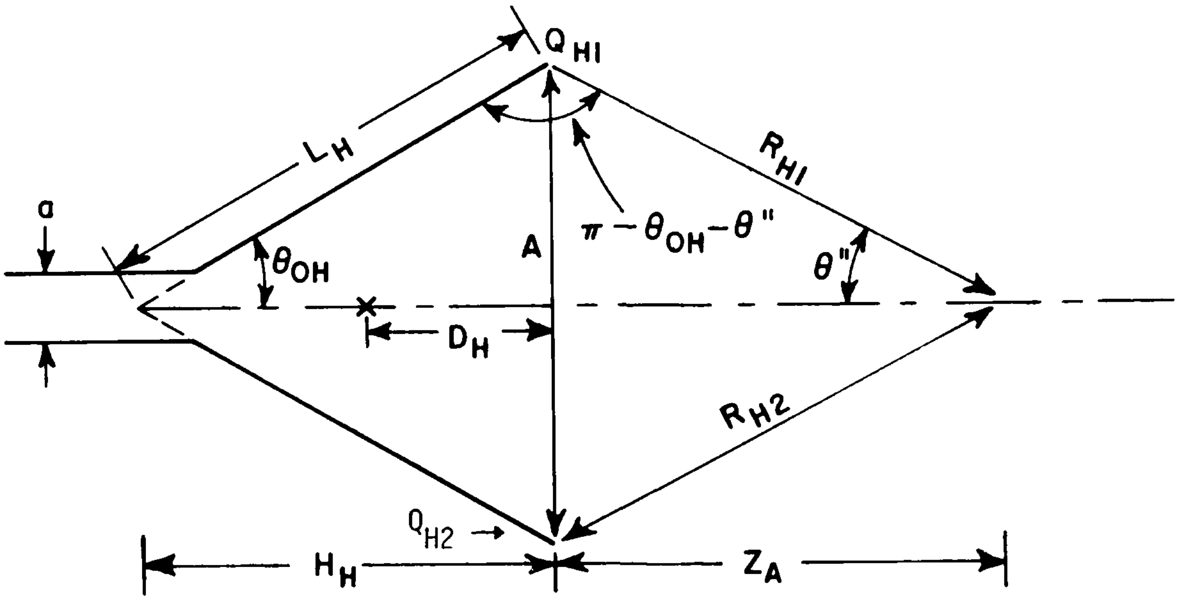

Figure 14. H-plane geometry.

The E-plane apex is chosen as the phase reference point such that the same phase point is used reference for both the E- and H-plane in the calculation. Therefore, in the H-plane, the diffracted field given in Equation (77) should be multiplied by the phase term $e^{jk(H_H-H_E)}$ then the sum of the diffracted fields from the diffraction points Q_{H1} and Q_{H2} in the H-plane becomes

$$H_{DIF} = 2\left(\frac{\pi}{2\theta_{oH}}\right)\frac{e^{-jkL_{HM}}}{jkL_H^{3/2}} \cdot D_{PI}\left(\frac{L_H R_{H1}}{L_H+R_{H1}}, \pi-\theta_{oH}-\theta'', \frac{\pi}{2}, 2\right)\cdot\frac{e^{jkR_{H1}}}{\sqrt{R_{H1}(R_{H1}+L_H)}} \tag{78}$$

where

$$L_{HM} = L_H - (H_H-H_E)\cos\theta_{oH} \quad . \tag{79}$$

Finally, the on axis total field at the observation point is the sum of the geometrical optics and the diffracted fields from the four diffraction points as given by

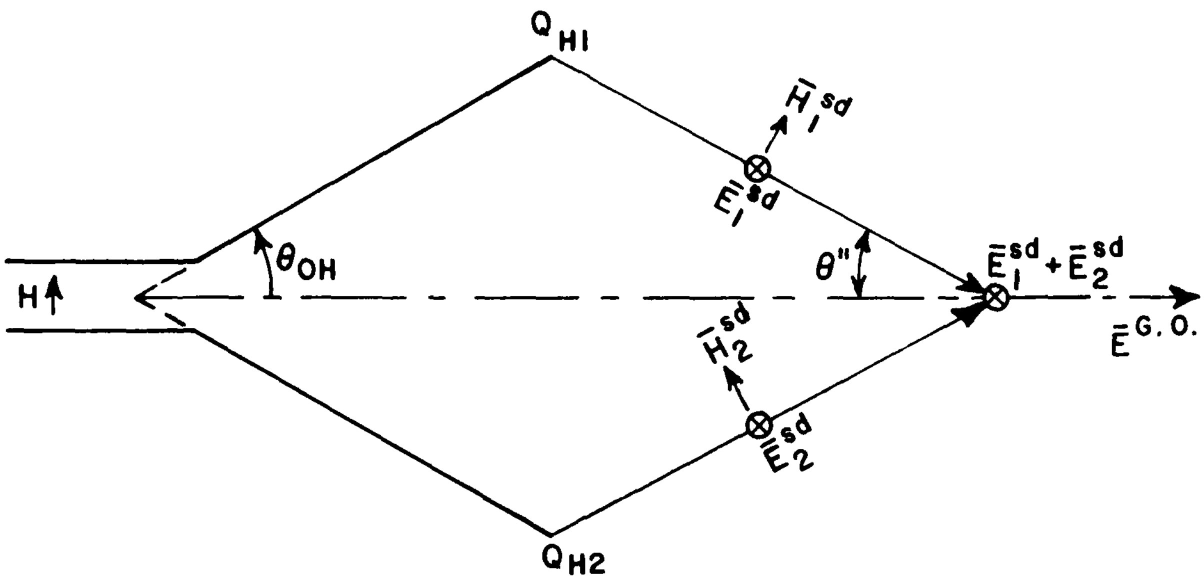

Figure 15. Basic field contributions for the pyramidal horn at the observation point.

$$E^{TOT} = E^{G.O.} + E_{DIF} + H_{DIF}$$

$$= \frac{e^{-jkR_o}}{R_o}\left[1+2D_I\left(\frac{L_E R_{E1}}{L_E+R_{E1}},\ -\pi_{oE}-\theta',\frac{\pi}{2},2\right)\frac{e^{-jkL_E}}{\sqrt{L_E}}\cdot e^{jk(R_o-R_{E1})}\right.$$

$$\cdot\frac{R_o}{\sqrt{R_{E1}(R_{E1}+L_E)}}\cos\theta'+2D_{PI}\left(\frac{L_H R_{H1}}{L_H+R_{H1}},\ \pi-\theta_{oH}-\theta'',\frac{\pi}{2},2\right)$$

$$\left.\cdot\frac{\pi}{2\theta_{oH}}\cdot\frac{e^{-jkL_{HM}}}{jkL_H^{3/2}}\cdot\frac{R_o}{\sqrt{R_{H1}(R_{H1}+L_H)}}\cdot e^{jk(R_o-R_{H1})}\right] \tag{80}$$

However, for small horn dimensions, the normal GTD calculations are not accurate enough. In that case, the accuracy can be improved by using the LSI method for non-corrugated horns and by using API method for corrugated horns which are discussed in Appendix A and B, respectively.

CHAPTER V
AMPLITUDE CENTER FOR ON-AXIS WAVE

The on-axis gain of a horn antenna is not uniquely defined in the near field. In this research the near field gain G(R) is defined through the following equation for the incident power density at points on the horn axis:

$$S^i = \frac{P_T G(R)}{4\pi R^2} \tag{81}$$

where P_T is the transmitted power. Still, the near field gain G(R) depends on how the range R is defined. In most published research the range is defined as that from the horn aperture. Thus the aperture to aperture distance is usually used to define the gains of two horn antennas through the coupling formula

$$\frac{P_R}{P_T} = \left(\frac{\lambda}{4\pi R}\right)^2 G_T(R)\ G_R(R) \tag{82}$$

Then near field corrections [7-11] are applied to determine the far field gain.

A more appropriate way to define the range R is to use the concept of an astigmatic ray tube which is often used in GTD. In an astigmatic ray tube there are two caustics from which the power appears to emanate as shown in Figure 16. A spherical wave is radiated when the two caustics are coincident to form an ordinary focus.

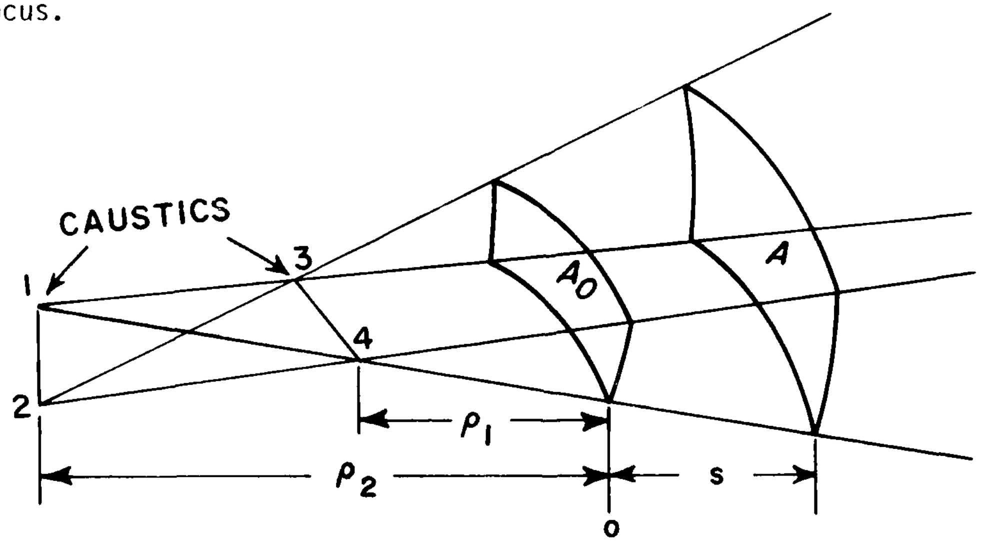

Figure 16. Astigmatic tube of rays.

The on-axis wave of a pyramidal horn can be represented as an astigmatic ray tube in which the E- and H-plane phase centers of the horn form the caustics.

The power spread in an astigmatic ray tube is given by

$$S^i(s) = C_1 \frac{\rho_1\rho_2}{(\rho_1+s)(\rho_2+s)} = \frac{C_2}{R^2} \tag{83}$$

where each distance is shown in Figure 16. For the horn, $\rho_1=D_E$ and $\rho_2=D_H$, the distances of the E- and H-plane phase centers from the aperture. The distance s is measured from the aperture to the observation point. Thus the range R is defined through Equation (83) as

$$R^2 = (s+D_E)(s+D_H) = s^2+(D_E+D_H)S+D_ED_H \tag{84}$$

For distances s large compared to the distances of the phase centers from the aperture,

$$R \approx s + \frac{1}{2}(D_E+D_H) \tag{85}$$

Thus the amplitude center is located half way between the E- and H-plane phase centers, or a distance

$$D = \frac{D_E + D_H}{2} \tag{86}$$

from the horn aperture.

Thus one should first compute the phase centers for the E- and H-planes. The phase center of a horn can be determined from the far field pattern. In our calculation of the E- and H-plane patterns the horn apex was used as our phase reference. Therefore, the far field can be represented by

$$E(\theta) = |F(\theta)|e^{j\phi(\theta)}e^{-jkR_o} \tag{87}$$

where $\phi(\theta)$ is the phase of the calculated pattern and R_o represents the distance from the apex to the observation point as shown in Figure 17. The equivalent line source integration (LSI) method was used to calculate the H-plane phase centers because the slope diffraction method is not as accurate for small horns. For far distances,

$$R_o = R_p + \Delta x \cos\theta \tag{88}$$

where Δx is the distance from the apex to the phase center.

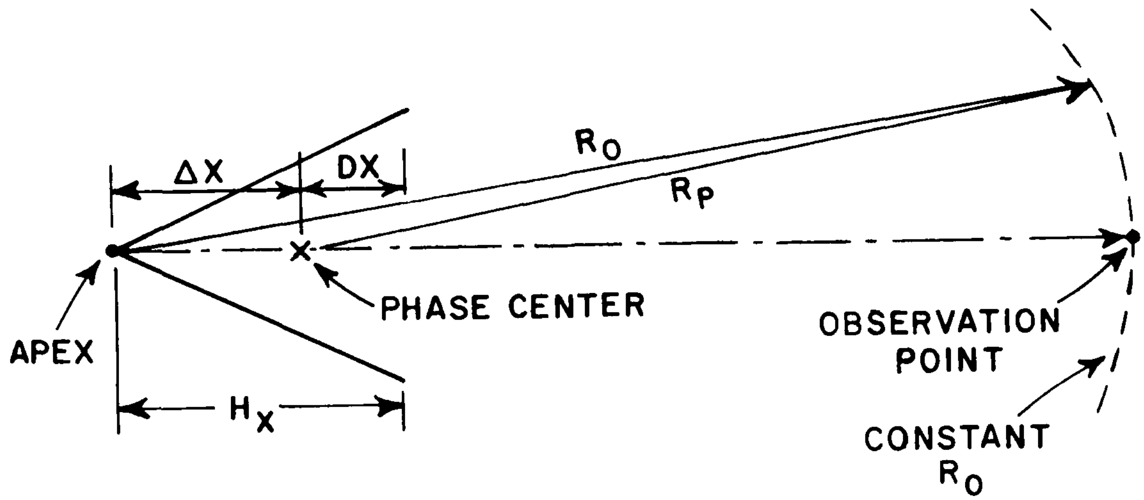

Figure 17. Phase center of the horn.

For small pattern angles the pattern will have no phase variation when referred to the phase center for the on-axis wave. Thus the far field also can be represented by

$$E(\theta) = |F(\theta)|e^{jB}\, e^{-jkR_p} \tag{89}$$

where B is a constant phase and R_p represents the distance from the phase center to the observation point. From Equations (37) and (89), one obtains

$$B = \phi(\theta) - k\Delta x \cos\theta \ . \tag{90}$$

Therefore

$$\Delta x = \frac{\phi(\theta) - \phi(0)}{k(\cos\theta - 1)} \ . \tag{91}$$

In free space medium,

$$k = \frac{2\pi}{\lambda} \tag{92}$$

thus

$$\frac{\Delta x}{\lambda} = \frac{\phi(\theta) - \phi(0)}{2\pi(\cos\theta - 1)} \tag{93}$$

The distance from the aperture to the phase center is given by

$$D_x = H_x - \Delta x \ , \tag{94}$$

where H_x is the distance from the apex to the aperture.

The following examples show the calculation of the E- and H-plane phase centers for the Scientific Atlanta 12-8.2 horn at 10 GHz. The computer listings give the pattern magnitude in dB and the phase in degrees.

Example of determining the phase center of E-plane:

```
WIDTH=    4.801  (LAMBA)
LENGTH=  10.397  (LAMBA)
FREQUENCY=10.000  GHZ
*** E PLANE ***
```

THETA	MAG.	PHASE
-10.00	-5.75060	9.70596
-9.00	-4.74633	7.00847
-8.00	-3.52313	5.53553
-7.00	-2.26580	5.42624
-6.00	-1.09745	6.31997
-5.00	-0.08109	7.76276
-4.00	0.75675	9.37060
-3.00	1.40758	10.86202
-2.00	1.87055	12.04648
-1.00	2.14723	12.80216
0.00	2.23924	13.06105
1.00	2.14723	12.80256
2.00	1.87056	12.04684
3.00	1.40759	10.86237
4.00	0.75675	9.37018
5.00	-0.08109	7.76254
6.00	-1.09744	6.32045
7.00	-2.26580	5.42597
8.00	-3.52313	5.53583
9.00	-4.74633	7.00857
10.00	-5.75059	9.70641

$\phi(1^0) = 12.80256^0$

$\phi(0^0) = 13.06105^0$

$$\Delta x_E = \frac{\phi(1^0)-\phi(0^0)}{360(\cos 1-\cos 0)} = 4.724^{(\lambda)}$$

$\therefore D_E = 10.397-4.724 = 5.67^{(\lambda)}$

Example of determining the phase center of H-plane:

WIDTH= 6.477 (LAMDA)
LENGTH= 10.947 (LAMDA)
FREQUENCY=10.000 GHZ
*** H-PLANE ***

THETA	MAG.	PHASE
-10.00	-5.23606	-11.25019
-9.00	-4.43553	-8.93096
-8.00	-3.63083	-6.81771
-7.00	-2.84653	-4.78290
-6.00	-2.11113	-2.79789
-5.00	-1.45086	-0.90495
-4.00	-0.88683	0.81359
-3.00	-0.43463	2.26580
-2.00	-0.10495	3.36932
-1.00	0.09535	4.05762
0.00	0.16252	4.29179
1.00	0.09535	4.05806
2.00	-0.10495	3.36932
3.00	-0.43463	2.26624
4.00	-0.88683	0.81314
5.00	-1.45086	-0.90494
6.00	-2.11113	-2.79787
7.00	-2.84653	-4.78290
8.00	-3.63083	-6.81724
9.00	-4.43553	-8.93097
10.00	-5.23606	-11.25018

$\phi(1^{o}) = 4.05762^{o}$

$\phi(0^{o}) = 4.29179^{o}$

$$\Delta x_H = \frac{\phi(1^{o})-\phi(0^{o})}{360(\cos 1-\cos 0)} = 4.271^{(\lambda)}$$

$\therefore D_H = 10.947 - 4.271 = 6.68^{(\lambda)}$.

CHAPTER VI
ANALYSIS OF HORN GAIN

The incident power density at the observation point is given by

$$S^i(R) = \frac{|E^{TOT}(R)|^2}{Z_o} \qquad (94)$$

where $E^{TOT}(R)$ is given by Equation (80) and Z_o is the free space intrinsic impedance. From Equations (81) and (94),

$$G(R) = \frac{4\pi R^2}{P_T} \frac{|E^{TOT}(R)|^2}{Z_o} \qquad (95)$$

where G(R) is the near field gain of transmitting horn at a distance R from the amplitude center of the horn. In the coupling analysis the range R is the distance between the amplitude centers of the two horns as shown in Figure 18. Thus the observation point of the transmitting horn is located at the amplitude center of the receiving horn. P_T is the transmitting power which is obtained through the geometric optics field

$$E^{G.O.}(R_o) = \cos\frac{\pi\theta_y}{2\theta_{oy}} \frac{e^{-jkR_o}}{R_o} \qquad (96)$$

and

$$P_T = \int_{-\theta_{ox}}^{\theta_{ox}} \int_{-\theta_{oy}}^{\theta_{oy}} \frac{|E^{G.O.}(R_o)|^2}{Z_o} R_o^2 d\theta_x d\theta_y$$

$$= \int_{-\theta_{ox}}^{\theta_{ox}} \int_{-\theta_{oy}}^{\theta_{oy}} \frac{\cos^2 \frac{\pi\theta_y}{2\theta_{oy}}}{Z_o} d\theta_x d\theta_y$$

$$= \frac{2\theta_{ox}\theta_{oy}}{Z_o} = \frac{AB}{2L_E L_H Z_o} \qquad (97)$$

where R_o is the distance from the apex of one horn as shown in Figure 18. The geometric optics gain is given by

$$G^{G.O.} = \frac{4\pi R_o^2}{P_T} \frac{|E^{G.O.}(R_o)|^2}{Z_o}, \text{ or}$$

$$G^{G.O.} = \frac{8\pi L_E L_H}{AB} \qquad (98)$$

Dividing Equation (95) by Equation (98)

$$\frac{G(R)}{G^{G.O.}} = \left(\frac{R}{R_0}\right)^2 \left| \frac{E^{TOT}(R)}{E^{G.O.}(R_0)} \right|^2 = \left(\frac{R}{R_0}\right)^2 \left| E^{GTD}(R) \right|^2 \tag{99}$$

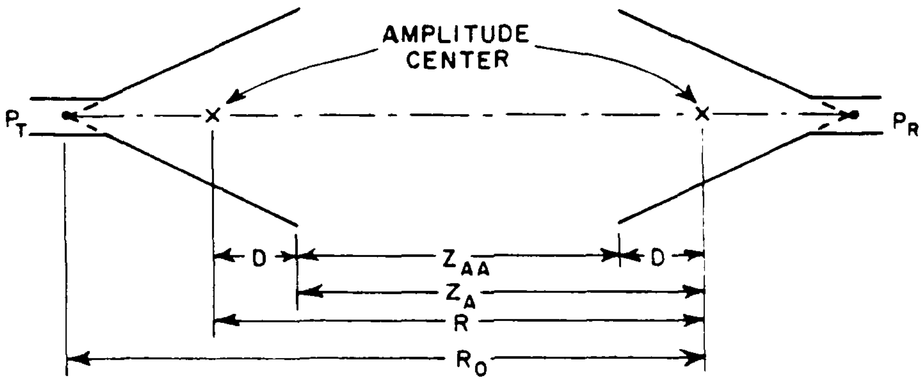

Figure 18. Transmitting and receiving horn antenna geometry.

where $E^{GTD}(R)$ is the on-axis normalized near field and is given by

$$E^{GTD}(R) = 1 + 2D_I\left(\frac{L_E R_{E1}}{L_E + R_{E1}}, \pi - \theta_{oE} - \theta', \frac{\pi}{2}, 2\right) \frac{e^{-jkL_E}}{\sqrt{L_E}} \cdot \frac{R_0}{\sqrt{R_{E1}(R_{E1} + L_E)}} \cdot e^{jk(R_0 - R_{E1})} \cos\theta'$$
$$+ 2D_{PI}\left(\frac{L_H + R_{H1}}{L_H + R_{H1}}, \pi - \theta_{oH} - \theta', \frac{\pi}{2}, 2\right) \frac{\pi}{2\theta_{oH}} \cdot \frac{je^{-jkL_{HM}}}{kL_{LH}^{3/2}} \cdot \frac{R_0}{\sqrt{R_{H1}(R_{H1} + L_H)}} \cdot e^{jk(R_0 - R_{H1})} \tag{100}$$

For far distances, i.e., as R approaches infinity, the far field gain is given by

$$G(\infty) = G^{F.F.} = G^{G.O.} \left| E^{GTD}(\infty) \right|^2 , \quad \text{since } \frac{R}{R_0} \to 1 \tag{101}$$

Then, the gain correction (gain ratio) is given by

$$R_{GAN} = \frac{G(R)}{G^{F.F.}} = \left(\frac{R}{R_0}\right)^2 \left| \frac{E^{GTD}(R)}{E^{GTD}(\infty)} \right|^2 \tag{102}$$

For the convenience of the reader, Tables 2 and 3 give summaries of the variables used in the horn analysis.

Table 2
Summary of Horn Parameters

Parameter	Description	Figure
a	H plane width of the waveguide	14
b	E-plane width of the waveguide	12
A	H plane aperture width of the horn	14
B	E-plane aperture width of the horn	12
L_E	E-plane slant length of the horn (length between Q_{E1} and the E plane apex)	12
L_H	H-plane slant length of the horn (length between Q_{H1} and the H-plane apex)	14
H_E	Horn antenna length in the E-plane (length between the E-plane apex and aperture)	12
H_H	Horn antenna length in the H-plane (length between the H-plane apex and the aperture)	14
θ_{oE}	E-plane half-angle	12
θ_{oH}	H-plane half-angle	14
R_{E1}	Distance between Q_{E1} and the observation point on the axis of horn in the E plane	12
R_{H1}	Distance between Q_{H1} and the observation point on the axis of horn in the H-plane	14
Z_{AA}	Aperture separation	18
Z_A	Distance between the aperture of the transmitting horn and the amplitude center of the receiving horn	18
R	Distance between the amplitude center of each horn	18
R_o	Distance between the apex of the transmitting horn and the amplitude center of the receiving horn	18
D_E	Distance between the aperture and the phase center of the horn in the E-plane	12
D_H	Distance between the aperture and the phase center of the horn in the H-plane	14

Table 3
Summary of Horn Geometry Relationships

1) $$D = \frac{D_E + D_H}{2}$$

2) $$Z_A = Z_{AA} + D$$

3) $$R = Z_{AA} + 2D$$

4) $$R_o = Z_{AA} + D + H_E$$

5) $$R_{E1} = \sqrt{\left(\frac{B}{2}\right)^2 + Z_A^2}$$

6) $$R_{H1} = \sqrt{\left(\frac{A}{2}\right)^2 + Z_A^2}$$

7) $$\theta' = \tan^{-1}\left(\frac{B}{2Z_A}\right)$$

8) $$\theta'' = \tan^{-1}\left(\frac{A}{2Z_A}\right)$$

CHAPTER VII
ON-AXIS COUPLING AND NEAR FIELD CORRECTION

The near field gain of an antenna is often defined through the coupling equation

$$\frac{P_R}{P_T} = \left(\frac{\lambda}{4\pi R}\right)^2 G_T(R)G_R(R) \tag{103a}$$

However, this definition causes the near field gain of each antenna to be dependent on the antenna with which it is measured, especially at close range. We have defined the near field gain through its on-axis power density in Equation (81). This gives a definition which is independent of the other antenna.

However, Equation (103a) is then not exact because the coupling depends on how the two antennas react. Equation (103a) is equivalent to assuming each antenna would radiate a uniform spherical wave from its amplitude center. A more accurate equation for coupling is derived in Appendix C which approximates the near axis fields of each antenna more accurately at close range. The more accurate coupling equation is given by

$$\frac{P_R}{P_T} = \left(\frac{\lambda G(R)}{4\pi R}\right)^2 \frac{1}{\sqrt{1+T_E^2}} \frac{1}{\sqrt{1+T_H^2}} \tag{103b}$$

where $G(R) = \sqrt{G_T(R)G_R(R)}$, $G_T(R)$ and $G_R(R)$ are the near field gains of the transmitting and receiving horns at distance R between the amplitude centers of the horns. The factors $[1+T_{E,H}^2]^{-\frac{1}{2}}$, derived in Appendix C, give more accuracy at close range. From Equation (103b), we get

$$G(R) = \frac{4\pi R}{\lambda} \sqrt{\frac{P_R}{P_T}} \left[(1+T_E^2)(1+T_H^2)\right]^{\frac{1}{4}} \tag{104}$$

From Equation (102) and Equation (104), we get the far-field gain

$$G^{F.F.} = \frac{G(R)}{R_{GAN}} = \frac{4\pi R}{\lambda R_{GAN}} \sqrt{\frac{P_R}{P_T}} \left[(1+T_E^2)(1+T_H^2)\right]^{\frac{1}{4}} \tag{105}$$

Therefore, we can express the far field gain in dB as

$$G_{dB}^{F.F.} = R_{GC} + \frac{1}{2}\left(\frac{P_R}{P_T}\right)_{dB}^{Meas.} \tag{106}$$

where R_{GC} includes the near field gain correction and is given in dB as

$$R_{GC} = 10 \log\left\{\frac{4\pi R}{\lambda R_{GAN}} \left[(1+T_E^2)(1+T_H^2)\right]^{\frac{1}{4}}\right\} \tag{107}$$

and $\left(\frac{P_R}{P_T}\right)_{dB}^{Meas.}$ is the measured coupling in dB.

It is convenient to express the range correction parameter R_{GC} as

$$R_{GC} = R_{GU} + F_C \tag{108}$$

where

$$R_{GU} = 10 \log\left[\frac{4\pi R}{\lambda R_{GAN}}\right] \tag{109}$$

is the basic range correction parameter (assumes wide beams or large separations). The correction factor for narrow beams at close range is given by

$$F_C = 10 \log \left[(1+T_E^2)(1+T_H^2)\right]^{\frac{1}{4}} = 2.5 \log[(1+T_E^2)(1+T_H^2)] \tag{110}$$

where, from Appendix C,

$$T_E = \frac{C_E}{R} \tag{111a}$$

$$C_E = \begin{cases} \frac{2\lambda}{\pi} A_E & \text{for like horns} \\ \frac{\lambda}{\pi} (A_{E1}+A_{E2}) & \text{for different horns} \end{cases} \tag{111b}$$

$$T_H = \frac{C_H}{R} \tag{112a}$$

and

$$C_H = \begin{cases} \frac{2\lambda}{\pi} A_H & \text{for like horns} \\ \frac{\lambda}{\pi} (A_{H1}+A_{H2}) & \text{for different horns} \end{cases} \tag{112b}$$

It is necessary to measure the coupling over a range of aperture separations in order to average out the ripple caused by interactions between the horn structures. For practical purposes, the coupling value used in Equation (106) can be obtained by drawing a smooth curve through the coupling data as shown in Figure 19.

In summary, we can determine the far field gain by the following procedure:

1. Measure the coupling data, P_R/P_T.

2. Compute the range corrected gain parameter R_{GC}.

3. Determine the far field gain from Equation (106).

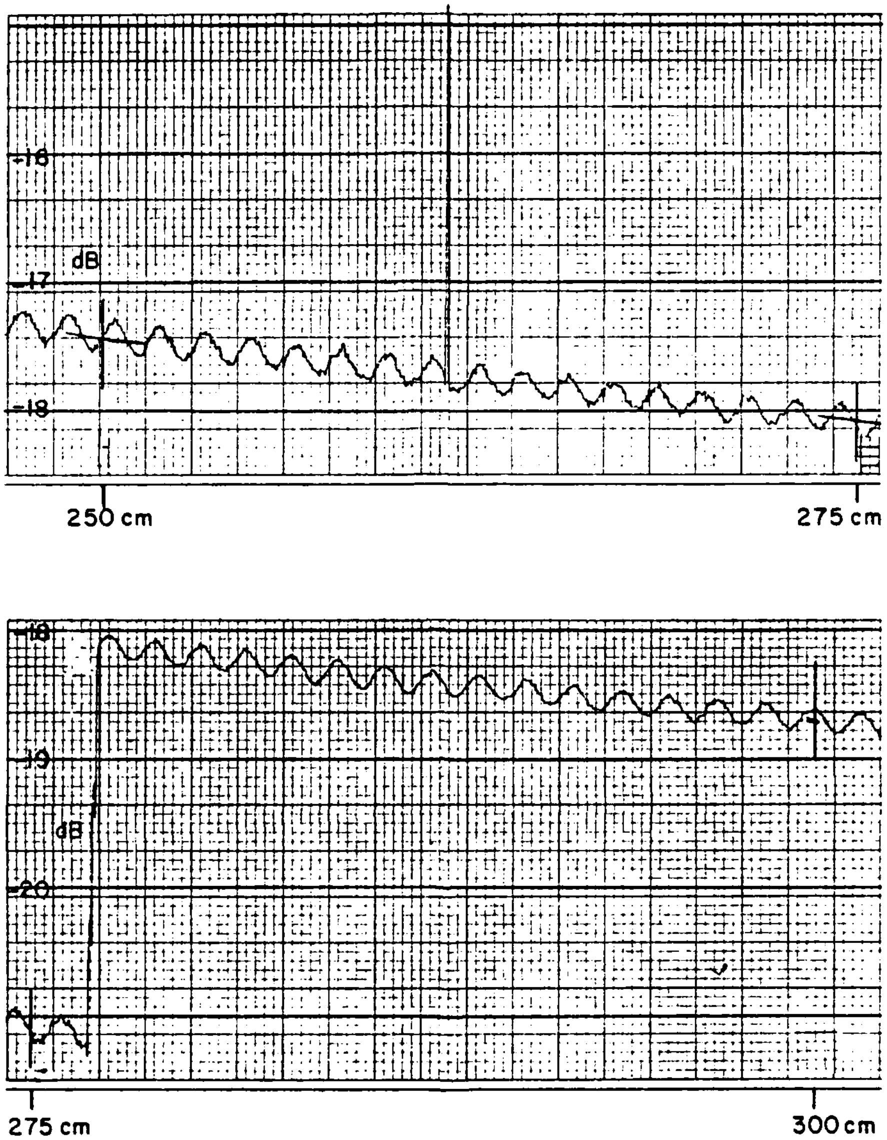

Figure 19. Measured coupling between two SA model 12-8.2 horns at 10 GHz.

CHAPTER VIII
RESULTS AND DISCUSSION

The procedure for determining the far field gain from the near field measurement data of coupling between two horns, using the near field range correction (R_{GC}) data, is presented in this chapter. The measured coupling data used in the examples are based on measurements taken at the Measurement Standards and Microwave Laboratory at Newark Air Force Station. The line source integration (LSI) method is used for conventional standard gain horns and the aperture integration (API) method is used for corrugated horns because they are considered to be more accurate than the basic GTD method.

Figure 20a shows the gain ratio or gain correction (R_{GAN}) curve for the Scientific-Atlanta Model 12-8.2 standard gain horn at 10 GHz. We can see here that the gain correction is small (less than 0.2 dB), because the range is measured between the amplitude centers of each horn. For example, the gain correction is less than 0.01 when the separation (distance between the horn apertures) is 300 cm (100λ at 10 GHz). Figure 20b shows the calculated coupling (P_R/P_T) between two Scientific-Atlanta standard gain horns at 10 GHz. Figure 20c shows the near field range correction of gain (R_{GC}) for two Scientific-Atlanta standard gain horns at 10 GHz. Figures 21 and 22 shows the near field correction and coupling curves for the Narda model 640 and corrugated horns, respectively. Figures 23 and 24 show the far field gain variation with frequency for the Scientific-Atlanta and Narda standard gain horns, respectively, as calculated from Equation (105).

The range correction data are given for 10 GHz in Tables 5 through 9 for both standard gain horns and the corrugated horn. Tables are given for both GTD and LSI for the non-corrugated horns. It is noted that the R_{GC} values for each horn model by GTD and those by LSI (Tables 5 through 8) agree within about 0.1 dB for aperture separations greater than 200 cm. The range correction data for 11 GHz are given in Tables 10 through 12 for both standard gain horns and the corrugated horn. A list of the variables in each column is given below:

ZAA = Aperture separation in cm.
R = Distance between amplitude centers in cm.
RGAN = Ratio of near field gain to far field gain.
PRPT = Calculated coupling.
NFGAIN = G(R) = calculated near field gain.
RGU = Basic range correction parameter.
RGC = Final range correction parameter.

Note that the calculated coupling values PRPT are given only for information purposes. Only the actual measured coupling values should be used with the theoretical range correction parameter RGC to determine the gain.

Procedure for Horns of Same Model

As an example of how to use the near field range correction tables, consider the following case in which the gain is determined from the measured coupling between two Scientific-Atlanta standard gain horns. The measured coupling curve for aperture separations between 250 cm and 300 cm is shown in Figure 19. The ripple caused by interactions between the horns and their mounting structures has a period of about 1.5 cm for each cycle, which corresponds to $\lambda/2$ as expected. The 0.25 dB peak to peak ripple at 250 cm corresponds to a multipath level from horn interactions of about -37 dB below the direct coupling. A -37 dB multipath will cause a ripple maximum of +0.122 dB and a ripple minimum of -0.124 dB with respect to the direct coupling. Consequently the direct coupling can be accurately measured by drawing a smooth curve through the average of the ripple minima and maxima.

The procedure for determining the far field gain is outlined below:

1. The coupling values are sampled at 250, 275 and 300 cm and are recorded in Table 4.

2. Next the theoretical range correction values are read from the appropriate table (Table 5 for SA model 12-8.2 at 10 GHz). These values are recorded in Table 4.

3. The far field gain values are determined for each point from Equation (106) which is repeated below:

$$G^{FF} = R_{GC} + \frac{1}{2} (P_R/P_T)_{dB} \tag{106}$$

TABLE 4
Example of Procedure for Range Correction

Z_{AA} cm	Coupling dB	R_{GC} dB	G^{FF} dB
250	-17.44	30.95	22.23
275	-18.12	31.29	22.23
300	-18.70	31.61	22.26

For example, the coupling at 250 cm is -17.44 dB. The R_{GC} value from Table 5 is 30.95 dB. We set the desired far field gain from Equation (106) as

$$G_{S/A} = 30.95 + \frac{1}{2}(-17.44) = 22.23 \text{ dB.}$$

Note that the spread in gain values in Table 4 is 22.26-22.23=0.03 dB. Thus this coupling measurement indicates an effective gain for the two horns of 22.24 dB.

Procedure for Horns of Different Models

The next example shows how to use the tables to determine the range correction for coupling measured between two horns of different models. Three coupling values should be checked as was done in the previous example. However, only one coupling value is used in this example to illustrate the use of the range correction tables for coupling between horns of different models.

First, the phase center information must be used to calculate the distance between the amplitude centers of the two horns. Referring to Tables 6 and 7,

$$(D_E+D_H)_{S/A} = (16.98+22.55)_{S/A} = 39.53^{(CM)}$$

$$(D_E+D_H)_{NARDA} = (1.09+1.55)_{NARDA} = 2.64^{(CM)}$$

$$(D_E+D_H)_{AVG} = (39.53+2.64)/2 = 21.08^{(CM)}$$

For an aperture separation of Z_{AA} = 150 cm this gives an effective range between horns as

$$R = 150+21.08 = 171.1^{(CM)}$$

We get the near field range correction of gain at R = 171.1^{CM} by interpolating the R_{GU} values from Tables 5 and 7 as follows:

$$(R_{GU})_{S/A} = 28.67 \text{ dB}$$

$$(R_{GU})_{NARDA} = 28.54 \text{ dB}$$

$$(R_{GU})_{AVG} = (28.67+28.54)/2 = 28.60 \text{ dB}$$

Note that the R_{GC} value cannot be directly obtained from the R_{GC} values of the individual horns because the F_c factor in Equation (110) has a non-linear relationship for the two horns. The values of C_E and C_H in Equations (111) and (112) can be calculated by averaging the values for the individual horns as given at the top of Tables 5 and 7. Thus

Horn	C_E cm	C_H cm
S/A	66.39	52.71
Narda	12.41	11.59
Average	39.40	32.15

Since R = 171.1 cm for this example, T_E = 0.230 and T_H = 0.188. The correction factor for close range is calculated from Equation (110) as F_c = 0.094 dB. The final range correction R_{GC} for the S/A to Narda coupling at ZAA = 150 cm is calculated from

$$(R_{GC})_{AVG} = R_{GU} + F_c$$

$$= 28.60 \text{ dB} + 0.09 \text{ dB}$$

$$= 28.69 \text{ dB}.$$

The measured coupling for 150 cm between the Scientific-Atlanta to Narda horns was -18.80 dB. Thus the effective far field gain of the two horns is determined as

$$G^{Meas}_{S/A\text{-}Narda} = (R_{GC})_{AVG} + \frac{1}{2}\left(\frac{P_R}{P_T}\right)_{Meas}$$

$$= 28.69 + \frac{1}{2}(-18.80) = 19.29 \text{ dB}.$$

The results of coupling measurements taken at the Measurements Standards Laboratory at NAFS are summarized in Tables 13 through 17 for 10 GHz and Tables 18 through 22 for 11 GHz. The Scientific Atlanta model 12-8.2 and the Narda model 640 were used along with an experimental corrugated horn (Ladar Systems model CX-20). The procedure for range corrected gain was used to determine the far field gain values for aperture separations Z_{AA} from 100 cm to 320 cm in each table. Tables 13 and 18 show the coupling data, the range correction R_{GC}, and the far field gain when two horns of the same model are measured together at 10 and 11 GHz, respectively. The next three tables in each series shows the results of measuring coupling between horns of different models. In each of these cases the basic range correction parameter R_{GU} is the average of those for the two individual horn models. However, the two R_{GU} values must correspond to the distance R between the amplitude centers of the two orns and not the aperture separation Z_{AA}. The correction factor F_c for narrow beams at close range, as calculated from Equation (I10) is thenused to calculate the final range correction parameter R_{GC}. The measured gain value G_{AVG} represents the mean gain (average in dB) of the two horns. The last table for each frequency summarizes the far field gain values when the three horn models are measured in the six possible combinations.

Referring to Table 17, there are six combinations of measurements, we find they are good agreement except for the corrugated to Narda horns case. There is about 0.23 dB difference between $G^{Meas.}_{Corr-Narda}$ and $(G_{Corr-Narda})_{AVG}$. This difference may be caused by measurement errors. The $(G_{Corr-Narda})_{AVG}$ is the average of individual horn gain measurements from columns 3 and 4; and is gotten as follows

$$Z_{AA} = 150 \text{ cm}$$

$$G_{Corr} = 20.48 \text{ dB}$$

$$G_{Narda} = 16.25 \text{ dB}$$

$$(G_{Corr-Narda})_{AVG} = \frac{G_{Corr}+G_{Narda}}{2} = 18.36 \text{ dB} .$$

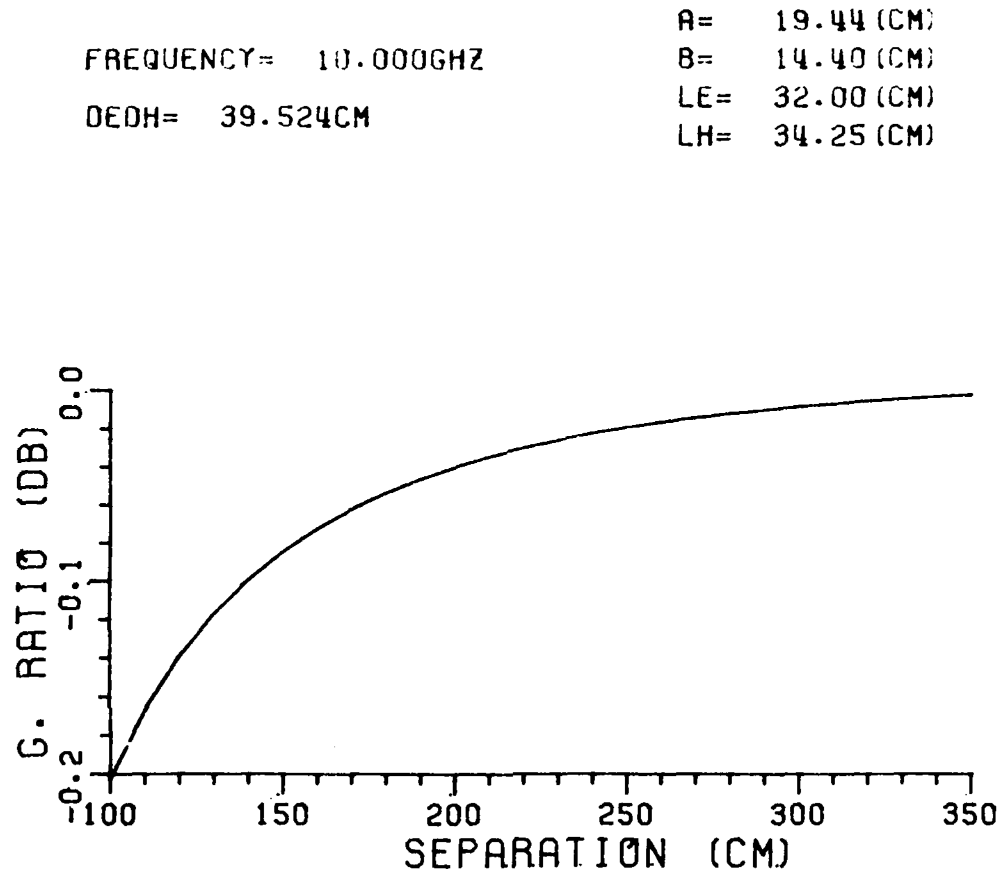

Figure 20a. Gain ratio curve for Scientific-Atlanta standard gain horn at 10 GHz (R_{GAN}).

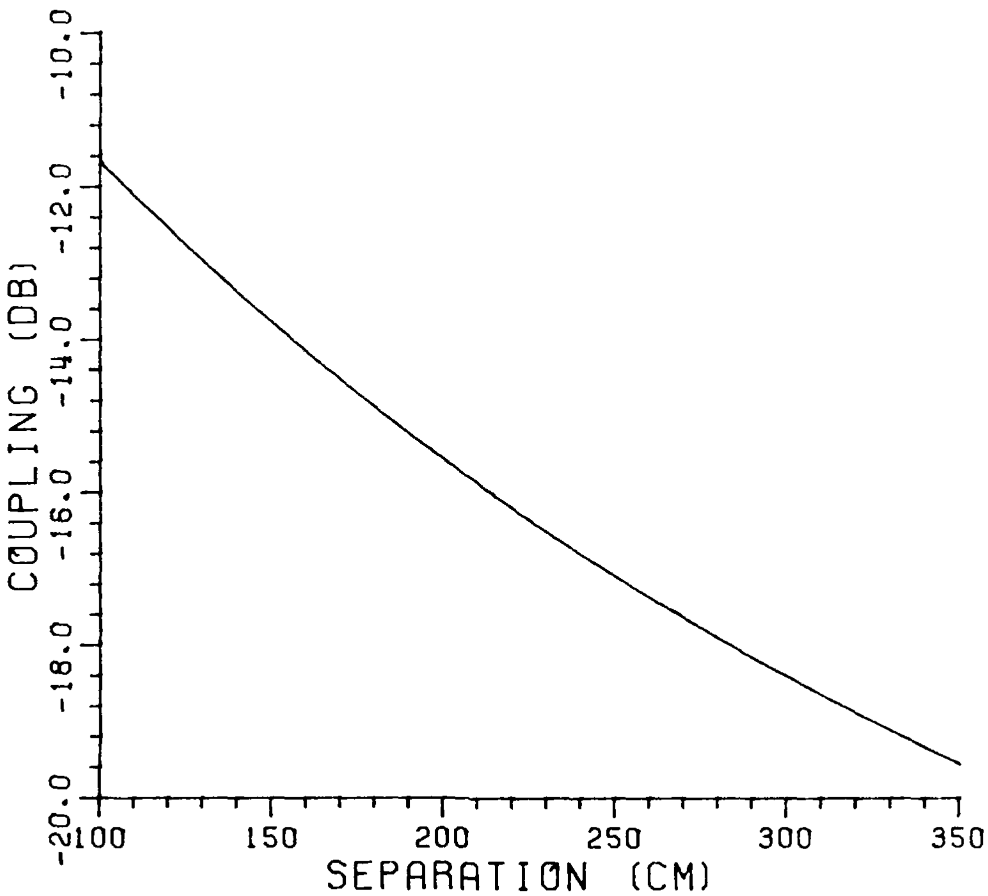

Figure 20b. Coupling between two Scientific-Atlanta standard gain horns at 10 GHz (P_R/P_T).

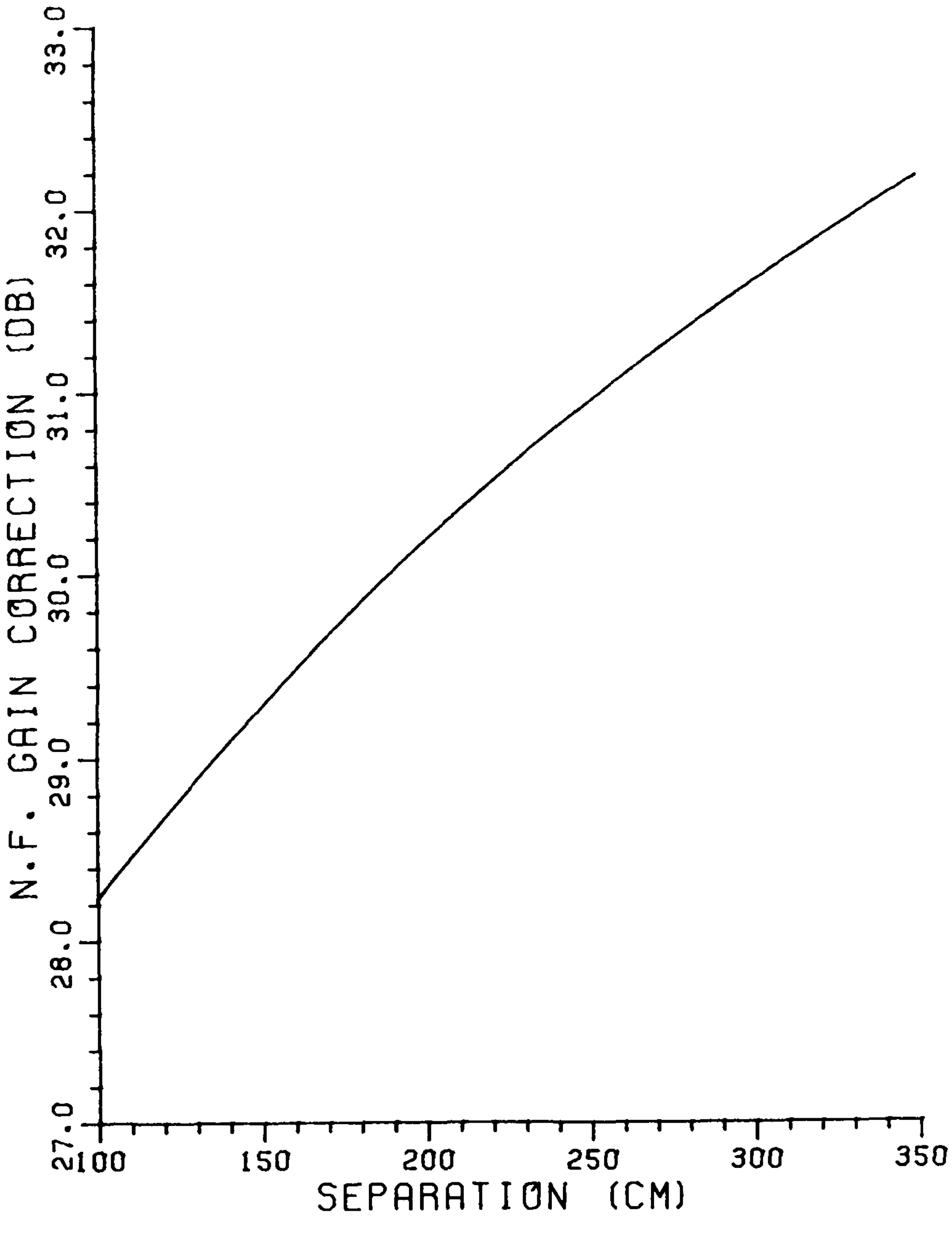

Figure 20c. Near field range correction of gain for two Scientific-Atlanta standard gain horns at 10 GHz (R_{GC}).

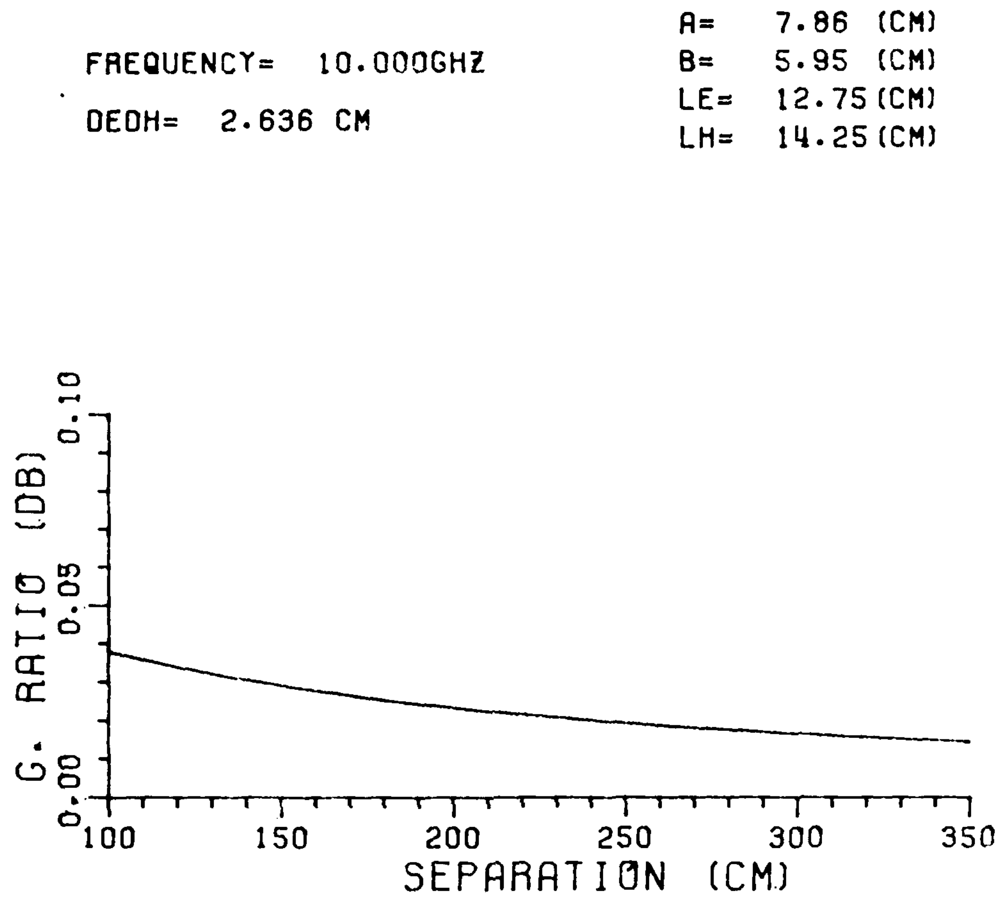

Figure 21a. Gain ratio curve for Narda standard gain horn at 10 GHz (R_{GAN}).

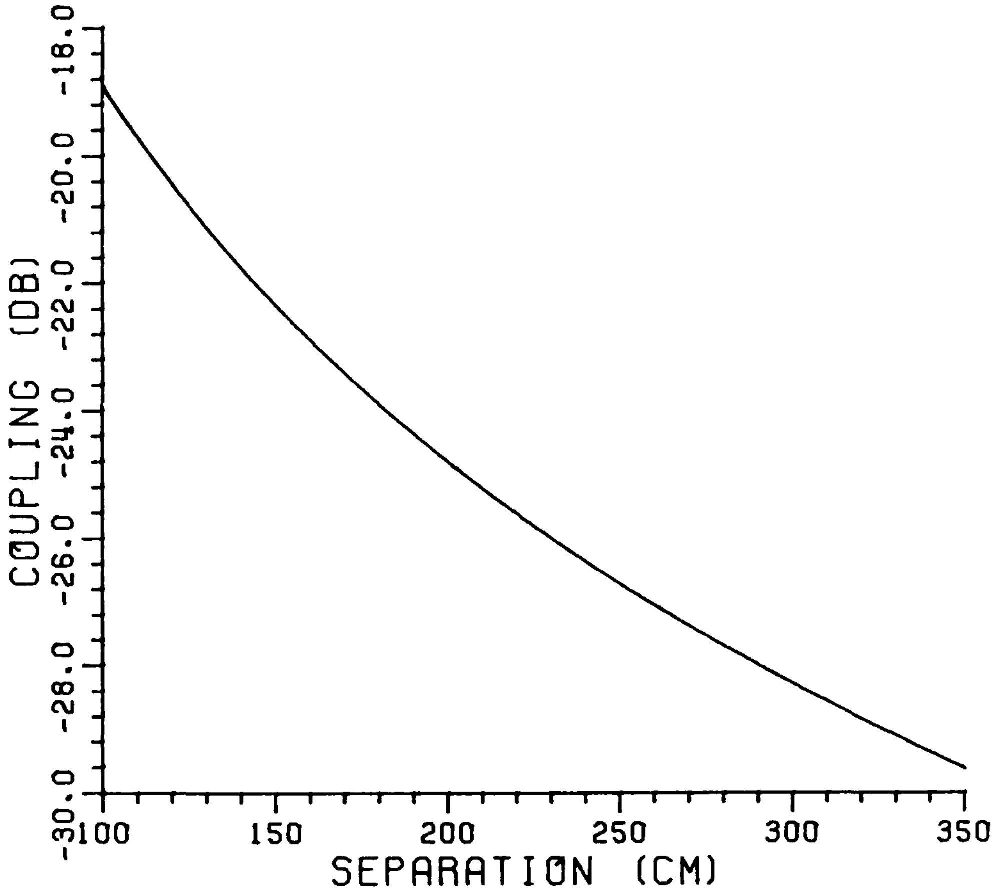

Figure 21b. Coupling between two Narda standard gain horns at 10 GHz (P_R/P_T)

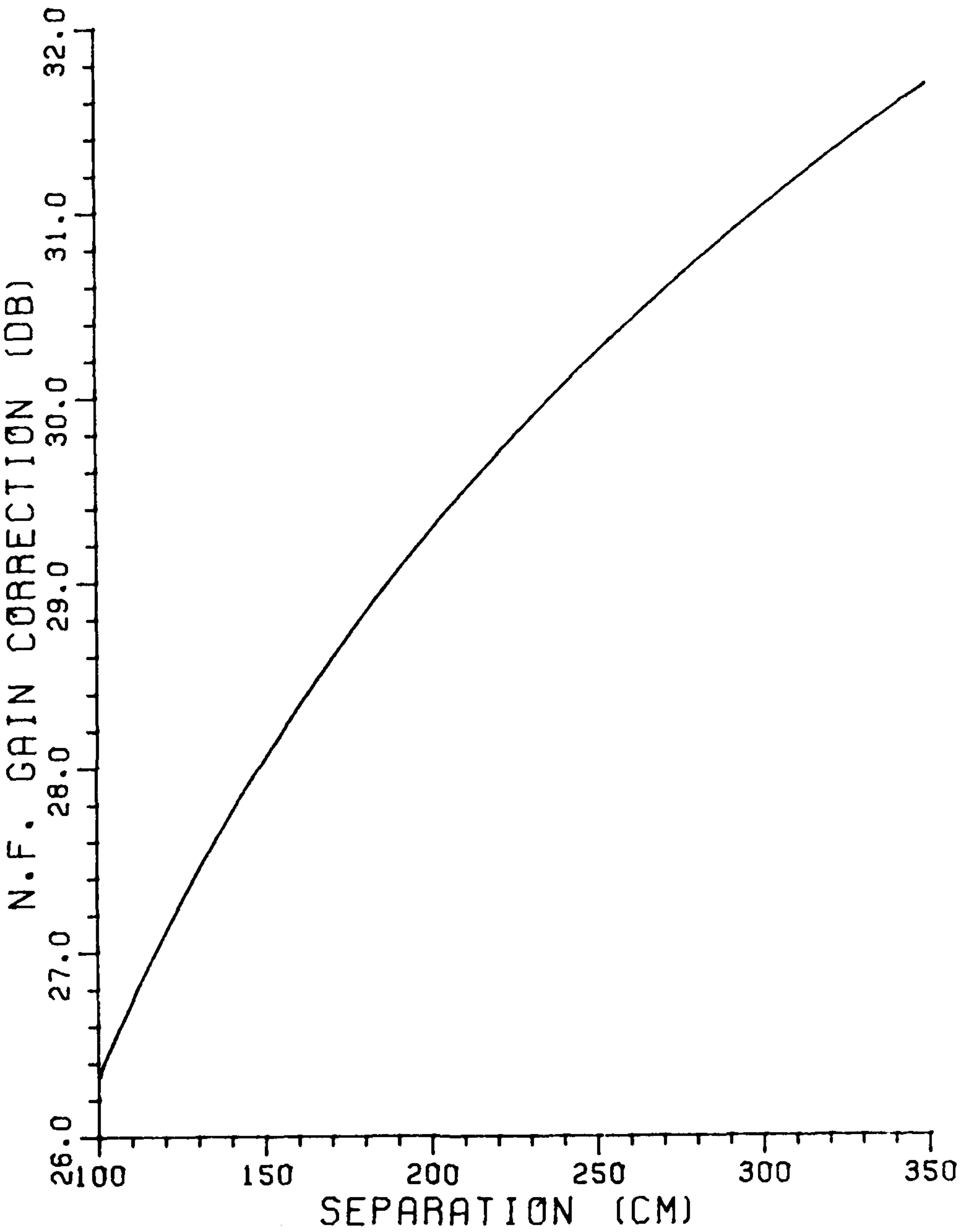

Figure 21c. Near field range correction of gain for two Narda standard gain horns at 10 GHz (R_{GC}).

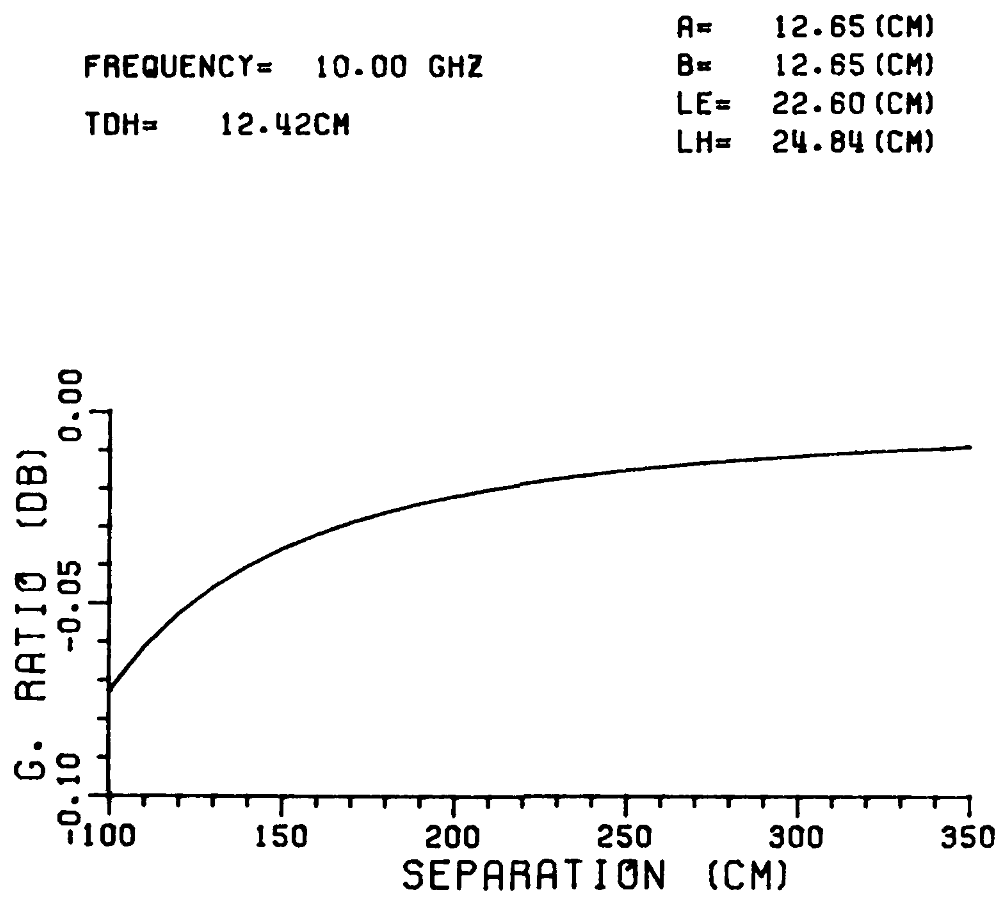

Figure 22a. Gain ratio curve for corrugated horn at 10 GHz (R_{GAN}).

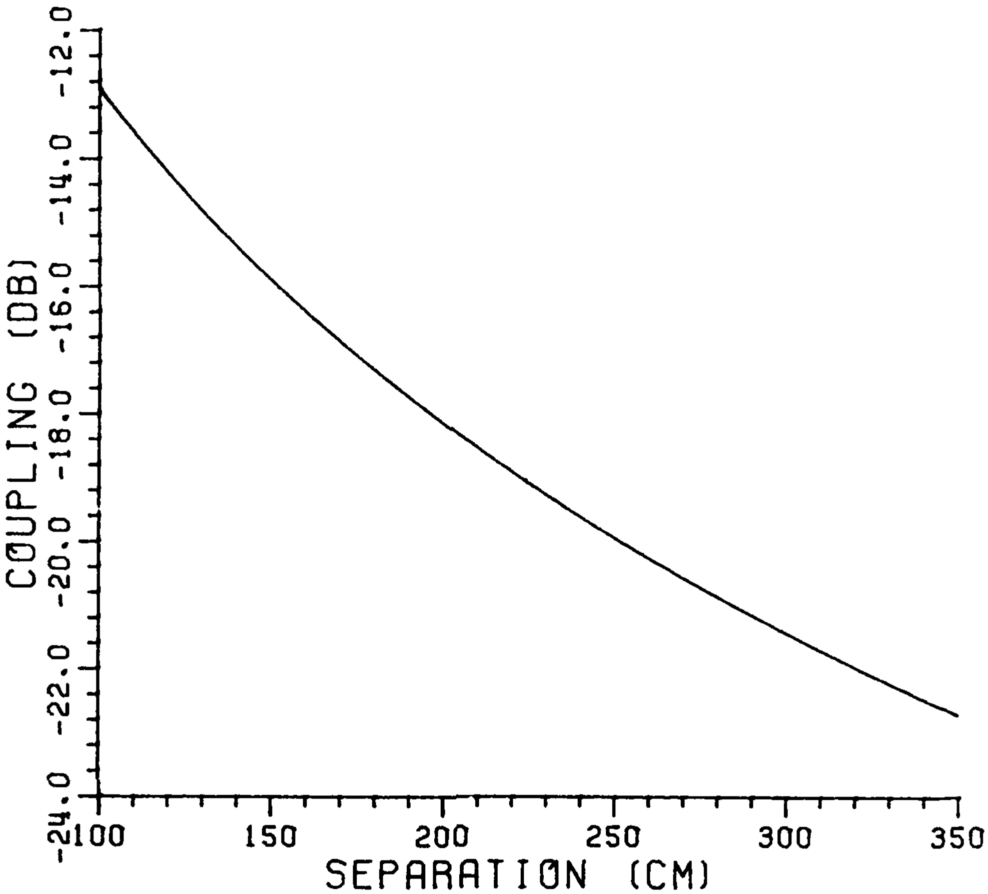

Figure 22b. Coupling between two corrugated horns at 10 GHz (P_R/P_T).

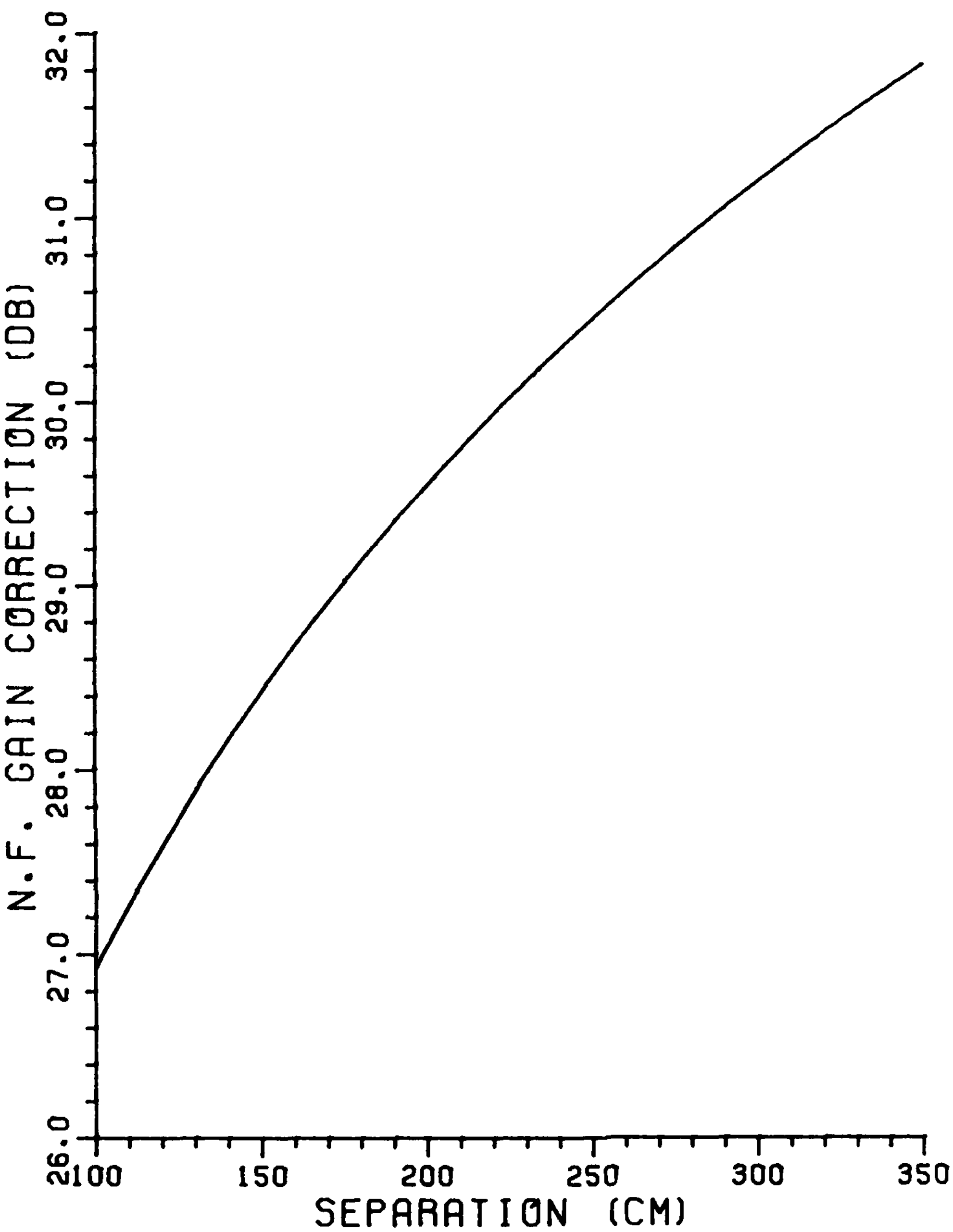

Figure 22c. Near field range correction of gain for two corrugated horns at 10 GHz (R_{GC}).

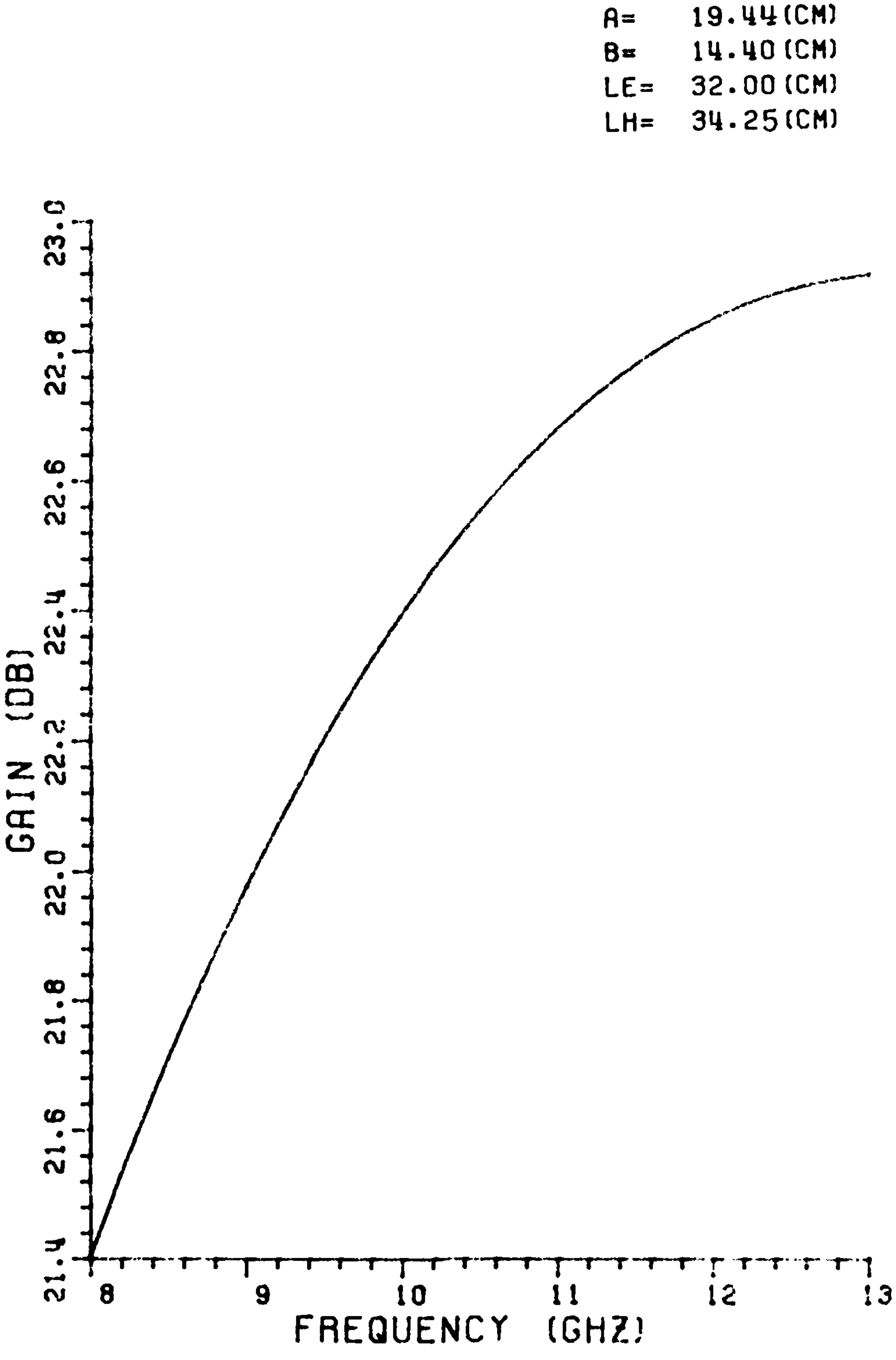

Figure 23. Far field gain vs. frequency curve for Scientific-Atlanta standard gain horn.

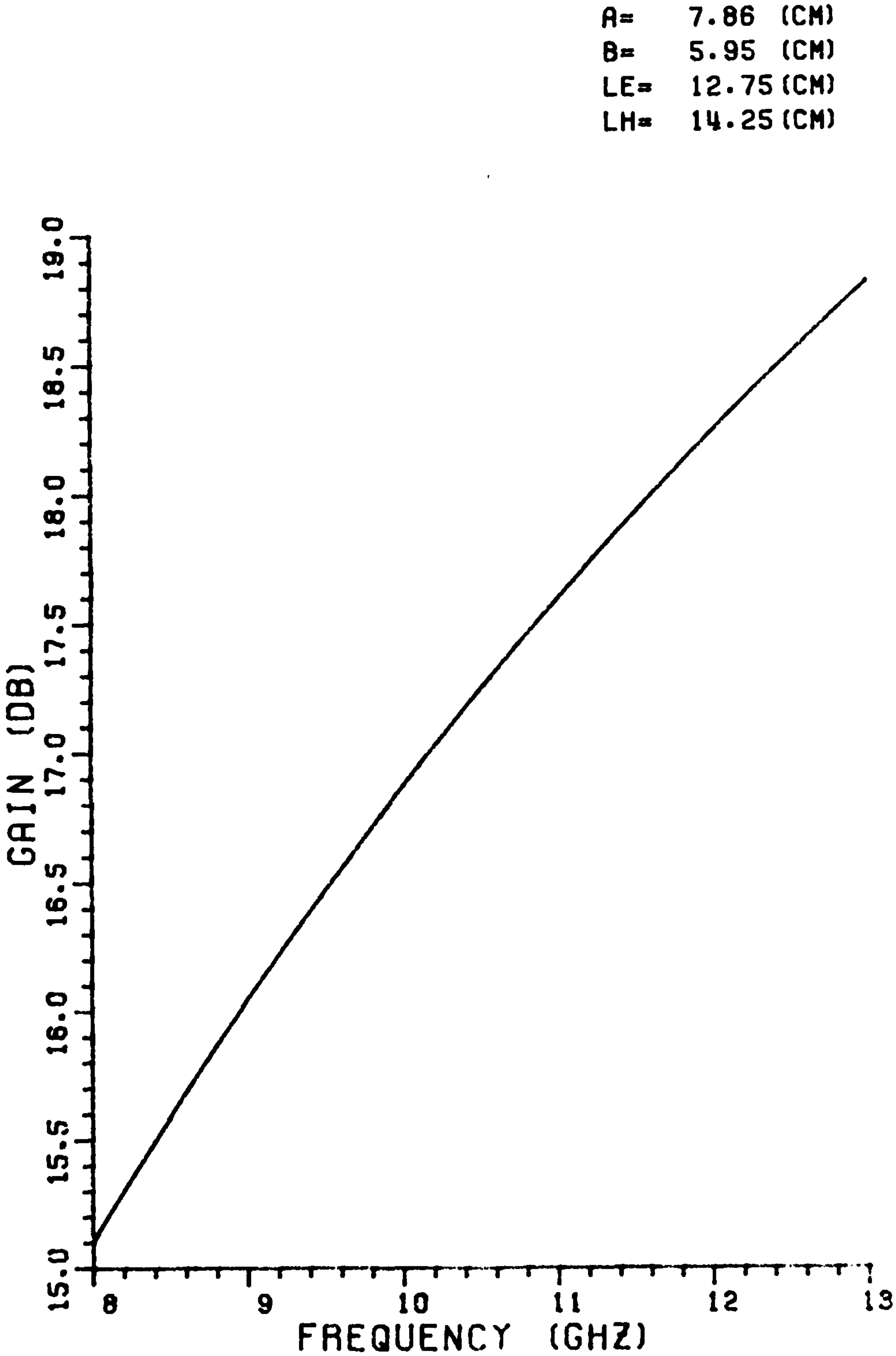

Figure 24. Far field gain vs. frequency curve for Narda standard gain horn.

Table 5: Range correction data for Scientific-Atlanta (model 12-8.2) standard gain horn by LSI method.

*****LSI***** ((FREQUENCY= 10.000 GHZ))
DE= 16.98 CM DH= 22.55 CM CE= 66.39 CM CH= 52.71 CM
B= 14.40 CM(4.8000 LAMDA) A= 19.44 CM(6.4800 LAMDA)
EL= 32.00 CM(10.6667 LAMDA) HL= 34.25 CM(11.4167 LAMDA)
****

ZAA (CM)	R (CM)	RGAN DB	PRPT DB	NFGAIN DB	RGU DB	RGC DB
7558.27	7597.81	0.00000	-45.261	22.397	45.028	45.028
100.00	139.54	-0.20558	-11.685	22.192	27.873	28.240
110.00	149.54	-0.17060	-12.128	22.227	28.139	28.461
120.00	159.54	-0.14298	-12.562	22.254	28.392	28.678
130.00	169.54	-0.12085	-12.984	22.276	28.634	28.889
140.00	179.54	-0.10289	-13.394	22.294	28.865	29.094
150.00	189.54	-0.08814	-13.790	22.309	29.086	29.293
160.00	199.54	-0.07591	-14.174	22.321	29.297	29.484
170.00	209.54	-0.06567	-14.545	22.332	29.499	29.670
180.00	219.54	-0.05704	-14.903	22.340	29.693	29.849
190.00	229.54	-0.04971	-15.250	22.348	29.879	30.022
200.00	239.54	-0.04345	-15.585	22.354	30.058	30.190
210.00	249.54	-0.03805	-15.909	22.359	30.230	30.352
220.00	259.54	-0.03336	-16.223	22.364	30.396	30.509
230.00	269.54	-0.02930	-16.527	22.368	30.556	30.661
240.00	279.54	-0.02579	-16.822	22.372	30.711	30.809
250.00	289.54	-0.02265	-17.109	22.375	30.861	30.952
260.00	299.54	-0.01992	-17.386	22.377	31.005	31.090
270.00	309.54	-0.01753	-17.656	22.380	31.146	31.225
280.00	319.54	-0.01536	-17.918	22.382	31.281	31.356
290.00	329.54	-0.01346	-18.173	22.384	31.413	31.484
300.00	339.54	-0.01175	-18.422	22.386	31.542	31.608
310.00	349.54	-0.01028	-18.663	22.387	31.666	31.729
320.00	359.54	-0.00892	-18.899	22.388	31.787	31.847
330.00	369.54	-0.00769	-19.128	22.390	31.905	31.962
340.00	379.54	-0.00660	-19.352	22.391	32.020	32.073
350.00	389.54	-0.00561	-19.571	22.392	32.132	32.183
360.00	399.54	-0.00474	-19.784	22.393	32.241	32.290
370.00	409.54	-0.00398	-19.993	22.393	32.348	32.394
380.00	419.54	-0.00320	-20.197	22.394	32.452	32.496
390.00	429.54	-0.00248	-20.396	22.395	32.553	32.595
400.00	439.54	-0.00202	-20.591	22.395	32.653	32.693

Table 6: Range correction data for Scientific-Atlanta (model 12-8.2) standard gain horn by GTD method.

*****GTD***** ((FREQUENCY= 10.000 GHZ))

DE= 16.98 CM DH= 20.04 CM CE= 66.39 CM CH= 48.51 CM

B= 14.40 CM(4.8000 LAMDA) A= 19.44 CM(6.4800 LAMDA)

EL= 32.00 CM(10.6667 LAMDA) HL= 34.25 CM(11.4167 LAMDA)

****

ZAA (CM)	R (CM)	RGAN DB	PRPT DB	NFGAIN DB	RGU DB	RGC DB
7558.27	7595.29	0.00000	-45.166	22.443	45.026	45.026
100.00	137.02	-0.43439	-11.874	22.009	28.023	28.380
110.00	147.02	-0.38813	-12.306	22.055	28.283	28.596
120.00	157.02	-0.35004	-12.729	22.093	28.531	28.808
130.00	167.02	-0.31823	-13.141	22.125	28.767	29.014
140.00	177.02	-0.29131	-13.541	22.152	28.992	29.214
150.00	187.02	-0.26830	-13.928	22.175	29.208	29.408
160.00	197.02	-0.24838	-14.303	22.195	29.414	29.595
170.00	207.02	-0.23106	-14.666	22.212	29.612	29.776
180.00	217.02	-0.21581	-15.017	22.228	29.802	29.952
190.00	227.02	-0.20238	-15.356	22.241	29.984	30.122
200.00	237.02	-0.19037	-15.684	22.253	30.159	30.286
210.00	247.02	-0.17965	-16.002	22.264	30.328	30.445
220.00	257.02	-0.16997	-16.310	22.274	30.491	30.599
230.00	267.02	-0.16124	-16.609	22.282	30.648	30.748
240.00	277.02	-0.15335	-16.899	22.290	30.799	30.893
250.00	287.02	-0.14608	-17.180	22.297	30.946	31.033
260.00	297.02	-0.13948	-17.453	22.304	31.088	31.170
270.00	307.02	-0.13342	-17.718	22.310	31.226	31.302
280.00	317.02	-0.12781	-17.976	22.316	31.360	31.431
290.00	327.02	-0.12265	-18.227	22.321	31.489	31.557
300.00	337.02	-0.11785	-18.471	22.326	31.615	31.679
310.00	347.02	-0.11339	-18.709	22.330	31.738	31.798
320.00	357.02	-0.10926	-18.941	22.334	31.857	31.914
330.00	367.02	-0.10541	-19.167	22.338	31.973	32.027
340.00	377.02	-0.10181	-19.388	22.342	32.086	32.137
350.00	387.02	-0.09838	-19.603	22.345	32.197	32.245
360.00	397.02	-0.09525	-19.814	22.348	32.304	32.350
370.00	407.02	-0.09226	-20.019	22.351	32.409	32.453
380.00	417.02	-0.08939	-20.220	22.354	32.512	32.554
390.00	427.02	-0.08675	-20.417	22.357	32.612	32.652
400.00	437.02	-0.08422	-20.609	22.359	32.710	32.748

Table 7: Range correction data for Narda (model 640) standard gain horn by LSI method.

```
      *****LSI*****    ((FREQUENCY=  10.000 GHZ))
DE=  1.08  CM   DH=  1.55  CM   CE= 12.41  CM   CH= 11.59  CM
 B=  5.95  CM(  1.9833  LAMDA)   A=  7.86  CM(  2.6200  LAMDA)
EL= 12.75  CM(  4.2500  LAMDA)  HL= 14.25  CM(  4.7500  LAMDA)
****************************************************************
```

ZAA (CM)	R (CM)	RGAN DB	PRPT DB	NFGAIN DB	RGU DB	RGC DB
1235.59	1238.22	0.00000	-40.556	16.871	37.149	37.149
100.00	102.63	0.03343	-18.917	16.905	26.300	26.330
110.00	112.63	0.03132	-19.719	16.903	26.706	26.730
120.00	122.63	0.02941	-20.454	16.901	27.077	27.098
130.00	132.63	0.02760	-21.132	16.899	27.420	27.437
140.00	142.63	0.02601	-21.762	16.897	27.737	27.752
150.00	152.63	0.02450	-22.350	16.896	28.033	28.046
160.00	162.63	0.02319	-22.900	16.894	28.310	28.321
170.00	172.63	0.02193	-23.419	16.893	28.570	28.580
180.00	182.63	0.02073	-23.908	16.892	28.816	28.825
190.00	192.63	0.01973	-24.371	16.891	29.048	29.057
200.00	202.63	0.01880	-24.811	16.890	29.269	29.277
210.00	212.63	0.01800	-25.230	16.889	29.479	29.486
220.00	222.63	0.01702	-25.629	16.888	29.680	29.686
230.00	232.63	0.01641	-26.011	16.888	29.871	29.877
240.00	242.63	0.01561	-26.378	16.887	30.055	30.060
250.00	252.63	0.01492	-26.729	16.886	30.231	30.236
260.00	262.63	0.01438	-27.066	16.886	30.400	30.404
270.00	272.63	0.01385	-27.391	16.885	30.563	30.567
280.00	282.63	0.01315	-27.705	16.884	30.720	30.724
290.00	292.63	0.01254	-28.008	16.884	30.871	30.875
300.00	302.63	0.01206	-28.300	16.883	31.018	31.021
310.00	312.63	0.01173	-28.583	16.883	31.159	31.163
320.00	322.63	0.01114	-28.857	16.882	31.297	31.300
330.00	332.63	0.01077	-29.123	16.882	31.430	31.433
340.00	342.63	0.01040	-29.380	16.882	31.559	31.561
350.00	352.63	0.01004	-29.631	16.881	31.684	31.687
360.00	362.63	0.00975	-29.874	16.881	31.806	31.808
370.00	372.63	0.00950	-30.110	16.881	31.924	31.926
380.00	382.63	0.00910	-30.341	16.880	32.040	32.042
390.00	392.63	0.00857	-30.566	16.880	32.152	32.154
400.00	402.63	0.00834	-30.785	16.880	32.262	32.263

Table 8: Range correction data for Narda (model 640) standard gain horn by GTD method.

```
    *****GTD*****     ((FREQUENCY=   10.000 GHZ))
DE=  1.08  CM   DH=  7.42  CM   CE= 12.41  CM   CH=  7.18  CM
 B=  5.95  CM(  1.9833  LAMDA)    A=  7.86  CM(  2.6200  LAMDA)
EL= 12.75  CM(  4.2500  LAMDA)  HL= 14.25  CM(  4.7500  LAMDA)
****************************************************************
```

ZAA (CM)	R (CM)	RGAN DB	PRPT DB	NFGAIN DB	RGU DB	RGC DB
1235.59	1244.09	0.00000	-39.671	17.334	37.169	37.170
100.00	108.50	0.36413	-17.791	17.698	26.211	26.230
110.00	118.50	0.33522	-18.609	17.669	26.623	26.639
120.00	128.50	0.31020	-19.358	17.644	27.000	27.013
130.00	138.50	0.28823	-20.049	17.622	27.347	27.359
140.00	148.50	0.26881	-20.691	17.603	27.669	27.679
150.00	158.50	0.25165	-21.289	17.586	27.969	27.978
160.00	168.50	0.23616	-21.849	17.570	28.251	28.258
170.00	178.50	0.22226	-22.376	17.556	28.515	28.522
180.00	188.50	0.20974	-22.873	17.544	28.764	28.770
190.00	198.50	0.19835	-23.343	17.532	29.000	29.006
200.00	208.50	0.18783	-23.790	17.522	29.224	29.229
210.00	218.50	0.17830	-24.215	17.512	29.437	29.442
220.00	228.50	0.16950	-24.621	17.504	29.640	29.644
230.00	238.50	0.16134	-25.009	17.495	29.834	29.838
240.00	248.50	0.15401	-25.379	17.488	30.020	30.024
250.00	258.50	0.14681	-25.736	17.481	30.199	30.202
260.00	268.50	0.14026	-26.078	17.474	30.370	30.373
270.00	278.50	0.13434	-26.407	17.468	30.535	30.538
280.00	288.50	0.12862	-26.725	17.463	30.694	30.696
290.00	298.50	0.12329	-27.031	17.457	30.847	30.850
300.00	308.50	0.11816	-27.327	17.452	30.995	30.998
310.00	318.50	0.11353	-27.613	17.448	31.138	31.141
320.00	328.50	0.10910	-27.890	17.443	31.277	31.279
330.00	338.50	0.10486	-28.159	17.439	31.412	31.414
340.00	348.50	0.10087	-28.420	17.435	31.542	31.544
350.00	358.50	0.09732	-28.672	17.431	31.668	31.670
360.00	368.50	0.09377	-28.918	17.428	31.791	31.793
370.00	378.50	0.09015	-29.158	17.424	31.911	31.913
380.00	388.50	0.08702	-29.390	17.421	32.028	32.029
390.00	398.50	0.08364	-29.618	17.418	32.142	32.143
400.00	408.50	0.08071	-29.839	17.415	32.252	32.253

Table 9: Range correction data for corrugated (model CX-20) horn by API method.

*****API*****   ((FREQUENCY= 10.000 GHZ))

DE= 5.94CM DH= 6.50 CM   CE= 28.46 CM   CH= 27.73 CM

B= 12.65 CM   A= 12.65 CM   EL= 22.60 CM   HL= 24.84 CM

****

ZAA (CM)	R (CM)	RGAN DB	PRPT DB	NFGAIN DB	RGU DB	RGC DB
3200.45	3212.89	0.00000	-41.639	20.470	41.290	41.290
100.00	112.44	-0.07020	-12.923	20.400	26.800	26.932
110.00	122.44	-0.05916	-13.601	20.411	27.159	27.271
120.00	132.44	-0.05058	-14.234	20.420	27.492	27.587
130.00	142.44	-0.04378	-14.827	20.427	27.801	27.884
140.00	152.44	-0.03829	-15.385	20.432	28.090	28.163
150.00	162.44	-0.03379	-15.911	20.437	28.362	28.426
160.00	172.44	-0.03006	-16.408	20.440	28.617	28.674
170.00	182.44	-0.02693	-16.879	20.443	28.859	28.910
180.00	192.44	-0.02428	-17.327	20.446	29.088	29.134
190.00	202.44	-0.02202	-17.754	20.448	29.306	29.347
200.00	212.44	-0.02006	-18.161	20.450	29.513	29.551
210.00	222.44	-0.01836	-18.551	20.452	29.711	29.746
220.00	232.44	-0.01688	-18.924	20.453	29.901	29.932
230.00	242.44	-0.01557	-19.282	20.455	30.083	30.112
240.00	252.44	-0.01442	-19.627	20.456	30.257	30.284
250.00	262.44	-0.01339	-19.958	20.457	30.425	30.449
260.00	272.44	-0.01247	-20.277	20.458	30.586	30.609
270.00	282.44	-0.01165	-20.586	20.459	30.742	30.763
280.00	292.44	-0.01091	-20.884	20.459	30.892	30.912
290.00	302.44	-0.01024	-21.172	20.460	31.038	31.056
300.00	312.44	-0.00963	-21.451	20.461	31.178	31.196
310.00	322.44	-0.00907	-21.721	20.461	31.314	31.331
320.00	332.44	-0.00857	-21.983	20.462	31.447	31.462
330.00	342.44	-0.00811	-22.238	20.462	31.575	31.589
340.00	352.44	-0.00768	-22.486	20.463	31.699	31.713
350.00	362.44	-0.00729	-22.726	20.463	31.821	31.834
360.00	372.44	-0.00693	-22.961	20.463	31.938	31.951
370.00	382.44	-0.00660	-23.189	20.464	32.053	32.065
380.00	392.44	-0.00629	-23.411	20.464	32.165	32.176
390.00	402.44	-0.00600	-23.628	20.464	32.274	32.284
400.00	412.44	-0.00573	-23.840	20.465	32.380	32.390

Table 10: Range correction data for Scientific-Atlanta (model 12-8.2) standard gain horn by LSI method.

```
    *****LSI*****    ((FREQUENCY=  11.000 GHZ))
DE= 20.80  CM   DH= 26.55  LM   CE= 71.32  CM   CH= 52.91  CM
 B= 14.40  CM(  5.2800  LAMDA)   A= 19.44  CM(  7.1280  LAMDA)
EL= 32.00  CM( 11.7333  LAMDA)  HL= 34.25  CM( 12.5583  LAMDA)
****************************************************************
```

ZAA (CM)	R (CM)	RGAN DB	PRPT DB	NFGAIN DB	RGU DB	RGC DB
8314.10	8361.45	0.00000	-46.354	22.681	45.858	45.858
100.00	147.35	-0.24572	-12.486	22.435	28.564	28.924
110.00	157.35	-0.20647	-12.896	22.475	28.810	29.129
120.00	167.35	-0.17514	-13.300	22.506	29.046	29.331
130.00	177.35	-0.14976	-13.694	22.531	29.273	29.528
140.00	187.35	-0.12898	-14.079	22.552	29.490	29.721
150.00	197.35	-0.11175	-14.453	22.569	29.699	29.908
160.00	207.35	-0.09735	-14.816	22.584	29.899	30.089
170.00	217.35	-0.08519	-15.168	22.596	30.092	30.265
180.00	227.35	-0.07489	-15.510	22.606	30.277	30.436
190.00	237.35	-0.06606	-15.841	22.615	30.455	30.601
200.00	247.35	-0.05844	-16.161	22.623	30.626	30.762
210.00	257.35	-0.05188	-16.472	22.629	30.792	30.917
220.00	267.35	-0.04613	-16.774	22.635	30.952	31.068
230.00	277.35	-0.04113	-17.067	22.640	31.106	31.215
240.00	287.35	-0.03669	-17.351	22.644	31.256	31.357
250.00	297.35	-0.03282	-17.628	22.648	31.400	31.495
260.00	307.35	-0.02941	-17.896	22.652	31.541	31.629
270.00	317.35	-0.02633	-18.158	22.655	31.677	31.760
280.00	327.35	-0.02362	-18.412	22.657	31.809	31.887
290.00	337.35	-0.02115	-18.659	22.660	31.937	32.011
300.00	347.35	-0.01898	-18.900	22.662	32.061	32.131
310.00	357.35	-0.01701	-19.135	22.664	32.183	32.249
320.00	367.35	-0.01526	-19.365	22.666	32.301	32.363
330.00	377.35	-0.01369	-19.588	22.667	32.416	32.475
340.00	387.35	-0.01229	-19.807	22.669	32.528	32.584
350.00	397.35	-0.01100	-20.020	22.670	32.638	32.691
360.00	407.35	-0.00977	-20.228	22.671	32.744	32.795
370.00	417.35	-0.00867	-20.432	22.672	32.848	32.897
380.00	427.35	-0.00775	-20.632	22.673	32.950	32.997
390.00	437.35	-0.00683	-20.826	22.674	33.050	33.094
400.00	447.35	-0.00596	-21.017	22.675	33.147	33.190

Table 11: Range correction data for Narda (model 640) standard gain horn by LSI method.

*****LSI*****   ((FREQUENCY= 11.000 GHZ))

DE= 1.34 CM DH= 1.88 CM CE= 13.56 CM CH= 12.63 CM

B= 5.95 CM(2.1817 LAMDA) A= 7.86 CM(2.8820 LAMDA)

EL= 12.75 CM(4.6750 LAMDA) HL= 14.25 CM(5.2250 LAMDA)

****

ZAA (CM)	R (CM)	RGAN DB	PRPT DB	NFGAIN DB	RGU DB	RGC DB
1359.15	1362.37	0.00000	-40.758	17.599	37.978	37.978
100.00	103.22	0.03289	-18.350	17.632	26.740	26.774
110.00	113.22	0.03103	-19.146	17.630	27.143	27.172
120.00	123.22	0.02930	-19.875	17.628	27.512	27.537
130.00	133.22	0.02772	-20.549	17.627	27.853	27.874
140.00	143.22	0.02611	-21.176	17.625	28.169	28.187
150.00	153.22	0.02471	-21.760	17.624	28.463	28.479
160.00	163.22	0.02347	-22.308	17.622	28.739	28.753
170.00	173.22	0.02231	-22.824	17.621	28.998	29.011
180.00	183.22	0.02125	-23.311	17.620	29.243	29.254
190.00	193.22	0.02024	-23.772	17.619	29.475	29.485
200.00	203.22	0.01930	-24.210	17.618	29.695	29.704
210.00	213.22	0.01840	-24.628	17.617	29.905	29.913
220.00	223.22	0.01765	-25.026	17.617	30.104	30.112
230.00	233.22	0.01678	-25.407	17.616	30.296	30.303
240.00	243.22	0.01606	-25.772	17.615	30.479	30.485
250.00	253.22	0.01539	-26.122	17.614	30.654	30.660
260.00	263.22	0.01464	-26.459	17.614	30.823	30.829
270.00	273.22	0.01404	-26.784	17.613	30.986	30.991
280.00	283.22	0.01365	-27.096	17.613	31.142	31.147
290.00	293.22	0.01311	-27.398	17.612	31.294	31.298
300.00	303.22	0.01266	-27.690	17.612	31.440	31.444
310.00	313.22	0.01212	-27.972	17.611	31.581	31.585
320.00	323.22	0.01172	-28.245	17.611	31.718	31.722
330.00	333.22	0.01130	-28.510	17.610	31.851	31.854
340.00	343.22	0.01086	-28.768	17.610	31.980	31.983
350.00	353.22	0.01023	-29.018	17.609	32.105	32.108
360.00	363.22	0.01002	-29.261	17.609	32.226	32.229
370.00	373.22	0.00965	-29.497	17.609	32.345	32.347
380.00	383.22	0.00912	-29.727	17.608	32.460	32.463
390.00	393.22	0.00886	-29.951	17.608	32.572	32.575
400.00	403.22	0.00887	-30.169	17.608	32.681	32.684

Table 12: Range correction data for corrugated (model CX20) horn by API method.

```
*****API*****    ((FREQUENCY=  11.000 GHZ))
DE=  7.15CM  DH=  7.81 CM   CE= 30.60 CM   CH= 29.65 CM
B= 12.65 CM   A= 12.65 CM   EL= 22.60 CM   HL= 24.84 CM
**************************************************************
```

ZAA (CM)	R (CM)	RGAN DB	PRPT DB	NFGAIN DB	RGU DB	RGC DB
3520.49	3535.45	0.00000	-42.142	21.048	42.119	42.119
100.00	114.96	-0.08356	-12.840	20.965	27.324	27.468
110.00	124.96	-0.07056	-13.495	20.978	27.673	27.796
120.00	134.96	-0.06042	-14.109	20.988	27.997	28.103
130.00	144.96	-0.05235	-14.686	20.996	28.300	28.391
140.00	154.96	-0.04584	-15.230	21.002	28.583	28.663
150.00	164.96	-0.04049	-15.744	21.008	28.849	28.920
160.00	174.96	-0.03604	-16.231	21.012	29.100	29.164
170.00	184.96	-0.03231	-16.693	21.016	29.338	29.395
180.00	194.96	-0.02914	-17.133	21.019	29.563	29.615
190.00	204.96	-0.02643	-17.552	21.022	29.778	29.824
200.00	214.96	-0.02408	-17.953	21.024	29.982	30.025
210.00	224.96	-0.02205	-18.337	21.026	30.178	30.216
220.00	234.96	-0.02027	-18.704	21.028	30.365	30.400
230.00	244.96	-0.01870	-19.058	21.029	30.544	30.577
240.00	254.96	-0.01732	-19.397	21.031	30.717	30.747
250.00	264.96	-0.01609	-19.725	21.032	30.883	30.911
260.00	274.96	-0.01498	-20.040	21.033	31.042	31.068
270.00	284.96	-0.01400	-20.345	21.034	31.197	31.221
280.00	294.96	-0.01310	-20.640	21.035	31.346	31.368
290.00	304.96	-0.01230	-20.925	21.036	31.490	31.511
300.00	314.96	-0.01157	-21.201	21.037	31.629	31.649
310.00	324.96	-0.01091	-21.469	21.037	31.764	31.783
320.00	334.96	-0.01029	-21.729	21.038	31.895	31.913
330.00	344.96	-0.00974	-21.981	21.038	32.022	32.039
340.00	354.96	-0.00922	-22.226	21.039	32.146	32.161
350.00	364.96	-0.00876	-22.465	21.039	32.266	32.281
360.00	374.96	-0.00833	-22.697	21.040	32.383	32.397
370.00	384.96	-0.00793	-22.924	21.040	32.497	32.510
380.00	394.96	-0.00755	-23.145	21.041	32.608	32.620
390.00	404.96	-0.00721	-23.360	21.041	32.716	32.728
400.00	414.96	-0.00689	-23.570	21.041	32.822	32.833

Table 13: Range corrected gain measurements.

Frequency : 10 GHz									
	NARDA (Model 640) CE=12.41 cm, CH=11.59 cm			CORR. (Model CX-20) CE=28.46 cm, CH=27.73 cm			S/A (Model 12-8.2) CE=66.39 cm, CH=52.71 cm		
Z_{AA} / cm	R_{GC} (dB)	Coupl. (dB)	Gain (dB)	R_{GC} (dB)	Coupl. (dB)	Gain (dB)	R_{GC} (dB)	Coupl. (dB)	Gain (dB)
100	26.33	-20.16	16.25	26.93	-12.85	20.51	28.24	-11.96	22.26
150	28.05	-23.60	16.25	28.43	-15.90	20.48	29.29	-14.08	22.25
200	29.28	-26.06	16.25	29.55	-18.15	20.48	30.19	-15.88	22.25
250	30.24	-28.00	16.24	30.45	-19.92	20.49	30.95	-17.44	22.23
300	31.02	-29.52	16.26	31.20	-21.40	20.50	31.61	-18.70	22.26
320	31.20	-30.10	16.25	31.46	-21.98	20.47	31.85	-19.18	22.26
Meas. Date	7-19-1979			8-6-1979			7-19-1979		
Xmtr.	Narda #06137			Corrugated #41			S/A #1221		
Revr.	Narda #07057			Corrugated #42			S/A #1222		

* Measured Coupling Data from NAFS.

Table 14: Range corrected gain measurements

Frequency = 10 GHz			CE=39.39 cm, CH=32.15 cm					
			R_{GU}					
Z_{AA} (cm)	Meas. Coupling (dB)	R (cm)	S/A (dB)	Narda (dB)	AVG (dB)	F_C	R_{GC}	G_{AVG}^{Meas}
100	-16.10	121.1	27.36	27.03	27.20	0.18	27.38	19.33
150	-18.80	171.1	28.67	28.54	28.61	0.09	28.70	19.30
200	-20.92	221.1	29.72	29.66	29.69	0.06	29.75	19.29
250	-22.60	271.1	30.58	30.54	30.56	0.04	30.60	19.30
300	-24.06	321.1	31.30	31.28	31.29	0.03	31.32	19.29
320	-24.60	341.1	31.56	31.54	31.55	0.02	31.57	19.27

1. Transmitter: S/A (12-8.2) #1221: Receiver: Narda (640) #06137
2. $R = Z_{AA} + (D_E+D_H)_{AVG}$
3. $(D_E+D_H)_{AVG} = \left[(D_E+D_H)_{S/A} + (D_E+D_H)_{Narda}\right]/2 = 21.1$ cm
4. Measurement at NAFS on 17 July, 1979

Table 15: Range corrected gain measurements.

Frequency = 10 GHz   CE=47.42 cm;   CH=40.22 cm

Z_{AA} (cm)	Meas. Coupling (dB)	R (cm)	R_{GU} Corr (dB)	R_{GU} S/A (dB)	R_{GU} AVG (dB)	F_c	R_{GC}	G_{AVG}^{Meas}
100	-12.50	126.0	27.28	27.50	27.39	0.25	27.64	21.39
150	-15.00	176.0	28.70	28.73	28.72	0.13	28.85	21.35
200	-17.00	226.0	29.77	29.81	29.79	0.08	29.87	31.37
250	-18.65	276.0	30.64	30.65	30.65	0.05	30.70	21.37
300	-20.05	326.0	31.36	31.36	31.36	0.04	31.40	21.38
320	-20.56	346.0	31.62	31.61	31.62	0.03	31.65	21.37

1. Transmitter: Corr (CX20) #41;   Receiver: S/A (12-8.2) #1221
2. $R = Z_{AA} + (D_E+D_H)_{AVG}$
3. $(D_E+D_H)_{AVG} = \left[(D_E+D_H)_{Corr.} + (D_E+D_H)_{S/A}\right]/2 = 26$ cm
4. Measurement at NAFS on 7 August, 1979

Table 16: Range corrected gain measurements

Frequency = 10 GHz   CE=20.44 cm,   CH=19.66 cm

Z_{AA} (cm)	Meas. Coupling (dB)	R (cm)	P_{GU} Corr (dB)	P_{GU} Narda (dB)	P_{GU} AVG (dB)	F_c	R_{GC}	G_{AVG}^{Meas}
100	-17.00	107.5	26.61	26.50	26.56	0.07	26.63	18.13
150	-20.20	157.5	28.23	28.17	28.20	0.03	28.23	18.13
200	-22.56	207.5	29.41	29.37	29.39	0.02	29.41	18.13
250	-24.42	257.5	30.34	30.31	30.33	0.01	30.34	18.13
300	-25.95	307.5	31.11	31.09	31.10	0.01	31.11	18.14
320	-26.50	327.5	31.38	31.36	31.37	0.01	31.38	18.13

1. Transmitter: Corr (CX20) #41; Receiver: Narda (640) #06137
2. $R = Z_{AA} + (D_E+D_H)_{AVG}$
3. $(D_E+D_H)_{AVG} = \left[(D_E+D_H)_{Corr} + (D_E+D_H)_{Narda}\right]/2 = 7.5$ cm
4. Measurement at NAFS on 7 August, 1979

Table 17: Summary of range corrected gain measurements

Frequency = 10 GHz									
				$G_{S/A}$-Narda		$G_{Corr.}$-S/A		$G_{corr.}$-Narda	
Z_{AA} (cm)	$G_{S/A}$ (dB)	G_{Narda} (dB)q	$G_{Corr.}$ (dB)	Meas. (dB)	Avg. (dB)	Meas. (dB)	Avg. (dB)	Meas. (dB)	Avg. (dB)
100	22.26	16.25	20.51	19.33	19.26	21.39	21.39	18.13	18.38
150	22.25	16.25	20.48	19.30	19.25	21.35	21.37	18.13	18.36
200	22.25	16.25	20.48	19.29	19.25	21.37	21.37	18.13	18.36
250	22.23	16.24	20.49	19.30	19.24	21.37	21.36	18.13	18.36
300	22.26	16.26	20.50	19.29	19.26	21.38	21.38	18.14	18.38
320	22.26	16.25	20.47	19.27	19.26	21.37	21.37	18.13	18.36
Meas. Date	7-19-79	7-19-79	8-6-79	7-17-79		8-7-79		8-7-79	
Xmtr.	S/A#1221	Narda #06137	Corr. #41	S/A #1221		Corr. #41		Corr. #41	
Rcvr.	S/A#1222	Narda #07057	Corr. #42	Narda #06137		S/A #1221		Narda #06137	

*Measurement data from NAFS

**$(G_{x,y})_{AVG} = (G_x + G_y)/2$ Avg. of individual horn meas.

Table 18: Range corrected gain measurements

Frequency = 11 GHz									
	Narda (Model 640) CE=13.56cm, CH=12.63 cm			Corr. (Model CZ-20) CE=30.60 cm, CH=29.65 cm			S/A (Model 12-8.2) CE=71.32 cm, CH=52.91 cm		
Z_{AA} (cm)	R_{GC} (dB)	Coupl. (dB)	Gain (dB)	R_{GC} (dB)	Coupl. (dB)	Gain (dB)	R_{GC} (dB)	Coupl. (dB)	Gain (dB)
100	26.77	-19.80	16.87	27.47	-13.04	20.95	28.92	-13.16	22.34
150	28.48	-23.30	16.83	28.92	-15.96	20.94	29.91	-15.26	22.28
200	29.70	-25.76	16.82	30.03	-18.20	20.93	30.76	-16.98	22.27
250	30.66	-27.70	16.81	30.91	-19.96	20.93	31.50	-18.50	22.25
300	31.44	-29.24	16.82	31.65	-21.54	20.88	32.13	-19.78	22.24
320	31.72	-	-	31.91	-22.04	20.89	32.36	-20.24	22.24
Meas. Date	11-27-1979			11-28-1979			11-27-1979		
X mtr.	Narda #07057			Corrugated #41			S/A #1222		
Revr.	Narda #06137			Corrugated #43			S/A #616		

*Measured Coupling Data from NAFS.

Table 19 : Range corrected gain measurements

Frequency = 11 GHz   CE=42.44 cm   CH=32.77 cm

Z_{AA} (cm)	Meas. Coupling (dB)	R (cm)	R_{GU} S/A (dB)	R_{GU} Narda (dB)	R_{GU} AVG (dB)	F_c	R_{GC}	$G_{AVG}^{Meas.}$
100	-16.66	125.3	28.00	27.58	27.79	0.19	27.98	19.65
150	-19.28	175.3	29.22	29.05	29.14	0.10	29.24	19.60
200	-21.34	225.3	30.24	30.14	30.19	0.06	30.25	19.58
250	-23.12	275.3	31.07	31.01	31.04	0.04	31.08	19.52
300	-24.50	325.3	31.78	31.74	31.76	0.03	31.79	19.54
320	-25.04	345.3	32.03	32.00	32.02	0.03	32.05	19.53

1. Transmitter: S/A (12-8.2 #1222; Receiver: Narda (640) #07057
2. $R = Z_{AA} + (D_E+D_H)_{AVG}$
3. $(D_E+D_H)_{AVG} = \left[(D_E+D_H)_{S/A} + (D_E+D_H)_{Narda}\right]/2 = 25.3$ cm
4. Measurement at NAFS on 27 Nov., 1979

Table 20: Range corrected gain measurements.

Frequency - 11 GHz   CE=50.96 cm,   CH=41.28 cm

Z_{AA} (cm)	Meas. Coupling (dB)	R (cm)	G_U Corr. (dB)	G_U S/A	G_U AVG	F_c	R_{GC}	$G_{AVG}^{Meas.}$
100	-13.42	131.1	27.87	28.15	28.01	0.26	28.27	21.56
150	-15.90	181.1	29.25	29.36	29.31	0.14	29.45	21.50
200	-17.84	231.1	30.29	30.35	30.32	0.09	30.41	21.49
250	-19.50	281.1	31.14	31.16	31.15	0.06	31.21	21.46
300	-20.88	331.1	31.84	31.86	31.85	0.04	31.89	21.45
320	-21.38	351.1	32.10	32.11	32.11	0.04	32.15	21.46

1. Transmitter: Corr. (CX 20) #41; Receiver: S/A (12-8.2) #1222
2. $R = Z_{AA} + (D_E+D_H)_{AVG}$
3. $(D_E+D_H)_{AVG} = \left[(D_E+D_H)_{Corr.} + (D_E+D_A)_{S/A}\right]/2 = 31.1$ cm
4. Measurement at NAFS on 27 Nov., 1979

Table 21: Range corrected gain measurements.

Frequency - 11 GHz CE=22.09 cm, CH=21.14 cm

Z_{AA} (cm)	Meas. Coupling (dB)	R (cm)	R_{GU} Corr. (dB)	Narda	AVG (dB)	F_c	R_{GC}	$G_{AVG}^{Meas.}$
100	-16.70	109.1	27.10	26.98	27.04	0.08	27.12	18.77
150	-19.90	159.1	28.70	28.63	28.67	0.04	28.71	18.76
200	-22.20	209.1	29.87	29.82	29.85	0.02	29.87	18.77
250	-24.14	259.1	30.79	30.75	30.77	0.02	30.79	18.72
300	-25.68	309.1	31.55	31.52	31.54	0.01	31.55	18.71
320	-26.20	329.1	31.82	31.79	31.81	0.01	31.82	18.72

1. Transmitter: Corr. (CX 20) #41; Receiver: Narda (640) #07057
2. $R = Z_{AA} + (D_E+D_H)_{AVG}$
3. $(D_E+D_H)_{AVG} = \left[(D_E+D_H)_{Corr.} + (D_E+D_H)_{Narda}\right]/2 = 9.1$ cm
4. Measurement at NALS on 27 Nov., 1979

Table 22: Summary of range corrected gain measurements

Frequency = 11 GHz									
				$G_{S/A}$-Narda		$G_{Corr.}$-S/A		$G_{Corr.}$-Narda	
Z_{AA} (cm)	$G_{S/A}$ (dB)	G_{Narda} (dB)	$G_{Corr.}$ (dB)	Meas. (dB)	AVG. (dB)	Meas. (dB)	AVG. (dB)	Meas. (dB)	AVG. (dB)
100	22.34	16.87	20.95	19.65	19.61	21.56	21.65	18.77	18.91
150	22.28	16.83	20.94	19.60	19.56	21.50	21.61	18.76	18.89
200	22.27	16.82	20.93	19.58	19.55	21.49	21.60	18.77	18.88
250	22.25	16.81	20.93	19.52	29.53	21.46	21.59	18.72	18.87
300	22.24	16.82	20.88	19.54	19.53	21.45	21.56	18.71	18.85
320	22.24	-	20.89	19.53	-	21.46	21.57	18.72	-
Meas. Date	11-27-79		11-28-79	11-27-79		11-27-79		11-27-79	
X mtr.	S/A#1222	Narda #07057	Corr. #41	S/A #1222		Corr. #41		Corr. #41	
Rcvr.	S/A#616	Narda #06137	Corr. #43	Narda #07057		S/A #1222		Narda #07057	

*Measurement data from MAFS

**$(G_{x-y})_{ANG.} = (G_x+G_y)/2$. AVG. of individual horn meas.

CHAPTER IX
CONCLUSION

In the method developed here for determining the far field gain of pyramidal horn antennas, the range is defined as that between the calculated amplitude centers of the two horns. Consequently, the correction for near field gain is very small. At 10 GHz, the near field gain ratio for aperture separations greater than 150 cm is less than 0.1 dB for the Scientific-Atlanta X band standard gain horn and is less than 0.03 dB for the Narda X band standard gain horn. The accuracy of the calculated near field range correction data is estimated to be within 0.1 dB. Therefore, the accuracy of the far field gain measurements is practically limited by the accuracy of the measured coupling data.

The following observations demonstrate the validity and accuracy of the theory and the calculated results for the finite range correction data. The calculated finite range correction data given nearly the same value for far field gain of each horn over a wide range of aperture separations. When the finite range correction data were applied to coupling between mixed horns, the effective gain of each horn pair was consistent with the gains of the two horns when measured separately.

APPENDIX A
EQUIVALENT LINE SOURCE INTEGRATION METHOD (LSI)

The slope diffraction method described in Chapter I was used for the GTD calculations of the diffracted fields from the H-plane edges of the horn antennas. As seen from Equation (24) slope diffraction is exact for an incident wave with a $\sin\phi$ pattern where $\beta_o \approx 90^o$. This is equivalent to a $\sin(\theta_{oH}-\theta_H)$ pattern for the wave incident on the H-plane edge of the horn shown in Figure 5. However the geometrical optics or incident wave in the H-plane of a horn has a $\cos\frac{\pi\theta_H}{2\theta_{oH}}$ pattern. Furthermore, in the GTD calculations the diffracted field from each E-plane edge is calculated as that of a uniform spherical wave. Thus, the amplitude of the incident wave along the E-plane edges is assumed to be uniform when it actually varies as $\cos\frac{\pi\theta_H}{2\theta_{oH}}$. Nevertheless, for large horn dimensions, the normal GTD calculations are accurate. For small horn dimensions the accuracy can be improved by using LSI which integrates over the $\cos\frac{\pi\theta_H}{2\theta_{oH}}$ incident wave to calculate the diffracted fields from the E-plane edges, and performs a linear integration in the H-plane of the aperture to calculate diffracted fields from the H-plane edges.

The concept of the equivalent current method states that we can get the equivalent diffracted field from the equivalent line source current. We can assume that there is an equivalent magnetic current along each E plane edge and therefore it generates the electromagnetic field at the observation point.

Referring to [12], the magnetic field from the equivalent magnetic current M at the distance r is given by

$$H_z^d = -Y_o kM\sqrt{\frac{j}{8\pi kr}}\; e^{-jkr} \qquad \text{(A-1)}$$

$$E_\phi^d = -kM\sqrt{\frac{j}{8\pi kr}}\; e^{-jkr} \qquad \text{(A-2)}$$

The diffracted field at a distance r close to a wedge is given by

$$E^d = E^i(Q_E)D_I(L,\phi,\beta_o,n)\,\frac{e^{-jkr}}{\sqrt{r}} \qquad \text{(A-3)}$$

The diffraction coefficient D_I in Equation (A-3) becomes independent of the distance parameter L outside the transition regions around the shadow boundary. Furthermore, the diffraction coefficient can be approximated as that for the centerl diffraction point on the edge. Thus, comparing Equations (A-2) and (A-3), we get the equivalent magnetic current, as shown in Figure A-1,

$$M = \frac{2}{k} \sqrt{\frac{2\pi k}{j}}\ E^i D_I(L, \phi, \phi_0, n) \qquad \text{(A-4)}$$

The magnetic vector potential is given by

$$F = \frac{1}{4\pi} \int_{-\frac{A}{2}}^{\frac{A}{2}} \frac{Me^{-jkr}}{r}\, dx \qquad \text{(A-5)}$$

and the electric field is given by

$$E^d = -jkF \cos\psi \qquad \text{(A-6)}$$

$$E^d = \frac{1}{2\pi} \sqrt{\frac{2\pi k}{j}}\ D_I(L, \phi, \phi_0, n) \cos\psi \int_{-\frac{A}{2}}^{\frac{A}{2}} \frac{E^i e^{-jkr}}{r}\, dx \qquad \text{(A-7)}$$

The incident or geometric optics field is given by Equation (51) as

$$E^i = \frac{e^{-jkR}}{R} \cos \frac{\pi\psi}{2\psi_0} \qquad \text{(A-8)}$$

$\psi_0 = \psi_{0H}$, is half angle of the H-plane (A-9)

Define the integral

$$I = \int_{-\frac{A}{2}}^{\frac{A}{2}} \frac{E^i e^{-jkr}}{r}\, dx$$

$$= \int_{-\frac{A}{2}}^{\frac{A}{2}} \cos \frac{\pi\psi}{2\psi_0}\ \frac{e^{-jkR}}{R} \cdot \frac{e^{-jkr}}{r}\, dx \qquad \text{(A-10)}$$

$$L_{EM} = \frac{H_H}{\cos\theta_{oE}} \tag{A-11}$$

$$R = \sqrt{L_{EM}^2 + x^2}$$

$$\approx L_{EM} + \frac{x}{2L_{EM}} \quad , \text{ for } L_{EM} >> x \tag{A-12}$$

$$r \approx R_{E1} + \frac{x^2}{2R_{E1}} \quad , \quad \text{for } R_{E1} >> x \tag{A-13}$$

$$\theta = \tan^{-1} \frac{x}{L_{EM}} \tag{A-14}$$

$$\therefore I \approx \frac{j}{L_{EM} R_{E1}} e^{-jkR_{E1}} \int_{-\frac{A}{2}}^{\frac{A}{2}} \cos \frac{\pi\theta}{2\theta_o} e^{-j\frac{kx^2}{2R_{E1}}} e^{-jkR} dx \tag{A-15}$$

The convenience in checking the computer programs the following factor F_{CTR} is defined for calculating the diffracted field from the E-plane edges:

$$F_{CTR} = \frac{\int_{-\frac{A}{2}}^{\frac{A}{2}} \cos \frac{\pi\theta}{2\theta_o} e^{-j\frac{kx^2}{2R_{E1}}} e^{-jkR} dx}{\int_{-\infty}^{\infty} e^{-j\frac{kx^2}{2R_{E1}}} e^{-jkR} dx}$$

$$= \frac{\int_{-\frac{A}{2}}^{\frac{A}{2}} \cos \frac{\pi\theta}{2\theta_o} e^{-j\frac{kx^2}{2R_{E1}}} e^{-jkR} dx}{e^{-jkL_{EM}} \int_{-\infty}^{\infty} e^{-j\frac{kx^2}{2}\left(\frac{1}{R_{E1}} + \frac{1}{L_{EM}}\right)} dx} \tag{A-16}$$

$$\int_{-\infty}^{\infty} e^{-j\frac{kx^2}{2}\left(\frac{1}{R_{E1}}+\frac{1}{L_{EM}}\right)} dx = e^{j\frac{\pi}{4}}\sqrt{\frac{R_{E1}L_{EM}}{R_{E1}+L_{EM}}} \qquad \text{(A-17)}$$

The diffracted electric field on the horn axis by using LSI method can be gotten from Equation (70) multiplied by F_{CTR},

$$E^d = E_{DIF} \times F_{CTR}$$

$$= 2D_I \frac{e^{-jkL_E}}{\sqrt{L_E}} \cdot \frac{e^{-jkR_{E1}}}{\sqrt{R_{E1}(R_{E1}+L_E)}} \cos\alpha' \cdot \frac{\int_{-\frac{A}{2}}^{\frac{A}{2}} \cos\frac{\pi x}{2a_0}\, e^{-j\frac{kx^2}{2R_{E1}}} e^{-jkR} dx}{e^{-jkL_{EM}}\, e^{j\frac{\pi}{4}}\sqrt{\frac{R_{E1}L_{EM}}{R_{E1}+L_{EM}}}}$$

$$= 2D_I \frac{e^{-jk(L_E - L_{EM})}}{\sqrt{L_{EM}L_E}} \cdot \frac{e^{-jkR_{E1}}}{R_{E1}}\sqrt{\frac{R_{E1}L_E}{R_{E1}+L_{EM}}} \cos\alpha'\, e^{-j\frac{\pi}{4}}$$

$$\times \int_{-\frac{A}{2}}^{\frac{A}{2}} \cos\frac{\pi x}{2a_0}\, e^{-j\frac{kx^2}{2R_{E1}}} e^{-jkR} dx \qquad \text{(A-18)}$$

Referring to Figure A-2, the sum of the geometric optics field and the H-plane diffracted field is given by

$$E^{G.O.} + H_{DIF} = F_H \times E_{INC.} \qquad \text{(A-19)}$$

where F_H is defined by

$$F_H = \frac{\int_{-\frac{A}{2}}^{\frac{A}{2}} \cos\frac{\pi x}{2a_0}\, e^{jk\frac{x^2}{2\ell_A}} e^{-jkR'} dx}{\int_{-\infty}^{\infty} e^{-j\frac{kx^2}{2\ell_A}} e^{-jkR'} dx} \qquad \text{(A-20)}$$

$$R' = \sqrt{H_H^2 + x^2} \tag{A-21}$$

$$\approx H_H + \frac{x^2}{2H_H} \quad \text{for } H_H \gg x \tag{A-22}$$

$$\int_{-\infty}^{\infty} e^{-j\frac{kx^2}{2Z_A}} e^{-jkR'}\, dx = e^{-jkH_H} e^{j\frac{\pi}{4}} \sqrt{\frac{H_H Z_A}{H_H + Z_A}} \tag{A-23}$$

$$F_H = e^{-j\frac{\pi}{4}} \sqrt{\frac{H_H Z_A}{H_H + Z_A}}\, e^{-jkH_H} \int_{-\frac{A}{2}}^{\frac{A}{2}} \cos\frac{\pi\theta}{2\theta_o}\, e^{-j\frac{kx^2}{2Z_A}} e^{-jk\sqrt{H_H^2 + x^2}}\, dx \tag{A-24}$$

Therefore, the total electric field is given by

$$E^{TOT} = E_{DIF} \times F_{CTR} + F_H \times E_{INC}. \tag{A-25}$$

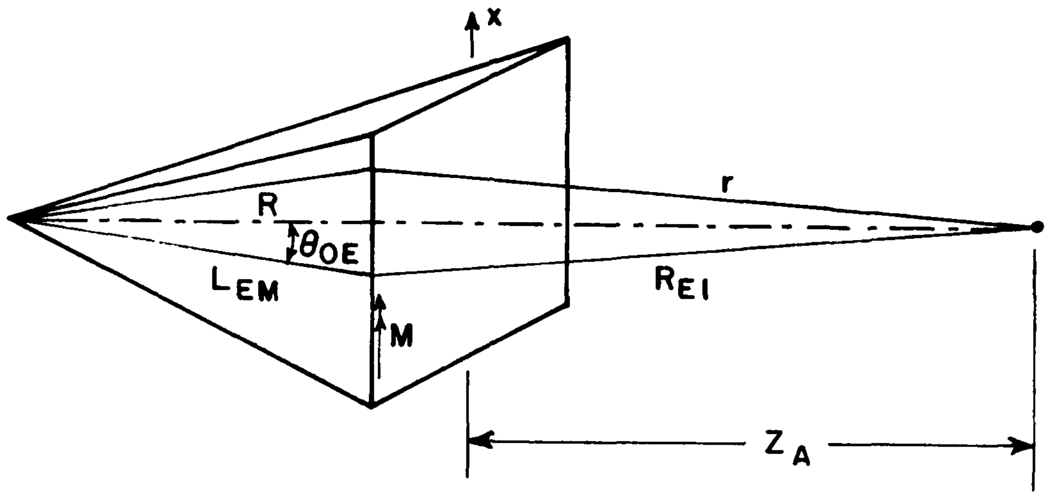

Figure A-1. Equivalent magnetic current along an E-plane edge.

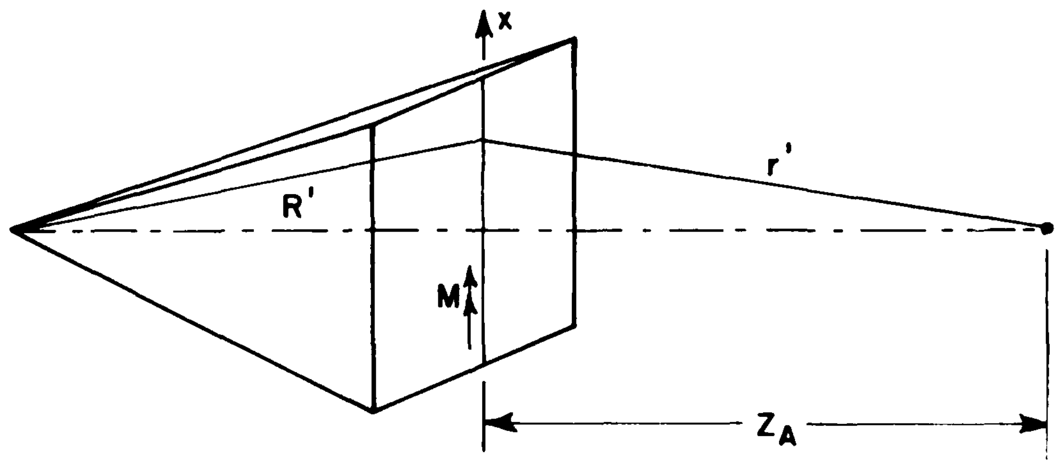

Figure A-2. Equivalent magnetic current along the central part of the H-plane.

APPENDIX B
APERTURE INTEGRATION METHOD (API)

The corrugated horn, as shown in Figure B-1, is formed by replacing the conventional E-plane horn walls by impedance walls which force the tangential magnetic field to zero along the walls. The effect of the capacitive corrugated surface is to modify the uniform field distribution in the E-plane to a cosine distribution in the horn aperture when the horn is properly designed, as shown in Figure B-2. The reason for using the LSI method for non-corrugated horns as discussed in Appendix A, also aplies in a similar way for corrugated horns. With corrugated horns, the aperture has a cosine distribution in both the E-plane and the H-plane. Therefore, the aperture integration method will be used here for computing the on-axis near field of the corrugated horn. The aperture field for a corrugated horn as shown in Figures B-2 and B-3 is given by

$$\bar{E}^i = \hat{y}\,\frac{e^{-jks'}}{s'}\cos\frac{\pi\theta_x}{2\theta_{ox}}\cos\frac{\pi\theta_y}{2\theta_{oy}} \qquad \text{(B-1)}$$

where

$$s' = \sqrt{H_{AVE}^2 + x^2 + y^2} \qquad \text{(B-2)}$$

$$\approx H_{AVE} + \frac{x^2}{2H_{AVE}} + \frac{y^2}{2H_{AVE}}$$

$$H_{AVE} = \frac{1}{2}(H_E + H_H) \qquad \text{(B-3)}$$

$$\theta_{ox} = \tan^{-1}\frac{A}{2H_H} \qquad \text{(B-4)}$$

$$\theta_x = \tan^{-1}\frac{x}{H_{AVE}} \qquad \text{(B-5)}$$

$$\theta_{oy} = \tan^{-1}\frac{B}{2H_E} \qquad \text{(B-6)}$$

$$\theta_y = \tan^{-1}\frac{y}{H_{AVE}} \qquad \text{(B-7)}$$

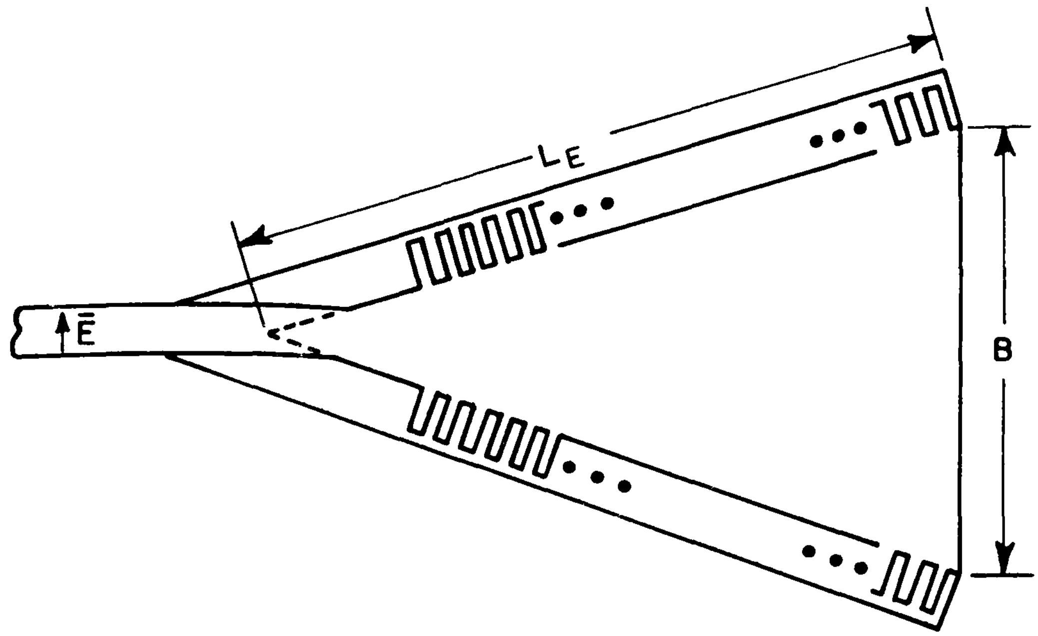

Figure B-1. Side view of corrugated horn.

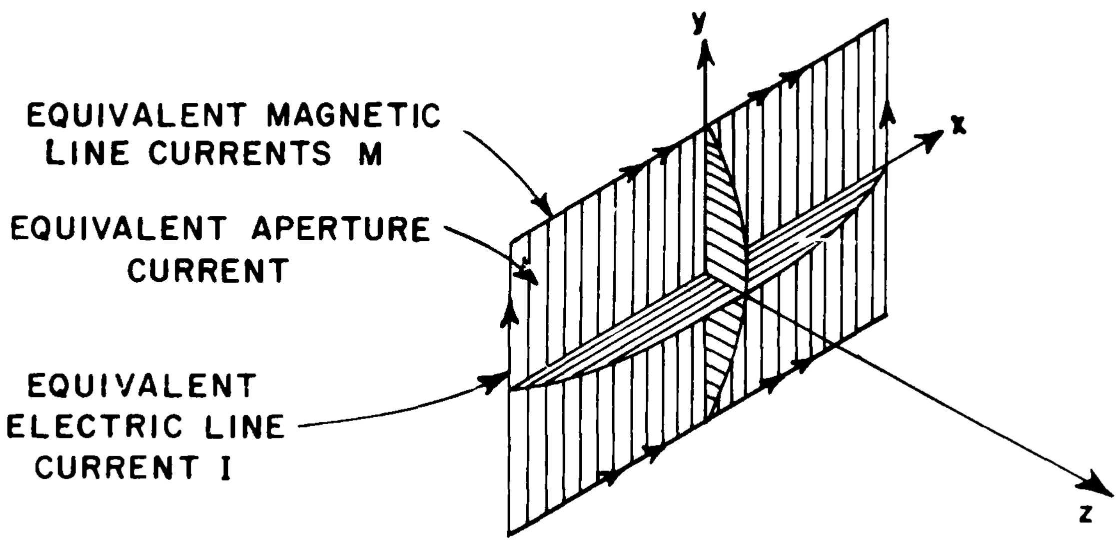

Figure B-2. Corrugated horn model.

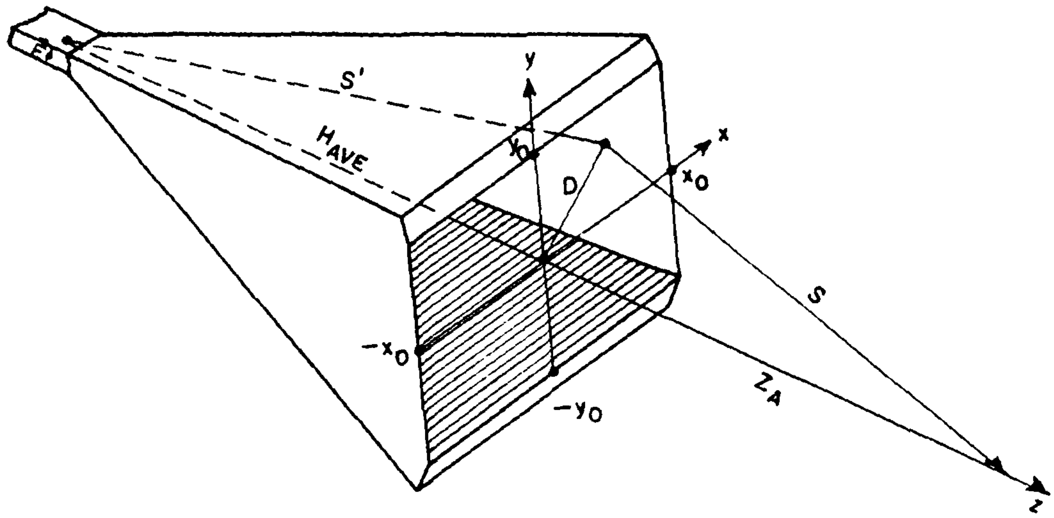

Figure B-3. Coordinate system.

The equivalent magnetic current is given by

$$\bar{M} = 2\bar{E}^i \times \hat{n}$$

$$= \hat{x}\, 2\, \frac{e^{-jks'}}{s'} \cos \frac{\pi\theta x}{2\theta_{ox}} \cos \frac{\pi\theta y}{2\theta_{oy}} \qquad \text{(B-8)}$$

Therefore, the total electric field on the horn axis is given by

$$E = \frac{jk}{4} \int_{-x_o}^{-x_o} \int_{-y_o}^{y_o} \frac{Me^{-jks}}{s}\, dx\, dy$$

$$= \frac{j}{\lambda} \int_{-x_o}^{x_o} \int_{-y_o}^{y_o} \frac{e^{-jks'}}{s'} \cos \frac{\pi\theta x}{2\theta_{ox}} \cos \frac{\pi\theta y}{2\theta_{oy}} \cdot \frac{e^{-jks}}{s} dx\, dy \qquad \text{(B-9)}$$

where

$$s = \sqrt{x^2+y^2+Z_A^2}$$

$$\approx Z_A + \frac{x^2}{2Z_A} + \frac{y^2}{2Z_A} \qquad \text{(B-10)}$$

$$\therefore E = \frac{je^{-jkZ_A} e^{-jkH_{AVE}}}{Z_A\, H_{AVE}} \int_{-x_o}^{x_o} \int_{-y_o}^{y_o} e^{-j\frac{kx^2 H_{ZA}}{2}}\, e^{-j\frac{ky^2 H_{ZA}}{2}}$$

$$\cdot \cos \frac{\pi\theta x}{2\theta_{ox}} \cos \frac{\pi\theta y}{2\theta_{oy}}\, dx\, dy \qquad \text{(B-11)}$$

where

$$H_{ZA} = \frac{1}{H_{AVE}} + \frac{1}{Z_A} = \frac{H_{AVE}+Z_A}{H_{AVE}Z_A} \qquad \text{(B-12)}$$

The geometric optics field can be expressed as

$$E^{G.O.} = \frac{je^{-jk(H_{AVE}+Z_A)}}{\lambda H_{AVE} Z_A} \int_{-\infty}^{\infty} \int_{\infty}^{\infty} e^{-j \frac{kx^2 H_{ZA}}{2}} \, e^{-j \frac{ky^2 H_{ZA}}{2}} \, dx \, dy$$

$$\int_{-\infty}^{\infty} e^{-j \frac{kx^2 H_{ZA}}{2}} \, dx = \int_{-\infty}^{\infty} e^{-j \frac{ky^2 H_{ZA}}{2}} \, dy \tag{B-13}$$

$$= \sqrt{\frac{1}{H_{ZA}}} \, e^{-j \frac{\pi}{4}} \tag{B-14}$$

For convenience in checking the computer programs the following factors F_{cx} and F_{cy} are defined as

$$F_{cx} = \frac{\int_{-x_o}^{x_o} e^{-j \frac{kx^2 H_{ZA}}{2}} \cos \frac{\pi \theta_x}{2\theta_{ox}} \, dx}{\int e^{-j \frac{kx^2 H_{ZA}}{2}} \, dx} = \sqrt{H_{ZA}} \, e^{j \frac{\pi}{4}} \int_{-x_o}^{x_o}$$

$$e^{-j \frac{kx^2 H_{ZA}}{e}} \cos \frac{\pi \theta_x}{2\theta_{ox}} \, dx \tag{B-15}$$

$$F_{cy} = \frac{\int_{-y_o}^{y_o} e^{-j \frac{ky^2 H_{ZA}}{2}} \cos \frac{\pi \theta_y}{2\theta_{oy}} \, dy}{\int_{-\infty}^{\infty} e^{-j \frac{ky^2 H_{ZA}}{2}} \, dy} = \sqrt{H_{ZA}} \, e^{j \frac{\pi}{4}} \int_{-y_o}^{y_o}$$

$$e^{-j \frac{ky^2 H_{ZA}}{2}} \cos \frac{\pi \theta_y}{2\theta_{oy}} \, dy \tag{B-16}$$

Therefore, the total electric field on the axis is given by

$$E^{TOT} = F_{cx} \times F_{cy} \tag{B-17}$$

APPENDIX C
COUPLING BETWEEN NON ISOTROPIC SOURCES

The near field coupling between two antennas with wide beamwidths (i.e., assuming each antenna would illuminate the other antenna with a nearly uniform spherical wave from its amplitude center) can be expressed as

$$\frac{P_{Ro}}{P_T} = \left(\frac{\lambda}{4\pi R}\right)^2 G_T(R) G_R(R) \qquad \text{(C-1)}$$

where

P_{ro} = Power received assuming uniform amplitude waves.

P_T = Power transmitted

R = Effective range (between amplitude centers)

$G_T(R), G_R(R)$ = Near field gains at distance R as defined by Equation (95) for transmitting and receiving antennas, respectively.

However, Equation (C-1) is not highly accurate if the two antennas are separated by a small distance compared to their beam widths. An improved calculation of the coupling can be derived for close antenna separations by using the principle of reaction [12]. This principle is based on two sets of sources which represent the transmitting and receiving antennas as shown in Figure C-1. The current I_a of source a produces the fields E_a, H_a; and I_b produces E_b, H_b. The reaction principle is based on the following Equation

$$-\oint\!\!\oint_S (\bar{E}_a \times \bar{H}_b - \bar{H}_b \times \bar{H}_a)\, d\bar{s}$$

$$= \iiint_V (\bar{E}_a \cdot \bar{J}_b - \bar{H}_a \cdot \bar{M}_b - \bar{E}_b \cdot \bar{J}_a + \bar{H}_b \cdot \bar{M}_a)\, dv \qquad \text{(C-2)}$$

Since each source is represented by electric currents only, the magnetic currents are zero ($M_a = M_b = 0$). The volume V of integration will be taken as the right half-space as shown in Figure C-1. Thus the volume integral in Equation (C-2) reduces to

$$\iiint_V \bar{E}_a \cdot \bar{J}_b dv = \int_b \bar{E}_a \cdot I_b d\bar{\ell} = V_{ab} I_b \qquad \text{(C-3)}$$

where V_{ab} is voltage induced by source a into source b when it is receiving.

Let both sources be identical to represent the coupling between like horns. Also assume unit currents for both sources $I_a = I_b = 1$. Then Equation (C-2) can be written as

$$V_{ab} = - \iint (E_{ta}H_{tb} - E_{tb}H_{ta})ds \qquad (C-4)$$

where E_{ta}, H_{tb}, E_{tb} and H_{ta} are the tangential field components on surface S. From Figure C-1 note that

$$E_{ta} = E_{tb} \approx E_a \qquad (C-5)$$

$$H_{ta} = -H_{tb} \approx H_a \qquad (C-6)$$

which can be approximated as the total field components for small angles. Then the received voltage can be approximated as

$$V_{ab} \approx 2 \iint_S E_a H_a \, dS \approx \frac{2}{Z_0} \iint_S E_a^2 \, dS \qquad (C-7)$$

where Z_0 is the impedance of free space.

As seen from Chapter VII the coupling between two horns is represented as that between two point sources located at the respective amplitude centers of each horn as shown in Figure C-2. In Equation (C-1) the spherical wave from each amplitude center is assumed to have uniform amplitude. In this derivation the spherical wave from each amplitude center is assumed to have a Gaussian amplitude. Thus a more accurate representation of the near axis pattern is given by

$$F(\theta) = C\, e^{-A\theta^2} \qquad (C-8)$$

where A is a constant which can be determined from the calculated horn patterns as follows: First, use the normalized field pattern given by

$$F_n(\theta) = \frac{F(\theta)}{F(0)} = e^{-A\theta^2} \qquad (C-9)$$

Then A can be evaluated for a small angle (let's choose $\theta = 1^\circ = \pi/180$ radians). Thus

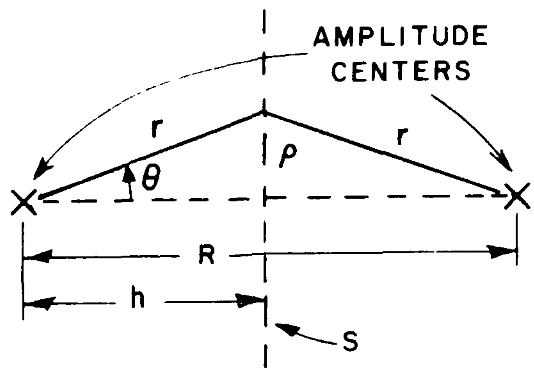

Figure C-1. Fields of source a and source b over sourface S of integration.

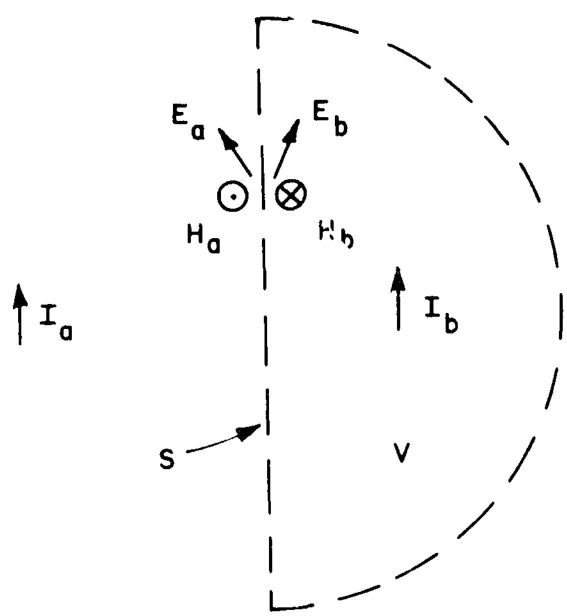

Figure C-2. Coupling between two horns.

$$A = \frac{-\ln F_n(1^o)}{(\pi/180)^2} \tag{C-10}$$

Calculated horn paterns are usually expressed in dB as

$$F_{dB}(\theta) = 20 \log F_n(\theta) \tag{C-11}$$

Then

$$F_n(\theta) = (10)^{F_{dB}/20} \tag{C-12}$$

Thus

$$A = -\left(\frac{180}{\pi}\right)^2 \frac{\ln 10}{20} F_{dB}(1^o) \tag{C-13}$$

$$A = -378 F_{dB}(1^o) \tag{C-14}$$

where $F_{dB}(1^o)$ is the value of the normalized horn pattern in dB at $\theta = 1^o$.

The field of each horn on surface S as shown in Figure C-2 is given by

$$E(r,\theta,\phi) = F_E(\theta_E)F_H(\theta_H) \frac{e^{-jkr}}{r} \tag{C-15}$$

where F_E and F_H are the E- and H-plane patterns, respectively. Thus the voltage received by one horn with an identical transmitting horn is given by Equation (C-7) as

$$V_R = \frac{2}{Z_o} \iint_S E^2 ds = \frac{2}{Z_o} \iint_S \left[F_E(\theta_E)F_H(\theta_H) \frac{e^{-jkr}}{r}\right]^2 dS \tag{C-16}$$

Because of stationary phase effects most of the contributions to the integral in Equation (C-16) will result from the near-axis region where

$$r \approx h + \frac{\rho^2}{2h} \tag{C-17}$$

$$x \approx h\theta_E \tag{C-18}$$

$$y \approx h\theta_H \tag{C-19}$$

and

$$\rho^2 = x^2 + y^2 \approx h^2(\theta_E^2+\theta_H^2) \tag{C-20}$$

Using these approximations in Equation (C-14) gives the received voltage as

$$V_R = \frac{2e^{-j2kh}}{Z_0 h^2} \int_{-\pi/2}^{\pi/2} e^{-(2A_E+jkh)\theta_E^2}\, h\, d\theta_E$$

$$\times \int_{-\pi/2}^{\pi/2} e^{-(2A_H+jkh)\theta_H^2}\, h\, d\theta_H \tag{C-21}$$

where the Gaussian pattern of Equation (C-9) has been used.

The coupling power ratio in Equation (C-1) assumes spherical waves with uniform amplitudes, i.e., $A_E=A_H=0$. Thus the ratio of the received voltage V_R to the voltage V_{Ro} received with assumed uniform amplitude waves is given by

$$\frac{V_R}{V_{Ro}} = \frac{\int_{-\infty}^{\infty} e^{-(2A_E+jkh)\theta_E^2}\, d\theta_E \int_{-\infty}^{\infty} e^{-(2A_H+jkh)\theta_H^2}\, d\theta_H}{\int_{-\infty}^{\infty} e^{-jkh\theta_E^2}\, d\theta_E \int_{-\infty}^{\infty} e^{-jkh\theta_H^2}\, d\theta_H} \tag{C-22}$$

Because of stationary phase effects the limits of integration in Equation (C-22) can be treated as infinite. Then the integrals can be analytically evaluated by

$$\int_{-\infty}^{\infty} e^{-(2A+jB)\theta^2}\, d\theta = \frac{\sqrt{\pi}}{\sqrt{2(A+jB)}} \tag{C-23}$$

Then Equation (C-23) can be evaluated as

$$\frac{V_R}{V_{Ro}} = \sqrt{\frac{jkh}{2A_E+jkh}}\sqrt{\frac{jkh}{2A_H+jkh}} = \frac{1}{\sqrt{1-jT_E}}\ \frac{1}{\sqrt{1-jT_H}} \tag{C-24}$$

where

$$T_E = \frac{2A_E}{kh} = \frac{4A_E}{kR} = \frac{C_E}{R} \tag{C-25a}$$

$$C_E = \frac{2\lambda\ A_E}{\pi} \tag{C-25b}$$

$$T_H = \frac{2A_H}{kh} = \frac{4A_H}{kR} = \frac{C_H}{R} \tag{C-26a}$$

$$C_H = \frac{2\lambda A_H}{\pi} \tag{C-26b}$$

and R is the range between amplitude centers. Finally the ratio of the received powers is given by

$$\frac{P_R}{P_{Ro}} = \left|\frac{V_R}{V_{Ro}}\right|^2 = \frac{1}{\sqrt{1+T_E^2}}\ \frac{1}{\sqrt{1+T_H^2}} \tag{C-27}$$

Thus combining Equation (C-27) and (C-1) the coupling between two horns can be more accurately calculated from

$$\frac{P_R}{P_T} = \left(\frac{\lambda}{4\pi R}\right)^2 G_T(R)G_R(R)\ \frac{1}{\sqrt{1+T_E^2}}\ \frac{1}{\sqrt{1+T_H^2}} \tag{C-28}$$

where T_E and T_H are calculated by using Equations (C-25), (C-26) and (C-14).

For different horn models the patterns for each horn can be used in Equations (C-4) and (C-16). Thus coupling between horns of different dimensions can be calculated from Equation (C-27) with

$$T_E = \frac{2A_{E1}+2A_{E2}}{kR} = \frac{C_E}{R} \tag{C-29a}$$

and

$$C_E = \frac{\lambda}{\pi}(A_{E1}+A_{E2}) \tag{C-29b}$$

The pattern constants A_{E1} and A_{E2} are those for the E-plane patterns of horns 1 and 2, respectively. Similarly, for the H-plane, we have

$$T_H = \frac{2A_{H1}+2A_{H2}}{kR} = \frac{C_H}{R} \tag{C-30a}$$

and

$$C_H = \frac{\lambda}{\pi}(A_{H1}+A_{H2}) \ . \tag{C-30b}$$

REFERENCES

1. R. C. Rudduck, "Application of Wedge Diffraction to Antenna Theory," Report 1691-13. 30 June 1965. The Ohio State University ElectroScience Laboratory, Department of Electrical Engineering; prepared under Grant No. NSG-448 for National Aeronautics and Space Administration. Washington, D.C. Also published as NASA Report CR-372.

2. P. M. Russo, R. C. Rudduck, and L. Peters, Jr.. "A Method for Computing E-Plane Patterns of Horn Antennas," IEEE Trans. on Antennas and Propagation. AP-13, No. 2 March 1965, pp. 219-224

3. J. S. Yu, R. C. Rudduck, and L. Peters, Jr. "Comprehensive Analysis for E Plane of Horn Antennas for Edge Diffraction Theory," IEEE Trans. Antennas and Propagation, Vol. AP-14 March 1966, pp. 138-149.

4. J. S. Yu and R. C. Rudduck, "H-Plane Pattern of a Pyramidal Horn," IEEE Trans. on Antennas and Propagation Comm., Vol. AP-17, No. 5, September 1969.

5. C. A. Mentzer, L. Peters, Jr., and R. C. Rudduck, "Slope Diffraction and Its Application to Horns," IEEE Trans. on Ant. and Prop. AP-23, No. 2, March 1975.

6. R. G. Kouyoumjian and P. H. Pathak, "A Uniform Geometrical Theory of Diffraction for an Edge in a Perfectly-Conducting Surface," Proc. IEEE, vol. 62, November 1974, pp. 1448-1461.

7. T. S. Chu and R. A. Semplak, "Gain of Electromagnetic Horns," The Bell System Technical Journal, March 1965, pp. 527-537, Vol. 14, No. 3.

8. R. R. Bowman, "Absolute Gain Measurements for Horn Antennas," Technical Report No. RADC-TR-68-349, November 1968, Final Report.

9. E. V. Jull, "Finite Range Gain of Sectoral and Pyramidal Horns," Electron. Lett., Vol. 6. October 15, 1970.

10. A. C. Ludwig and R. A. Norman. "A New Method of Calculating Correction Factor for Near Field Gain Measurements," IEEE Trans. on Ant. and Prop. AP-21, No. 5, September 1973, pp. 623-628.

11. A. C. Newell, R. Baird and P. F. Wacker, "The Accurate Measurement of Antenna Gain and Polarization at Reduced Distances by an Extrapolation Technique," IEEE Trans. on Ant. and Prop., AP-21, No. 4, July 1973, pp. 418-431.

12. R. F. Harrington, Time-Harmonic Electromagnetic Fields, McGraw-Hill, 1961.